Multi-signature Search for Quark-Gluon Plasma Formation in High Multiplicity $\bar{p}p$ Interactions at $\sqrt{s}$=1.8 TeV

April 2, 1989

Fermilab Proposal P787

Submitted by Scientists at
Duke University, Fermi National Accelerator Laboratory,
Iowa State University, University of Notre Dame,
Purdue University, and University of Wisconsin

We propose to measure photon and e^+e^- pair production and to study the low p_t (<3 GeV/c) production characteristics of centrally produced hadrons such as π, ρ, K, K*, ϕ, p, Λ and deuterons in $\bar{p}p$ collisions at $\sqrt{s}$ = 1.8 TeV. This will be done as a function of the energy density of the collision as measured by the charged particle rapidity density. Variation of the above particle production cross sections and transverse momentum spectra with collision energy density will provide information about quark-gluon plasma formation in $\bar{p}p$ interactions at 1.8 TeV. This experiment will also provide unique data for testing hadroproduction models at the highest available energy. To make these measurements we will increase the aperature, momentum resolution and particle identification capabilities of the existing E735 spectrometer and build a second spectrometer arm in the tunnel at the C0 collision hall. Both detector arms will have electromagnetic calorimetry.

Names of the Senior Experimenters

De Pauw University:	V. DeCarlo
Duke University:	A. T. Goshaw
	S. Oh
	W.J. Robertson
	W.D. Walker
Fermilab:	P. C. Bhat
	C. Hojvat
	F. Turkot
Iowa State University:	E. W. Anderson
	C. S. Lindsey
Notre Dame University:	J. Bishop
	N. N. Biswas
	J. M. LoSecco
	V. P. Kenney
	J. Piekarz
Purdue University:	A. T. Bujak
	D. D. Carmony
	Y. I. Choi
	R. J. De Bonte
	L. J. Gutay
	A. S. Hirsch
	N. K. Morgan
	N. T. Porile
	R. P. Scharenberg
	B. C. Stringfellow
University of Wisconsin:	A. R. Erwin
	C. Findeisen
	K. Nelson
	M. A. Thompson

Contents

1 Introduction **4**

1.1 Prologue 4

1.2 Evaluation and Summary of Experiment E735 5

1.3 Overview of P787 Physics Goals 8

1.3.1 Electron-Positron Pair Production 9

1.3.2 Photon Production 10

1.3.3 Hadron Production 11

1.4 Detector Overview 11

1.5 Time Table for Staging P787 13

2 Proposed Measurement and Analysis **16**

2.1 Dilepton Production 16

2.1.1 Introduction 16

2.1.2 Expected Rates 16

2.1.3 Electron Identification 17

2.1.4 Background Rejection 18

2.2 Photon Production 19

2.2.1 Introduction 19

2.2.2 Analysis of the photon data from P787 and preliminary results from E735 20

2.3 Hadron Production 21

2.3.1 Study of Λ production and search for Ξ and Ω production in the central region 22

2.3.2 Low p_t hadron physics 22

2.3.3 p_t of π, K, p, ρ, K*, and ϕ production up to $p_t = 3\mathrm{GeV/c}$ 23

3 The P787 Detector **24**

3.1 The Spectrometer Components 24

3.1.1 Pre-magnet Drift Chambers (PRDC) 24

3.1.2 Post-magnet Drift Chambers (PSDC) 25

3.1.3 Threshold Cherenkov Counter (TC) 25

3.1.4 RICH Cherenkov Counter (RICH) 26

3.1.5 Spectrometer Room Electromagnetic Calorimeter (NAI) 26

3.1.6 Tunnel Side E.M. Calorimeter (EM2) 28

3.1.7 Multiplicity Hodoscope (H) 28
3.1.8 TOF counters 29
3.1.9 Magnets 29
3.2 Trigger 29
3.2.1 Interaction Trigger 29
3.2.2 Hadron Production Trigger 30
3.2.3 Single and Dilepton Trigger 30
3.3 Data Acquisition System 30
3.4 Accelerator Issues 32

A Theoretical Arguments for Strangeness Enhancement in Deconfined Hadronic Matter 33
A.1 Production Mechanism 33
A.2 Production Rate and Chemical Equilibrium 34
A.3 Conversion from the QGP to Hadronic Phase 34

B Lepton Pair Production from the Centrally Produced Hadronic Matter 35
B.1 Drell-Yan Model for Lepton Pair Production. 36
B.2 Modification of the Drell-Yan Model 36
B.3 The low mass ($m_d < 600$ MeV) region 36

1 Introduction

1.1 Prologue

There is a general theoretical consensus that at temperatures of about 200 MeV and energy densities of about 2 GeV/fm^3 a first order deconfining phase transition of QCD matter will take place [Hagedorn *et al.*, 1980]. There is reasonable expectation that such conditions can be obtained in high energy particle collisions. Theoretical description of the formation, thermalization, and decay of centrally produced hadronic matter is complex. In particular some of the experimental signatures predicted for the existance of a quark-gluon plasma (QGP) can be arrived at without assuming its existance. But while the QGP signatures stem from a central idea, the alternate explanations are subject to a collection of assumptions. The first round of QGP search experiments, E735 at FNAL and heavy ion collisions at CERN, are under analysis, and although there are several suggestive particle production "anomalies," no one experiment has claimed the observation of a QGP. As stressed by Van Hove [Van Hove, 1986], "it will take a unified interpretation of several anomalies to provide the first basis for a serious claim that a QGP has been discovered." The proposed experiment, P787, is designed with this philosophy in mind, namely to look for multiple signatures of QGP formation in a single experiment.

Aside from speculations about the formation of a QGP, the measurement of particle production from highly inelastic $\bar{p}p$ collisions is of fundamental importance in its own right. There is little data on mass identified particle production at low p_t at the Tevatron Collider and the theoretical understanding of the hadronic production mechanism is poor. The measurements made in experiments E735 and P787 will strongly compliment the hard scattering measurements to be made at CDF and D0.

Both our test run in 1987 and the ongoing E735 experiment have shown that a viable experimental $\bar{p}p$ collider program can be sustained at the C0 intersection region. In particular, we have shown [Alexopoulous *et al.*, 1988] that it is possible to measure production characteristics of interactions with central charged particle rapidity

densities as high as 32. These extremely high multiplicity events allow us to examine the characteristics of hadronic matter compressed to an energy density of up to 7 GeV/fm^3. This energy density is a factor of three higher than that estimated for the onset of QGP formation. The present proposal is intended to appreciably broaden our experimental sensitivity to the production of a QGP and other unusual high energy density $\bar{p}p$ production phenomena. We would enlarge the momentum range of our study of π, K and p production and add measurements of the production of hadron resonances, photons and dilepton pairs. The potential for the discovery of important new high energy physics phenomena in these data is high. The opportunity is also uniquely available to Fermilab if the P787 proposal is approved.

The remainder of this introduction is organized as follows. Section 1.2 evaluates and summarizes the data expected from experiment E735. Section 1.3 then provides a brief overview of the new physics goals of proposed experiment P787. Sections 1.4 and 1.5 provide an overview of the detector and give a time table for staging the experiment. The details of our proposed measurements are presented in Section 2 and a complete detector description is given in Section 3. Some detailed information supporting the proposal is given the appendices.

1.2 Evaluation and Summary of Experiment E735

Experiment 735 has been installed in the C0 region of the Tevatron Collider since January 1987. We have shown that it is possible to study the momentum spectra of mass identified particles emerging in the central region for very high multiplicity collisions. As shown in Figure 1.2.1, the multiplicity detector was located in the accelerator tunnel and the 90° magnetic, time-of-flight spectrometer was in an adjoining room. This is a unique experiment as it explores the low energy particle spectrum emerging from the highest energy collisions at hadron colliders.

The study of the soft particle spectrum in $\bar{p}p$ collisions at the highest energies is complementary to the research now taking place with relativistic heavy ion collisions, as it explores a different, but

significant, range of the variables of interest for the formation of a Quark-Gluon Plasma. These variables are: the size of the region of hadronic matter created during the collision and the energy density within it. The range of the two variables covered by the present data is summarized in Figure 1.2.2. We have extended the heavy ion collisions to the expectations for the RHIC accelerator and, for the purpose of this comparison we have assumed that experiment E735 could reach a value of dn/dη of 50. For the size of the collision region in $\bar{p}p$ collisions we have used a simple linear extrapolation of the preliminary UA1 results [Fincke-Keeler, 1989]. Figure 1.2.2 clearly illustrates the complementarity of the two approaches; heavy ion collisions can explore the large volume of hot hadronic matter while $\bar{p}p$ collisions can explore hadronic matter to very high energy densities.

About 5x10^6 events were collected during the four month 1987 collider run. At that time the Central Tracking Chamber was not installed. All this data has now been analysed, resulting in two publications, each addressing a possible signature of phase transition in hadronic matter. A further article, presenting the results of particle identification utilizing the Time-of-Flight (TOF) system is near completion. In addition, during part of this run an additional 1x10^6 events were collected with converter plates (0.1 and 0.2 radiation lengths) within the spectrometer aperture in order to have a preliminary look at photon production. This data is under analysis and a publication will be ready by summer of 1989. The final sample has of the order of 4000 photons, originating from the collision region. Finally, data collected using a small NaI calorimeter will be used in the design of the $\gamma/e^{\pm}$ calorimeter for P787.

This research is discussed in more detail below.

1. Studies of $< p_t >$ vs. dn/dη

   The first published article from the 1987 collider run presents the correlation between the average transverse momentum and the associated charged particle multiplicity of the events [Alexopoulos *et al.*, 1988]. The measurement extends previous results from a maximum dn/dη of 18 to a value of 32. The UA1 data [Arnison *et al.*, 1982 and Dowell *et al.*, 1988], taken at center of mass energies of 546 GeV and 900 GeV, is in good

agreement with our results for the region of overlap in dn/dη (see Figure 1.2.3). In agreement with UA1 our data clearly shows the existence of a plateau in $< p_t >$. The data at the highest multiplicities may indicate a further rise, following the plateau, of $< p_t >$. The high multiplicity data available to E735 from the 1988/89 run will significantly increase the maximum value of dn/dη to which the $< p_t >$ vs. multiplicity correlation could be extended. The actual value reached will likely be determined by our ability to correct for backgrounds and sytematics. The new data should settle the question of a second rise of the $< p_t >$ vs. multiplicity.

2. Studies of $\Lambda/\bar{\Lambda}$

   The second published article from the 1987 collider run presents the measurement of strange baryon production (Λ^o and $\bar{\Lambda}^o$) and its p_t dependence [Banerjee *et al.*, 1988]. The 1987 data contained 400 Λ's. The increase in the number expected from the 1988/89 run could vary from a factor of 5 to a factor of 10. Most of the increased statistics is in the high multiplicity region. This data will allow us to make a first determination of the ratio of Λ production to other charged particles as a function of particle multiplicity. A comparison with the recent preliminary results from the CERN heavy ion experiments, showing a quadratic increase on the ratio Λ/π with multiplicity, will be interesting.

3. The Transverse Momentum Spectra of π's, K's, and p's

   Our pending publication addresses the production of π's, K's, p's and $\bar{p}$'s identified by the TOF system. The p_t dependence of their production will be presented. The statistical accuracy available will permit us to obtain particle ratios up to the order of dn/dη = 15. The 1988/89 data will increase the maximum dn/dη to 20.

At the completion of the 1988/1989 collider run, Experiment 735 would have been taking data for a period of the order of 9 months. The complete experimental setup was available for this run, including the Central Tracking Chamber. In addition, the increased segmentation of the $\bar{p}$ and p TOF counters for this run will provide

increased efficiency in determining the vertex position for high multiplicities. During part of this run, a NaI prototype was installed. We estimate that from the 9 months operation we will accumulate a total of 16×10^6 events. Of these, we predict that of the order of 1×10^6 reconstructed tracks will be available for good events with $dn/d\eta \geq 19$. This represents an increase in the data sample by about 50 times over the first run of the experiment. It should be noted here that the overall number of events recorded is limited by the data recording rate. The dramatic improvement of the accelerator performance and luminosity has allowed E735 to significantly increase the relative fraction of high multiplicity events.

1.3 Overview of P787 Physics Goals

The experience we have gained from experiment E735 has allowed us to design an experiment that appreciably broadens our study of very high energy density $\bar{p}p$ interactions.

We propose to:

- Measure direct e^+e^- pair ($p_t < 3$ GeV/c) and photon ($p_t < 10$ GeV/c) production with a double arm electromagnetic calorimeter.
- Increase the detector aperture, momentum resolution and trigger selection, allowing a broad survey of low p_t meson and baryon production.
- Extend the identified $\pi/K/p$ measurements up to 3 GeV/c and the pion measurement below 150 MeV/c.

The unifying physics goal is to explore the low p_t (<3GeV/c) production region as completely as possible for $\bar{p}p$ collisions at the highest energy density. These measurements will be unique and we believe have considerable potential for the discovery of a quark-gluon plasma. The experiment will also provide a broad survey of low p_t particle production characteristics.

1.3.1 Electron-Positron Pair Production

The production of prompt leptons has been investigated extensively [Mikano *et al.*, 1980]. For e^+e^- pair masses, M, greater than 3 GeV/c^2, the major contributions are from J/ψ decays and Drell-Yan production. For 1.0< M <3.0 GeV/c^2, the decay of charmed mesons is one of the main sources. Recently, the e/π ratios of 1.0x10^{-3} for p_t=0.1 GeV/c and 0.5x10^{-3} for p_t=0.25 GeV/c were observed at the ISR [Akesson *et al.*, 1985]. This is much higher than expected from either hadronic bremsstrahlung or the semileptonic decay of charmed mesons. Not only was an excess of electrons observed but also the electron production rate increased as the square of the charged particle multiplicity.

It was pointed out [Adachi *et al.*, 1981] that the large e/π ratio at low p_t and the multiplicity dependence of the e/π ratio can be explained by thermodynamic models. Leptons would be produced from the annihilation of quark and antiquark in a quark-gluon plasma.

In contrast to most hadrons, which are produced from the later stage of the quark-gluon plasma via surface emission, the leptons (like prompt photons) are expected to be produced throughout the lifetime of the plasma and from the entire plasma volume [Müller, 1985]. Leptons could, therefore, be a much cleaner probe of the plasma stage than the various proposed hadronic probes. For example, the p_t spectrum of dilepton pairs could tell us the internal temperature of the plasma.

In addition to $q\bar{q}$ annihilation, electrons can also come from resonance decays. Effects of plasma formation on these decays could be studied. For example, the ρ meson has a very short lifetime (1.5 fm/c). Once it is formed, it would tend to decay within the plasma volume before it is dissolved. If it decays hadronically (π^+ and π^-), then the decay products would not escape the plasma. If it decays electromagnetically, then the e^+e^- pairs would escape the plasma. In other words, the branching ratio of the hadronic decay mode would be suppressed compared to the electromagnetic decay mode. Using the double arm spectrometer, the production cross section of both decay modes can be measured as a function of p_t and multi-

plicity. It has also been suggested that the mass and width of the ρ would be changed if chiral symmetry is restored within the quark gluon plasma [Shuryak, 1981].

We propose to measure: (1) single electron and positron p_t spectra as a function of charged multiplicity; and (2) the invariant mass spectrum and p_t distribution of e^+e^- pairs from the continuum and from vector meson resonances such as ρ, ω, ϕ, and J/ψ. We will measure pairs with mass from 0.1 to 3 GeV/c^2 and p_t less than 10 GeV/c as a function of multiplicity.

1.3.2 Photon Production

We propose extending the scope of our study of low p_t processes by measuring the central production of photons with energies below 10 GeV. Photons provide a qualitatively different view of high energy density $\bar{p}p$ collisions since the direct photon spectrum is sensitive to the parton structure of the collision prior to hadronization. This would be a particularly valuable method of exploring the formation and evolution of a QGP. We would search for an increase of the $\gamma/\pi^{\pm}$ ratio and a change in the shape of the low energy gamma spectrum as a function of the collision energy density as measured by $dn/d\eta$. Any anomalous photon signals would then be correlated with other QGP signatures such as a rise in $< p_t >$, changes in K/π, Λ/p ratios, *etc.* Independent of the formation of a QGP, these photon data will provide constraints on hadroproduction models, being especially sensitive to central π° production.

Interest in the measurement of the low energy direct photon spectrum is enhanced by the observation of unexplained signals from two previous experiments. Data from collisions of K^+p at 70 GeV/c [Chliapnikov *et al.*, 1984] and p-Be at 450 GeV/c [Goerlach *et al.*, 1988] give evidence of large excesses of direct photons at low X_F and p_t. Theoretical attempts to explain these soft photons by standard hadronic production mechanisms have failed [Anderson *et al.*, 1988]. Recently Van Hove [Van Hove, 1988] speculated about the existence of a cold, non-thermal QGP state to explain these low energy photons and other low p_t hadron production phenomena.

1.3.3 Hadron Production

We will improve the π, K and p mass separation and extend identification from 1.2 GeV/c (E735) to 3 GeV/c (P787). These data, along with a larger detector acceptance and improved momentum resolution, will allow us to study a broad spectrum of low p_t hadron production. In particular, we will attempt to measure the $\pi : K : \phi$ and $p : \Lambda : \Xi : \Omega$ ratios as a function of n_c, p_t and $\sqrt{s}$. There are hints of strong variations of these ratios with these variables [Rafelski *et al.*, 1987]. It is important to make definitive measurements within a single experiment, especially at the highest collision energy currently available. The variation of these particle ratios may indicate the onset of new particle production mechanism thresholds. Our collaboration has already observed increases in the Λ/π and K/π ratios as a function of n_c, p_t and $\sqrt{s}$ in E735. A significant increase in these ratios would be an indication of abundant strange quark production via gluon-gluon collisions at high energy densities.

The presence of a low p_t peak in the pion spectrum has been reported in high multiplicity hadronic collisions [Willis, 1988]. Furthermore, low p_t direct photons and low mass dileptons have also been observed in these collisions. To test the idea of an extended (several fm) intermediate parton system [Van Hove, 1988] we will use a shorter flight path TOF detector to identify pions with p_t in the range 60 to 150 MeV/c interval. The detection of these low energy particles would provide important data for measuring the size of the intermediate parton system, which could be a QGP. In general these low p_t data will allow critical tests of ultrasoft hadron production models.

1.4 Detector Overview

The P787 detector will mass identify charged π's, K's, and p's with p_t between 50 MeV/c and 3 GeV/c. Electrons and γ's will be identified for energies less than 10 GeV. The design is based on experience gained from the E735 detector system. As shown in Figures 1.4.1a and 1.4.1b, the proposed detector is a double arm spectrom-

eter. One arm would consist of the present spectrometer with some major modifications, while the other arm would be new. Since the present E735 spectrometer arm worked very well, we decided to use the same basic design for the new arm: drift chambers for charged particle tracking before and after a dipole magnet (50MeV/c kick). Both arms would also have time of flight counters (250 *ps* FWHM) following the tracking chambers and new electromagnetic calorimeters. A RICH detector in one arm would provide mass identification for charged particles with momenta up to 3 GeV/c. Detailed descriptions of each component are given in Section 3.

The two spectrometer arms have sufficient acceptance to reconstruct mesons and baryons such as ρ's, K^*'s, ϕ's, K°'s, Λ°'s, Ξ's, *etc.* High resolution stereo drift chambers permit clear identification of the K° and Λ° decay vertices. The detector will also discriminate against e^+e^- pairs from Dalitz decays and pair conversions in the beam pipe. The high rejection of these pairs is very important in studying prompt e^+e^- production (see section 2.4 for details of background studies). The expected momentum resolution is

$$\frac{dp}{p} = \sqrt{(0.02)^2 + (\frac{0.03}{\beta^2})^2}$$

The electromagnetic calorimeters are designed to detect gammas and electrons with energy from 10 MeV to 10 GeV with resolution of

$$\frac{dE}{E} = \frac{2\%}{\sqrt{E(GeV)}}$$

The calorimeter in the detector room consists a front end and an absorber. The front end, consisting of a thin converter, TOF scintillators and drift chambers, rejects low energy neutrals using time of flight and measures the direction of photons. In section 2.2, we present a Monte Carlo study discussing the background rejection and the reconstruction of photons.

The absorber made of NaI is divided into two sections longitudinally to improve electron identification and reject pions by using longitudinal shower profile. Monte Carlo study shows that the calorimeter can reject pions better than 1 in 5000 for the energy

range above 100 Mev/c. With the aid of a Cherenkov counter the rejection will be better than 1 in 10^5. A detailed Monte Carlo study of the pion rejection is described in section 2.1.

The calorimeter in the tunnel side is similar to the one in the detector room with a less sophisticated front end. This detector is designed mainly to measure electrons and positrons. Since the radiation level is fairly high in the tunnel ($\sim$1 rad/hour) we will fabricate the E.M. calorimeter using radiation resistant, short radiation length materials such as CsI or BGO.

A scintillator hodoscope will cover most of the central region ($-3.2 < \eta < +3.2$). The hodoscope and the spectrometer drift chambers in front of the magnet provide multiplicity and trigger information. The present E735 multiplicity hodoscope will be modified in order to accommodate the new detector system.

A trigger based upon the E735 design will be used for P787. At present, two sets of 15 scintillator counters are located $\pm$200 cm from the interaction region. The trigger requires one or more hits in each set and that they must be in coincidence with the beam crossing. High multiplicity events can be selected preferentially by using the multiplicity hodoscope and a trigger processor especially designed for the experiment.

To enrich the electron and photon sample, an electron trigger system will be based on the pulse height from the electromagnetic calorimeter. The detailed description of the electron trigger is discussed in section 3.2.

1.5 Time Table for Staging P787

For the purpose of presenting the overall schedule for the experiment we shall assume that Fixed Target and Collider runs will alternate starting at the begining of December each year and lasting for about 9 month each. Collider runs will, therefore, be assumed to take place starting 12/01/90 and 12/01/92.

Due to the budgetary and manpower restrictions of our collaboration we have decided to set the following order of priorities to evolve from the present E735 apparatus to the full P787 experiment:

During the remainder of 1989:

1. Approval of P787 from Fermilab's Program Advisory Committee.
2. Complete processing of the E735 data to the DST stage. Physics analysis will continue concurrently with preparation for P787.
3. Studies finalizing the basic parameters of the P787 detector.
4. Detailed design of the spectrometer room electromagnetic calorimeter in order to place the first commercial purchase orders at the begining of the new budgetary year. We estimate of the order of 12 month for delivery.
5. Design and procurement of parts for the second magnet on the tunnel side of the experiment.

1990:

1. Development of prototypes for all the new components with the view to partial installation at C0 for testing during the next collider run starting 12/01/90. This will include one set of pre- and post- magnet drift chambers, one cell of the RICH counter, Be beam pipe, parts of the TOF hodoscope and NaI detector.
2. Construction of the second magnet.
3. Detailed design of the tunnel side electromagnetic calorimeter in order to place the first commercial purchase orders at the begining of the new budgetary year. We estimate of the order of 12 months for delivery.
4. Detailed design of remaining components and trigger electronics.
5. Request for PREP electronics.
6. Detailed design of support structures.
7. Start construction of components based upon the final design.
8. Partial delivery of PREP electronics.

9. Partial installation, including second magnet, at C0.

1991:

1. Continue construction of detector components.
2. *Data taking with partially installed experiment at C0.*

1992:

1. Full availability of additional PREP electronics.
2. Completion of all detector components.
3. *Installation of the full experimental apparatus following the Fixed Target run.*

2 Proposed Measurement and Analysis

2.1 Dilepton Production

2.1.1 Introduction

Analyses of prompt e^+e^- pair production [Mikano *et al.*, 1980] indicates that the dominant production mechanism varies with e^+e^- invariant mass, M. For M>3 GeV/c^2, the production is well explained by the Drell-Yan mechanism [Kajante *et al.*, 1986]. Below 3 GeV/c^2, however, there has been observed an excess above the Drell-Yan prediction. Bjorken and Weisberg [Bjorken *et al.*, 1976] used a model in which partons produced in the collision process contributed to the low-mass dileption production. Shuryak [Shuryak, 1978] later suggested these partons may be partons in a QGP. In the very low dileption mass range, M<600MeV, Domokos and Goldman [Domokos *et al.*, 1981] have also predicted that QGP produced dileptons would dominate. However, McLerran [McLerran *et al.*, 1985] has speculated that these low mass dilepton pairs may be produced from a hadron gas phase.

The P787 experiment will be sensitive to e^+e^- pair production with masses that span the range from about 100 MeV/c^2 to 3 GeV/c^2. We will therefore cover the production range appropriate to a QGP source.

2.1.2 Expected Rates

To make the proposed measurement, we must be able to cleanly identify electron and positrons and be able to reject prompt electron-positron pairs from Dalitz decay and photon pair production. In this section, we present a Monte Carlo study of electron identification and estimate the number of electrons and positrons and the e^+e^- pairs detected for a given luminosity.

Our calculation is based on an integrated luminosity of $0.1pb^{-1}$. The cross-section for lepton pair production from pp collision and p-nucleus collisions has been measured in various experiments. The

production cross section can be approximated by the expression:

$$\frac{(\frac{d\sigma}{dMdy})_{e^+e^-}}{(\frac{d\sigma}{dy})_{\pi^0}} = \frac{2.0 \times 10^{-5}}{M^2}\ GeV^{-1} \qquad (M\ in\ GeV)$$

This formula was used in our Monte Carlo detector simulation. We assumed that the rapidity distribution of the pairs is flat within our detector geometry, and that the p_t distribution is similar to the hadron p_t spectrum measured in E735.

In Figure 2.1.1, the expected number of single leptons $(e^+ + e^-)$ is shown as a function of p_t. The total number of leptons will be of the order of 250,000 to 500,000. We should be able to explore the p_t spectrum as a function of charged multiplicity in detail. In figure 2.1.3, the spectrometer arm acceptance is plotted as a function of p_t for different pair mass, M. The vertical axis is the probability that the pair is identified in the spectrometer when the pair is produced within the pseudo rapidity $-4.0 \leq \eta \leq 4.0$. The typical values are $\simeq 2 \times 10^{-3}$

The simulated dilepton mass spectrum is shown in Figure 2.1.2. We also estimate the number of expected vector mesons (ρ's, ω's, ϕ's and J/ψ's). The number of pairs for single a arm is very small. With the double arm configuration, the number of pairs would be large enough to study vector meson production as a function of multiplicity. The expected number of ρ's, ω's, and ϕ's is about 3000 to 5000 each. The expected number of J/ψ's is about 300. For J/ψ calculation, we use the same p_t slope and cross section measured at UA1 [Bains, 1988].

2.1.3 Electron Identification

The electrons are identified by four methods: (1) Time of flight; (2) comparison of momentum measured in the spectrometer arm to energy measured in the calorimeter; (3) longitudinal shower development in the calorimeter; and (4) Cherenkov counters.

In order to study the pion rejection, we have used EGS3 and Geihsha7 for the electromagnetic shower development and hadron shower development respectively. Figure 2.1.4 and 2.1.5 show the result of the Monte Carlo study for pions and kaons respectively. In

the figure, the rejection factor from different identification method is shown separately. The calorimeter as a whole provides about 1 to 5 $\times 10^{-3}$ rejection (method 2 above). Using longitudinal shower development information improves the rejection by about a factor of 5. The cuts we used to reject hadron are a function of momentum and about 85% of electrons pass the cuts. The measurement of the longitudinal shower development comes from the absorber which is divided into two sections longitudinally. (5 and 15 radiation lengths). The scatter plot of the energy deposited in the first section versus the second section is shown in Figure 2.1.6 for K^- and electrons. It clearly shows that the electron exhibit a very different shower shape compared to the K^-. TOF will help us to reject low energy pions, kaons and protons. Including the TOF, the hadron rejection is shown in the same figures. With TOF, the rejection is about 3 x 10^{-4}, which is not quite sufficient. To improve the rejection further, a Cherenkov counter will be used. Although a detailed study is not yet completed, we expect at least an additional factor of 20 to 50 rejection. With the Cherenkov counter, the overall probability of misidentifying pions would be much better than 1×10^{-5}.

2.1.4 Background Rejection

The major background to our signal is from the Dalitz decay of pions and η's and the pair conversion of photons from the beam pipe and from the chamber windows. The radiation length of the Be pipe and the chamber window of the pre-magnet drift chambers is less than 0.5%X_o.

We have made a Monte Carlo study of this background contribution. We generated 2γ and γe^+e^- decays of π^o's and η's. Some of the gammas are converted to e^+e^- pairs in the beam pipe and the first chamber's windows. Figure 2.1.1 shows the detected e^+ and e^- in the spectrometer arm. Here we assumed that the probability of the background pair rejection is 10^{-2}. The rejection method will be explained very shortly. In the same plot, the expected signal is plotted as described earlier. As can be seen, the background is at least an order of magnitude less than the signal.

The background e^+e^- pairs are rejected by three methods. All

the available information from the drift chamber just outside the beam pipe must be used.

First, for every identified electron or positron track from the spectrometer arm, the invariant mass will be calculated with other tracks, (other than identified hadrons) not only tracks in the spectrometer arm but also in the first drift chambers. We point out that the solid angle of the drift chamber is much larger than the solid angle of the spectrometer arm. We reject the e^+e^- pair if the invariant mass is less than 100 MeV/c^2.

The second method used to reject backgrounds is to look at the charge on each wire along the the track of interest. If the sum of the charges is larger than expected from a single track, we reject the track. This rejects two close tracks from a gamma conversion. To obtain the charge on the wires we plan to use the flash ADC's, which are presently being used in the central tracking chamber, to read out the drift chambers.

The third background rejection method is to look at the unused drift chamber hits near the tracks. This is useful to reject very asymmetric gamma conversions or Dalitz pairs, in which a second electron is of very low energy and cannot be reconstructed. Using the three methods, we believe that we can reject the background 99% of the time.

2.2 Photon Production

2.2.1 Introduction

We propose to measure the central production of photons with transverse momentum between a few 10's of MeV and 10 GeV. This measurement will overlap with the low energy range of photon detection at CDF and D0 and provide new information about the photon production spectrum below a few GeV.

In general, these data will establish constraints on high energy hadroproduction models, being particularly sensitive to central π° production characteristics. Figure 2.2.1 shows the photon energy spectrum near 90° from $\sqrt{s} = 1.8$ TeV $\bar{p}p$ collisions as predicted by an ISAJET simulation. Our photon detector would cover a rapidity

range $-0.23 < y < +0.41$ for which 99.5% of the photons have energy less than 10 GeV.

More specifically, with regard to the main thrust of this experiment, we will be able to measure the shape of the low energy photon spectrum and the rate of photon production relative to charged hadrons. An enhancement of low energy photon production could occur if a QGP was formed. As with other QGP signatures we will measure this low energy photon signal as a function of the energy density of the $\bar{p}p$ collision as measured by $dn/d\eta$. For events containing a QGP, an excess of soft photons could be produced by quark bremsstrahlung and $g + q \rightarrow \gamma + q$ Compton scattering within the plasma. On the other hand, low energy photon production arising from neutral hadron decay (π^0's ,η's ,...) will be proportional to charged hadron production. In addition the shape of photon production spectrum below 100 MeV is dominated by the hadron decay properties and relatively insensitive to production characteristics of the parent hadrons. See Section 2.2.2 below for more details.

Finally we mention that unexplained low energy photon signals have been observed in hadron collisions at lower energies [Chliapnikov *et al.*, 1984 and Goerlach *et al.*, 1988]. Standard hadronic production models, including hadronic bremsstrahlung, have not been able to explain the observed photon excess [Anderson *et al.*, 1988). We will be able to search for this soft photon production in $\bar{p}p$ collisions at $\sqrt{s} = 1.8$ TeV and, if an excess is observed, correlate it with other expected QGP signatures.

Section 3.1.5 describes the photon detector and reviews tests that have been made at the C0 collision region. Section 2.2.2 discusses the analysis approach we will use to search for an anamolous low energy photon signal.

2.2.2 Analysis of the photon data from P787 and preliminary results from E735

There is little known about the photon production characteristics from 1.8 TeV $\bar{p}p$ collisions. Our data will be used for two purposes. First, to study the photon spectrum from the electromagnetic decays of hadrons and second, to search for excess low energy photon signals.

The most basic analysis is to simply compare the measured photon p_t spectrum to that predicted by various QCD-based hadron production models (ISAJET, LUND, *etc.*). We are in the process of studying the ability of the photon spectrum below 10 GeV to distinguish between various models. A first look at the photon spectrum from hadrons generated by ISAJET is in general agreement with a preliminary measurement we have made using the E735 NaI prototype (see Figure 2.2.3). We will be able to study photon production with lower backgrounds, much higher statistics, better energy resolution and over a larger energy range with the P787 NaI detector.

To search for an excess low energy photon signal, we will estimate the contribution of low energy photons from hadron decay by fitting the photon spectrum above about 200 MeV, and extrapolating to low energies. This extrapolation is highly constrained by the hadron decay properties. This technique has been used in several previous experiments to search for low energy photon signals and has been capable of extracting the soft photons produced by hadronic bremstrahlung [Goshaw *et al.*, 1979 and Chliapnikov *et al.*, 1984]. The sensitivity of the P787 experiment to excess photons in the energy range from a few 10's of MeV to a few 100 MeV is currently under study using Monte Carlo simulations and the data being acquired from the E735 prototype detector.

2.3 Hadron Production

We propose to investigate three different kinematic domains of hadron production as a function of charged particle multiplicity. They are: (1) Production of strange particles (K, Λ, Ξ, and Ω^-) at intermediate p_t, (2) Low p_t (60 MeV/c$<$ p_t $<$200MeV/c) pion production, and (3) Measurement of the yields of particles ($\pi^\pm$, $K^\pm$, $p^\pm$) and low mass vector mesons with two body decays (ρ, ω, ϕ) up to $p_t \approx$3GeV/c.

These measurements may reveal information on a new form of matter and are of general interest for models of particle production.

2.3.1 Study of Λ production and search for Ξ and Ω production in the central region

In an earlier paper we discussed [Banerjee, *et al.*,1988] characteristics of Λ production at $\sqrt{s}$=1.8 TeV. Since our spectrometer arm can identify charged hadrons, it is also interesting to look for the $\Xi \rightarrow \Lambda + \pi$ and $\Omega \rightarrow$K+Λ final states with our improved tracking and acceptance. Monte Carlo acceptance calculations for Ξ and Ω acceptance are underway.

Making reasonable assumptions on production, equilibriation and decay of QGP a striking prediction for the Λ/p ratio was obtained [Koch *et al.*, 1986]. The detailed arguments are given in Appendix 1 and the result for the Λ/p ratio as a function of temperature is given in Figure 2.3.1. It is thus obvious that we must measure the Λ/p ratio as a function of n_c. It is crucial to minimize the background and its variation with n_c under the Λ peak. In order to achieve that, we will build a high resolution, stereo drift chamber with multi-hit capability for accurate Λ decay vertex determination (see section 3.1.1). In addition with the help of the drift chamber on the tunnel side, the primary vertex location will be accurately determined. Particle identification will be improved by the double signature of a Cherenkov counter and TOF. Finally, we will make a three constraint fit to all Λ candidates. Thus we will obtain a clear signal for the Λ/p ratio variation as a function of charged particle multiplicity.

2.3.2 Low p_t hadron physics

Reports of sharp peaks of $d\sigma/dp_t^2$ at p_t <100MeV/c have been reported [Willis, 1988] Tying together the above results with low p_t lepton and photon enhancement, Van Hove [Van Hove, 1988] suggested that they are all the manifestations of a cold QCD plasma. Since we can measure all three signatures in one experiment we can have conclusive experimental evidence for the existance or nonexistance of such a system. These events may also be related to enhancements in rapidity density $dn/d\eta$ as discussed by Pesanski [Pesanski, 1988].

The measurement will be made with the tunnel side magnetic-TOF spectrometer (see Figure 1.4.1) with the magnetic field in the

magnet lowered to ~1kG. We would make this measurement during the 1991 collider period.

2.3.3 p_t of π, K, p, ρ, K*, and ϕ production up to p_t = 3GeV/c

Using the magnetic-TOF spectrometer in E735, we were able to obtain mass indentified p_t distributions for π, K, and p up to 1.5 GeV/c. With the help of a Cherenkov counter the range of mass identification can be extended to 3 GeV/c. Since the single arm acceptance for ρ, K* and ϕ increases with p_t, we will be able to measure the n_c dependance of ϕ and, with lesser acceptance, that of ρ and K*.

3 The P787 Detector

The P787 experimental apparatus is shown in Figures 1.4.1a and 1.4.1b. A detailed description of the individual components is given in the following sections. With the exception of the proposed RICH counter, our collaboration has succesfully built similar devices for E735. Although the general description of each component is accurate, the detail will change as more design studies are made. For example, the exact number of sense wires assign to each chamber view and some of the readout details may change. The individual components are also identified by the abbreviations shown in the apparatus figures.

3.1 The Spectrometer Components

3.1.1 Pre-magnet Drift Chambers (PRDC)

Two of these chambers are required, one for each spectrometer arm. We have borrowed extensively from our experience with E735 Central Tracking Chamber (CTC) by adopting a similar design for the drift cells, as shown in Figure 3.1.1. Each drift cell will consist of 10 sense wires and 22 field shaping wires. Cells are separated by an additional 11 high voltage wires. A total of 46 cells divided into 3 views x, u, v will form one chamber. The overall geometry of the x cells are shown in Figure 3.1.2 and in Figure 3.1.3 for the u and v cells. The dimensions of a full chamber, including the cell locations is shown in Figure 3.1.4.

The two chambers will have a total of 920 sense wires. The same gas as for the CTC will be utilized (Argon, 4% methane, 1% CO_2), with a drift velocity of the order of 30 microns/ns. Readout of the pre-magnet chamber will utilize the 100 MHz Fast ADC system in use with E735 CTC. Only one end of each sense wire will be read, the FADC system providing multi-hit capability. As for the CTC we would expect a position resolution of less than 250 microns and a two track separation of the order of 3mm.

3.1.2 Post-magnet Drift Chambers (PSDC)

Two post-magnet drift chambers are required, one for each spectrometer. Their design follows from our experience with the straw drift chambers presently in use in E735. These are required because of the large angular range of the traversing particles. To obtain a more compact geometry we have chosen 2 cm diameter straws. The straw arrangement is shown in Figure 3.1.5. As per E735 they will operate with Argon-10% Methane gas. We expect a resolution of the order of 200 microns. The small diameter straws allows us to increase our multi-track capability and the efficiency for detecting tracks correlated in space. Each post-magnet chamber consists of two sections. One with vertical wires (10 rows of tubes) and the other with slanted wires (6 rows of tubes). A total of 960 sense wires per chamber will be instrumented with the same type of single hit TDC electronics presently used for the E735 spectrometer straw chambers.

3.1.3 Threshold Cherenkov Counter (TC)

A final decision on the necessity of the Threshold Cherenkov counters to be installed within the two magnet gaps awaits a more detailed Monte Carlo study. The purpose is to provide e/π separation at momenta below 1.0 GeV/c. Freon 12 at atmospheric pressure is one candidate for the radiative media. Each counter will contains 6 or more cells constructed from thin aluminized mylar reflectors in order to keep to expected particle occupancy per cell to less than one. Cherenkov light will be reflected backwards and towards the top of the magnet by a series of thin plane aluminized mirror installed on the downstream end of the detector. Ray-tracing studies are presently under way to study the photon efficiency of such a geometry. In addition, two possible detection schemes are under evaluation:

- Winston cones and light guides transmiting the light to phototubes on top of the magnets;
- a compact TEA chamber separated from the radiator by a quartz window installed just below the magnet coil. The design

of this chamber will be identical to the one to be built for the RICH counter below. A larger number of cells could then be considered.

3.1.4 RICH Cherenkov Counter (RICH)

The RICH counter under development follows closely a counter recently discussed in the literature [Arnold *et al.*, 1988]. The proposed counter is designed for particle identification below 3 GeV/c and has the advantage of a very short length, 20 cm, as sufficient number of photons are emitted from the 5 mm thick NaF radiator. The length of the counter is determined by the requirement that the radius of the rings becomes measurable in the photosensitive TEA or TMAE drift chamber. Due to the proximity of the electromagnetic calorimeter a TEA chamber appears more convenient in order to avoid operating at higher than room temperatures.

As shown in Figure 3.1.6, the counter will be built in 4 modules 20 cm wide and approximately 50 cm high at the NaF entrance radiator and 65 cm high at the exit CaF window. Within each module the NaF radiator will be constructed of 4 x (5" x 8") and the CaF drift chamber window of 4 x (6.5" x 8") crystals. The type of readout and optimum segmentation is under study. Two possibilities exist:

- A MWPC with the order of 5 mm wire spacing for charge amplification in conjunction with 1 cm x 1 cm pads for position readout. A total of 5200 electronic channels would then be required.
- A modification of the post-magnet straw drift chambers with open slots for the entrance of the photoelectrons. Charge division, in conjuction with the FADC pre-magnet chamber system, could be used for measuring the position along the wire. Eighty channels of FADC would then be necessary.

3.1.5 Spectrometer Room Electromagnetic Calorimeter (NAI)

The layout of the electromagnetic detector is shown in figure 3.1.7. It consists of a thin (0.1 radiation length) copper converter followed by y and z drift planes, a time of flight (TOF) scintillator hodoscope and a calorimeter composed of an array of NaI blocks.

The copper radiator will convert 5 to 8% of the incident photons, producing e^+e^- pairs which will traverse the drift planes. The drift planes are made up of 1.5 cm diameter straw tubes with four z measuring planes (vertical tubes) and four y measuring planes (horizontal tubes). Our experience with 2.5 cm drift tubes in the E735 spectrometer shows that we should be able to determine spatial position of charged tracks in the drift planes to an accuracy of 200 microns. There will be four z planes and four y planes.

The trajectory of a converting photon will be determined by measuring the positions of the produced e^+e^- in the y and z planes and reconstructing from these points the slopes for the gamma. This trajectory is then projected back to the beam line. Simulation studies with the shower program EGS indicate that we can use this method to predict the point of origin of the converted gammas at the beam line to within 10 cm (sigma) for photon energies as low as 50 MeV. The beam interaction vertex position will be known to a few mm from the reconstruction of produced charged tracks in the drift planes nearest the beam line.

The TOF hodoscope, situated between the drift planes and the calorimeter, will be used to determine whether a photon which converts in the copper radiator is synchronous with the beam interaction. Particles from the $\bar{p}p$ interaction which subsequently scatter in the spectrometer magnet yoke can result in neutrons, K^o's and photons which will enter the electromagnetic detector. They will arrive at the detector later in time than photons traveling directly from the beam interaction and can be discriminated against. The TOF hodoscopes employed in E735 provide timing resolution of 250 picosec FWHM. We should be able to reject photons that are out of time by 1 nanosec (4 sigma).

The NaI calorimeter consists of a 10 x 15 array of 10 cm square blocks; the front face is 125 cm from the beam line. The depth of the calorimeter will be 20 radiation lengths so as to be a total absorber for incident photons up to 10 GeV energy (punch through for 10 GeV photons $< 1.5\%$). The calorimeter will include a 2 radiation length NaI active converter in front of it which will provide information used to distinguish between charged hadrons and electrons incident on the calorimeter.

The signal from each NaI block will be split into two. One will

have high gain (full ADC count for 400 MeV energy deposition) and the other will have low gain (full ADC count for 10 GeV energy deposition). This will provide good energy resolution over a large dynamic range.

3.1.6 Tunnel Side E.M. Calorimeter (EM2)

The tunnel side electromagnetic calorimeter will be similar to the one in the spectrometer room except it will not have a front-end with drift chambers and TOF. However this detector will be subject to considerable radiation exposure over the entire length of the experiment. The actual choice of material (CsI, BGO, *etc.*) is presently under study.

3.1.7 Multiplicity Hodoscope (H)

The scintillator counter hodoscope will serve the same functions for P787 as it did for E735. Online, it will provide a fast indication of the event multiplicity so the trigger system can scale down the number of low multiplicity events written to tape in favor of the more interesting high multiplicity events. Offline, the hodoscope will serve in combination with the inner drift chambers to determine the charged multiplicity in the central region.

As much of the previous system will be used as possible. Although, the counters will have received as much as 15Krad by the end of the 1988-89 run, they still should be usable up to 50Krad dose [Lindsey *et al.*, 1987]. Any counters which show deterioration will be repaired or replaced.

In Figure 1.4.1a are shown the P787 endcap counter arrays' position. The two inner rings (of 24 counters each) from E735 will be brought closer to the intersection region in order to avoid particles showering from the edges of the magnet iron. Figure 1.4.1b shows the new position of the "barrel" counters (which previously surrounded the central tracking chamber). They will now cover the region above and below the beampipe.

This arrangement reduces the segmentation from 240 counters to about 120. Used in combination with the inner drift chambers, this should be sufficient for the trigger and for offline multiplicity deter-

mination. If further study shows that more segmentation is required, other counters can be added using either the previous counters or making new ones.

3.1.8 TOF counters

The TOF arrays used for triggering and interaction time measurement during E735 would need to be reconstructed to allow for the new geometry around the beam pipe. The TOF1 and TOF2 arrays from E735 would be dismantled and reconstructed to build the TOF counters at the entrance of the two electromagnetic calorimeters.

3.1.9 Magnets

The present E735 spectrometer magnet will be used with only minor mechanical modifications and a change in position in the C0 pit floor.

The second magnet design will follow closely the design of the first. A smaller magnet is required. We expect that the same mechanical drawings and tooling for the first magnet could be utilized with only some dimensional changes.

3.2 Trigger

3.2.1 Interaction Trigger

The lowest level trigger on the experiment is that of the detection that an interaction has taken place at the time of the crossing. As for the E735 detector this trigger will be provided by two sets of TOF counters located approximately 2.1 meters upstream and downstream of the C0 interaction point. This distance allows for a clean separation between beam-beam events and those originating upstream or downstream of the interaction region (Beam-Gas events). In addition, interactions due to beam present in neighboring bunches can also be rejected by timing. The TOF/TRIGGER counter hodoscopes "P" and "PBAR" utilized for E735, with a time resolution of 250ps FWHM are perfectly adequate for P787 as well. Two set of Beam Halo Veto hodoscopes from E735, located approximately 4.5 m on either side of the interaction point provide

a more clear time separation for Beam-Gas events associated with near bunches. During experiment E735 an "Interaction Trigger" rate of the order of 400 Hz was measured for CDF Luminosities of the order of $1x10^{30}$.

3.2.2 Hadron Production Trigger

A Trigger Processor (TP), providing trigger scaling based upon the hodoscope hit multiplicity will be utilized to reduce the 400 Hz first level trigger rate. This TP will be an upgraded version of the one that has worked well in E735.

3.2.3 Single and Dilepton Trigger

For a clean lepton signal, that is to optimize the amount of lepton events recorded on tape, a rejection of the order of $1x10^{-2}$ is necessary with respect to triggers originating from pions.

3.3 Data Acquisition System

The data acquisition system for FNAL P787 will utilize a VAX-6310 computer and an existing VME system, developed for FNAL E735, extended into a second crate. A possible configuration is shown in Fig. 3.2.1. The data from FADC's, CAMAC and FASTBUS are read out in parallel by frontend VME microcomputers, preprocessed and stored in their local memory buffers. The DMA device, under control of a supervisory processor, copies segments of an event from FEPs into contiguous, multievent buffers in memory ("stand alone" on VME bus), formatting the event appropriately for magnetic tape interface.

The mode of transfer (maximum or limited-rate, with or without-hold) is decided by the Supervisor on an event by event basis in order to minimize a bus and dual-port memory arbitration overhead. The Supervisor maintains an Output Queue, it administers DMA transfers to magnetic tape in an asynchronous manner. Every n^{th} event (n=1,2...) is transferred to the VAX for monitoring hardware performance, on-line track reconstruction, full event display, *etc.* The VAX may also request a specific type of event. There are two

6250 Bpi, 125 Ips tape drives in the system. A third tape drive on VAX-6310 is used to read (analyse) events taken earlier.

The existing VME system is based on Microsys' CPU07 microcomputer boards supporting standard (24 bit) addressing. Assuming, that no extended (32 bit) addressing CPU boards are introduced into the existing VME system (which potentially may create hardware, as well as software incompatibility problems), the proposed configuration does not give much room for further expansion: the 16 MByte address space is almost fully utilized.

This problem can be circumvented by connecting two crates in DR11W-DR11W type manner for which we have the necessary hardware. In that configuration two crates would operate as two independent 16 MByte computers, communicating with each other with a protocol similar to that of the CD driver. Additional advantage of that kind of solution would be a 50% decrease of bus traffic and consequently a substantial increase in system performance. In this "loosely coupled" system the front-end processors and interfaces to experimental apparatus would be kept all in one crate, the data buffers, magnetic tape and host interfaces in another crate. Additional CPUs (ACP-RISC type) could be easily incorporated into the system within the second crate for on-line or off-line data analysis.

The data acquisition programs are written mostly in RTF68K Fortran, some real-time routines in AS68K assembler. Both are available from CERN. They run as native compilers on CPU07 computer under CPM-68 operating system. This makes the system virtually independent from a host computer. This has proven to be very convenient, especially on a test stage of program development and hardware testing. The compilers are able to generate code for 68000, 68010 and 68020 processors. Data acquisition software runs without support of any operating system after it is downloaded from hard disk by one of the VME computers. The RTF68K cross-compiler under VMS exists. New version of RTF68K, greatly improved and supporting FASTBUS and DR11W interfaces is now available from CERN.

3.4 Accelerator Issues

In order to increase the lower momentum limit of particles towards the two spectrometer arms and to minimize the number of photon conversions, we would like to request the replacement of the existing aluminum beam pipe with a beryllium one. Assuming that the Tevatron proton abort line will not be utilized during collider running, the new beam pipe should be centered on the Tevatron beam and of dimensions comparable to the beryllium pipe presently installed at B0 (CDF).

A Theoretical Arguments for Strangeness Enhancement in Deconfined Hadronic Matter

In order to compute quantitive predictions for strangeness production in Centrally Produced Hadronic Matter (CPHM) one has to make general assumptions as well as detailed parametrizations. In this section we give a brief description of the important steps and results based on the paper of Koch *et al.*[Koch *et al.*, 1986].

A.1 Production Mechanism

There are two commonly accepted consequences of the standard model:

1. Both the gluon (g) density and small x collision cross section increases rapidly with $\sqrt{s}$.

2. There is a large cross section for strange quark (s) production via the elementary process:

$$g + g \rightarrow s + \bar{s}$$

   Based on considerable experimental evidence, it is further assumed that if the size of CPHM is greater than r$\geq$ 2 fm and the number of produced particles is sufficiently large, then:

3. The concept of temperature (T) (hadron thermodynamics) is meaningful. The parameter which controls decisively the predictions of strange quark abundance and yet least amenable to direct measurement is the strange quark mass (m_s). Fitting the stable particle mass spectrum one can deduce:

4. $m_s \simeq$170 MeV. Since the Deconfined Hadronic Matter or Quark Gluon Plasma (QGP) in CPHM has T$\geq$170 MeV, a profuse strange particle production is expected. We have to emphasize that the basic pair production subprocess $g + g \rightarrow s + \bar{s}$ is in principle the same for both phases of hadronic matter: hadron gas and QGP. However in the case of separated hadrons reaction 1 can only take place during the actual collision process,

which means that strange quark production has a strict constraint in space, time and phase space. On the otherhand, if QGP is formed with a reasonable space-time extension at high T with a very large phase space, a large enhancement of strange quark production is expected (r>2 fm, t$\simeq 2 \times 10^{-23}$ sec, T$\geq$ 170 MeV).

A.2 Production Rate and Chemical Equilibrium

In order to predict the strangeness abundance, one has to calculate the strangeness production rate per unit volume and the time constant for chemical equilibrium. The equilibrium time (t) must be less or of the order of QGP lifetime: t$< 2 \times 10^{-23}$ sec. The calculation assumes (1) the subprocesses

$$g + g \rightarrow s + \bar{s}$$

$$q + \bar{q} \rightarrow s + \bar{s}$$

and (2) Bose-Einstein and Fermi-Dirac distributions for the momentum distribution of the quarks and gluons. The results show that t depends on the strength of the coupling constant, the mass of the strange quark and the temperature. When $m_s \leq$ T and T$\simeq$ 200 MeV, one finds that t is comparable or less than the QGP lifetime (2×10^{-23} sec). In general, the higher t and the coupling strength, and lower m_s the more enhanced the strange quark production will become.

A.3 Conversion from the QGP to Hadronic Phase

The entropy of QGP is proportional to the number of quarks and gluons from which it is made. Since quark pairs form mesons and gluons in $g \rightarrow q + \bar{q}$ transitions also form mesons, after QGP $\rightarrow$ hadrons phase transition entropy would decrease. To be consistent with the Second Law of Thermodynamics, one has to assume that there must be a third elementary processes in hadronization. Since a $q\bar{q}$ pair is in a color singlet state in one out of nine cases, in the other eight cases the $q\bar{q}$ pair first must radiate a gluon in order to be able to recombine into a meson.

1. The three elementary processes which dominate hadronization are

$$q + \bar{q} \rightarrow \pi$$

$$q + \bar{q} \rightarrow \pi + g$$

$$g \rightarrow q + \bar{q}$$

The breakup process is assumed to proceed in a single direction: quarks coalesce to form hadrons. The inverse reactions are neglected. The above assumptions are combined with the Combinatorical Breakup Model, which assumes:

2. Quarks are distributed among final state hadrons by two constant probabilities: one for meson and one for baryon production. For example:

$$N_{nucleon} = \frac{\beta}{3!} \times N_q^3$$

$$N_Y = \frac{\beta}{2!} \times N_q^2 \times N_s$$

$$N_p = \alpha \times N_q \times N_{\bar{q}}$$

3. Combining thermal and chemical equilibrium with gluon radiation corrections $N_q, N_{\bar{q}}$ and N_s can be calculated and the prediction for $\rho_{\bar{Y}}/\rho_N$ ratio can be calculated (See Fig. 2.3.1). There is an order of magnitude enhancement for this ratio in QGP compared to hadron gas.

B Lepton Pair Production from the Centrally Produced Hadronic Matter

From lepton number conservation, leptons and antileptons are produced in pairs. Let Q_μ denote the sum of dilepton four momenta, then the mass of the dilepton system (m_d) is $m_d = \sqrt{Q_\mu Q_\mu}$. For the purpose of experimental study, the dilepton mass spectrum has been divided [Kajante *et al.*, 1986] into three regions:

$m_d > 3$ GeV	(Drell-Yan region)
1 GeV$< m_d < 3$ GeV	(QGP region)
140 MeV $< m_d <$ 600 MeV	(Hadronized gas region)

B.1 Drell-Yan Model for Lepton Pair Production.

According to this model the origin of the dileptons is electromagnetic: Constituents of the colliding hadrons annihilate into virtual (timelike) photons which converts into dilepton pairs. For massive lepton pairs ($m_d > 3$ GeV) the theoretical results are compatible with experiments. However, for small dilepton masses and small transverse momenta, the Drell-Yan formula needs to be corrected.

B.2 Modification of the Drell-Yan Model

Bjorken and Weisberg [Bjorken *et al.*, 1976] considered the contribution of parton's which were produced in the collision process. Thus the parton density function in inelastic hadron-hadron collision can be at least five times larger then the density function extracted from hadron structure function νW_2, which was measured by lepton probes. This modification brings the theoretical prediction in agreement with experiments. This implies that the excess lepton yield is made up of low-mass ($m_d < 3$ GeV) dileptons produced at high total transverse momentum. Viewing the time development of the QGP it was concluded by McLerran and Toimela [McLerran *et al.*, 1985] that massive, high p_t dileptons are emitted in the early stages of the collision. Thus there is a relationship between the age of the plasma and the dilepton mass. Approximately one has t $\propto$ m_d^{-1} [Adachi *et al.*, 1981].

B.3 The low mass ($m_d <$ 600 MeV) region

For this mass range there are contradictory predictions. While Domokos and Goldman predict [Domokos *et al.*, 1981] that QGP produced dilepton pairs dominate this mass range, McLerran predicts that these pairs are emitted from the matter after it has cooled down [Kajante *et al.*, 1986] below the hadron gas phase.

References

[Adachi *et al.*, 1981]
Adachi *et al.*, Phys. Rev. **D23**(1981) 1106;
Shuryak, Phys. Reports **61C**(1980) 71.

[Akesson *et al.*, 1985]
Akesson *et al.*, Phys. Lett. **152B**(1985) 411.

[Alexopoulous *et al.*, 1988]
Alexopoulous *et al.*, Phys. Rev. Lett. **60**(1988) 1622.

[Anderson *et al.*, 1988]
Anderson *et al.*, LUND pre-print LUTP 88-1.

[Arnison *et al.*, 1982]
Arnison *et al.*, Phys. Rev. Lett. **118B**(1982) 167.

[Arnold *et al.*, 1988]
Arnold *et al.*, NIM **A273**(1988) 466.

[Bains, 1988]
Bains, Ph.D. Thesis, University of Birmingham (1988) 99.

[Banerjee *et al.*, 1988]
Banerjee *et al.*, Phys. Rev. Lett. **62**(1988) 12.

[Bjorken *et al.*, 1976]
Bjorken and Weisberg, Phys. Rev. **D13**(1976) 1405

[Chliapnikov *et al.*, 1984]
Chliapnikov *et al.*, Phys. Lett. **B141**(1984) 276.

[Domokos *et al.*, 1981]
Domokos and Goldman, Phys. Rev. **D23**(1981) 203.

[Dowell *et al.*, 1988]

Dowell *et al.*, (1988) CERN-EP188-137.

[Fincke-Keeler, 1989]
Fincke-Keeler, Ph.D. thesis, University of Victoria (1989).

[Goerlach 1988]
Goerlach, Proc. 24th Int. Conf. on High Energy Physics, Munich (1988).

[Goshaw *et al.*, 1979]
Goshaw *et al.*, Phys. Rev. Lett. **43**(1979) 1065.

[Hagedorn *et al.*, 1980]
Hagedorn and Rafelski, Phys. Lett. **97B**(1980) 136;
McLerran and Svetitsky, Phys. Lett. **98B**(1981) 195
Kuti, Polonyi and Szlachanyi, Phys. Lett. **98B**(1981)199;
Van Hove, Phys. Lett. **118B**(1982) 138;
Bjorken, Fermilab Pub. 82/44-PHY;
Kogut *et al.*, Phys. Rev. Lett. **51**(1983) 869;
Engels *et al.*, Nucl. Phys. **B205**(1982) 545.

[Kajante *et al.*, 1986]
Kajante *et al.*, Phys. Rev. **D34**(1986) 2746;
Kajante and McLerran, Ann. Rev. Nucl. Part. Sci. **37**(1987) 293.

[Koch *et al.*, 1986]
Koch *et al.*, Phys. Reports **142**(1986) 162;
Barz *et al.*, Nucl. Phys. **A484**(1988) 661.

[Lindsey *et al.*, 1987]
Lindsey *et al.*, NIM **A254**(1987) 212.

[McLerran *et al.*, 1985]
McLerran and Toimela, Phys. Rev. **D32**(1985) 1109.

[Mikano *et al.*, 1980]
Mikano *et al.*, Phys. Rev. Lett. **D22**(1980) 2107;

Blockus *et al.*, Nucl. Phys. **B201**(1982) 205;
Adams *et al.*, Phys. Rev. **D27**(1971) 1983;
Anderson *et al.*, Phys. Rev. Lett. **37**(1976) 799.

[Müller 1985]
Müller, *The Physics of the Quark Gluon Plasma*, Springer-Verlag, (1985)46;
Kajante and McLerran, Ann. Rev. Nucl. Part. Sci. **37**(1987).

[Pesanski, 1988]

[Rafelski *et al.*, 1987]
Rafelski and Danos, Phys. Lett. **192**(1987) 432.

[Shuryak, 1978]
Shuryak, Phys. Lett. **78B**(1978) 150;

[Shuryak, 1981]

[Shuryak, 1988]
Shuryak, *The QCD Vacuum, Hadrons and the Superdense Matter*, World Scientific (1988);

[Van Hove, 1986]

[Van Hove, 1988]
Van Hove, CERN-TH, 5236/88.

[Willis 1988]
Willis, Nucl. Phys. **A478**(1988) 151.

Figures

Figure 1.2.1	The E735 detector.
Figure 1.2.2	Hadronic matter energy density versus radius. The regions accessible for $\bar{p}p$ collisions at FNAL and for heavy ion collisions at CERN and RHIC are shown.
Figure 1.2.3	$< p_t >$ versus dn/dη as measured in experiments E735 and UA1
Figure 1.4.1	Overview of P787 detector a) Plan view and b) Vertical cross section. H, hodoscope; TC, threshold Cherenkov counter; RICH, ring imaging Cherenkov counter; PRDC, pre-magnet drift chamber; PSTDC, post-magnet drift chamber; C, photon converter; DC1 and DC2, drift chambers; TOF, time-of-flight; NaI, NaI calorimeter; EM2, tunnel side calorimeter
Figure 2.1.1	Detected number of single electrons and positrons compared to the expected background from Dalitz and photon pair production. The background curve includes a rejection factor of 10^{-2}.
Figure 2.1.2	Detected pair mass distribution.
Figure 2.1.3	The probability that a pair can be detected when the pair is produced within the pseudo-rapidity -4.0 and 4.0. Each symbol represents different mass of pairs in GeV/c^2.
Figure 2.1.4	The π^- rejection probability using various detector components. With the threshold Cherenkov counter, the rejection should improve by at least a factor of 20-50.
Figure 2.1.5	Kaon rejection probability using various detector components. With a threshold Cherenkov counter, the rejection should increase by at least a factor of 20-50.
Figure 2.1.6	Fractional energy deposited by e^- and K$^-$ in the first versus second section of the NaI detector.
Figure 2.2.1	Photon spectrum into NaI calorimeter from $\bar{p}p$ collisions at $\sqrt{s}$=1.8TeV. (ISAJET prediction)
Figure 2.2.3	Comparison of photon energy spectrum measured from E735 NaI calorimeter (raw, uncorrected data) to the prediction of ISAJET.
Figure 2.3.1	Theoretical prediction for the hyperon-baryon ratio

	as a function of the plasma temperature. [Koch *et al.*, 1986]
Figure 3.1.1	Design of a X-U-V Cell Triplet Plane View of the Upper Plane
Figure 3.1.2	Design of a Single Cell X Chamber Cross Section
Figure 3.1.3	Design of a Single Cell U Chamber Cross Section
Figure 3.1.4	Design of the Whole Chamber Triplet Plane View
Figure 3.1.5	Post-magnet Chamber
Figure 3.1.6	One of four modules of the proposed RICH counter. A detail of the TEA drift chamber is shown.
Figure 3.1.7	Detector Room Electromagnetic Calorimeter
Figure 3.2.1	On Line Data Acquisition System (P787)

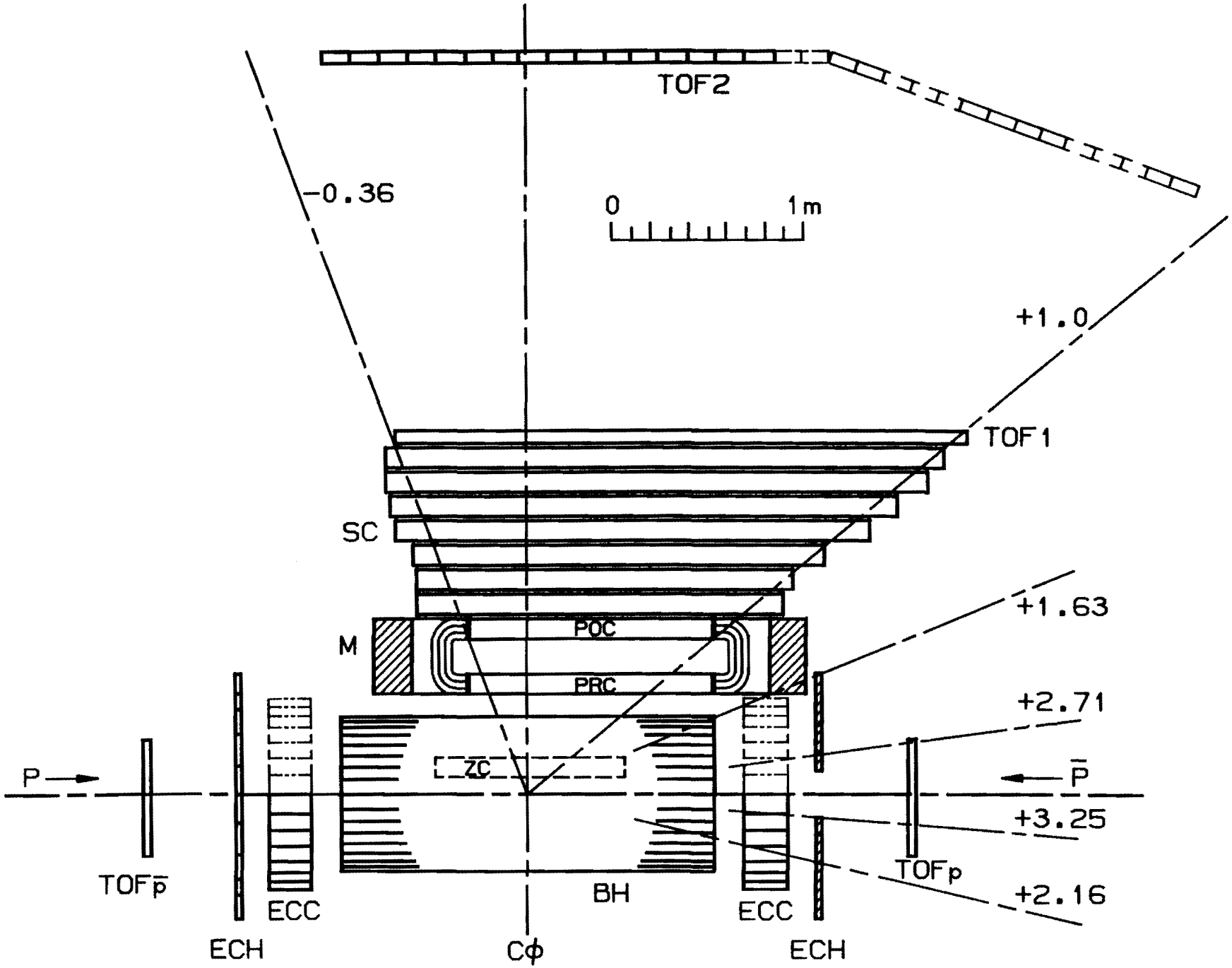

Figure 1.2.1 The E735 detector.

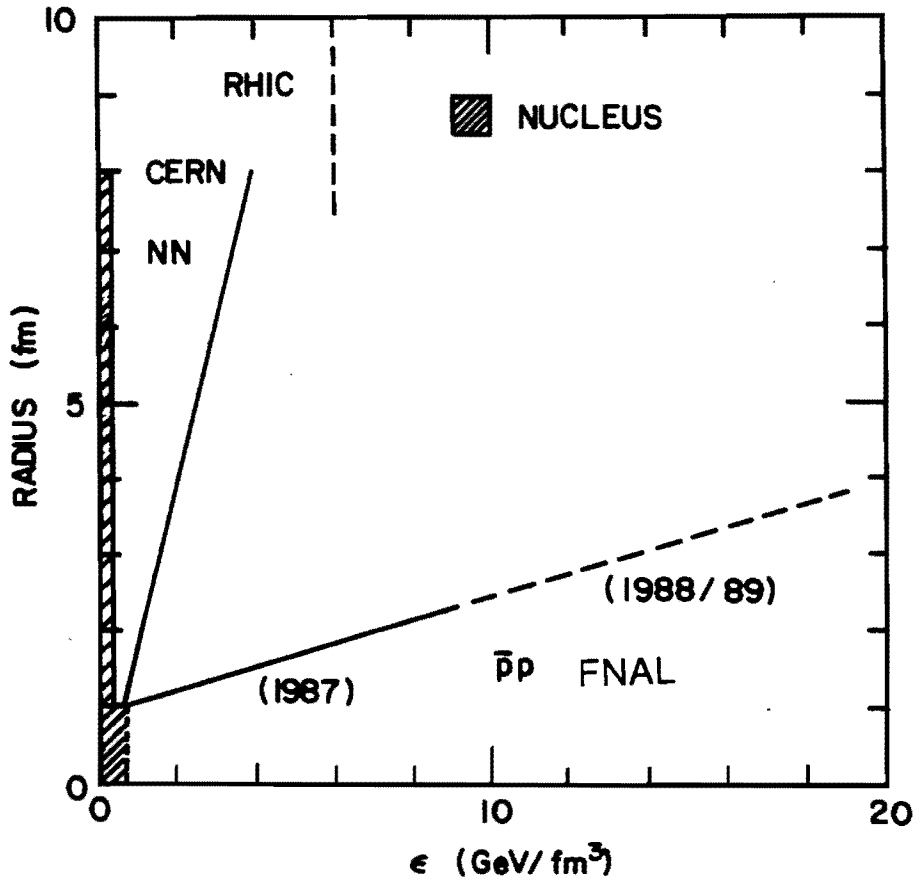

Figure 1.2.2 Hadronic matter energy density versus radius. The regions accessible for $\bar{p}p$ collisions at FNAL and for heavy ion collisions at CERN and RHIC are shown.

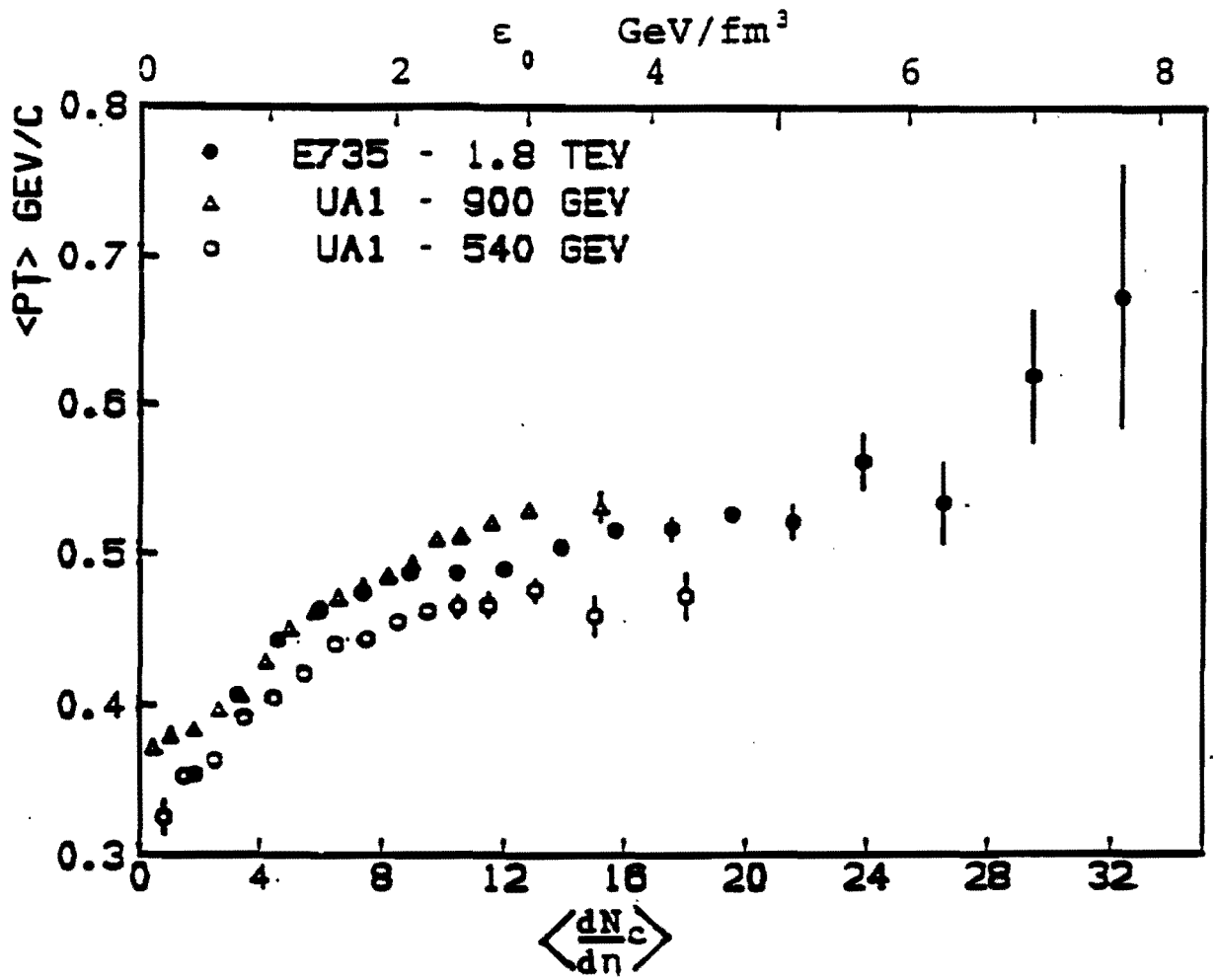

Figure 12.3 $< p_t >$ versus $dn/d\eta$ as measured in experiment E735 and UA1.

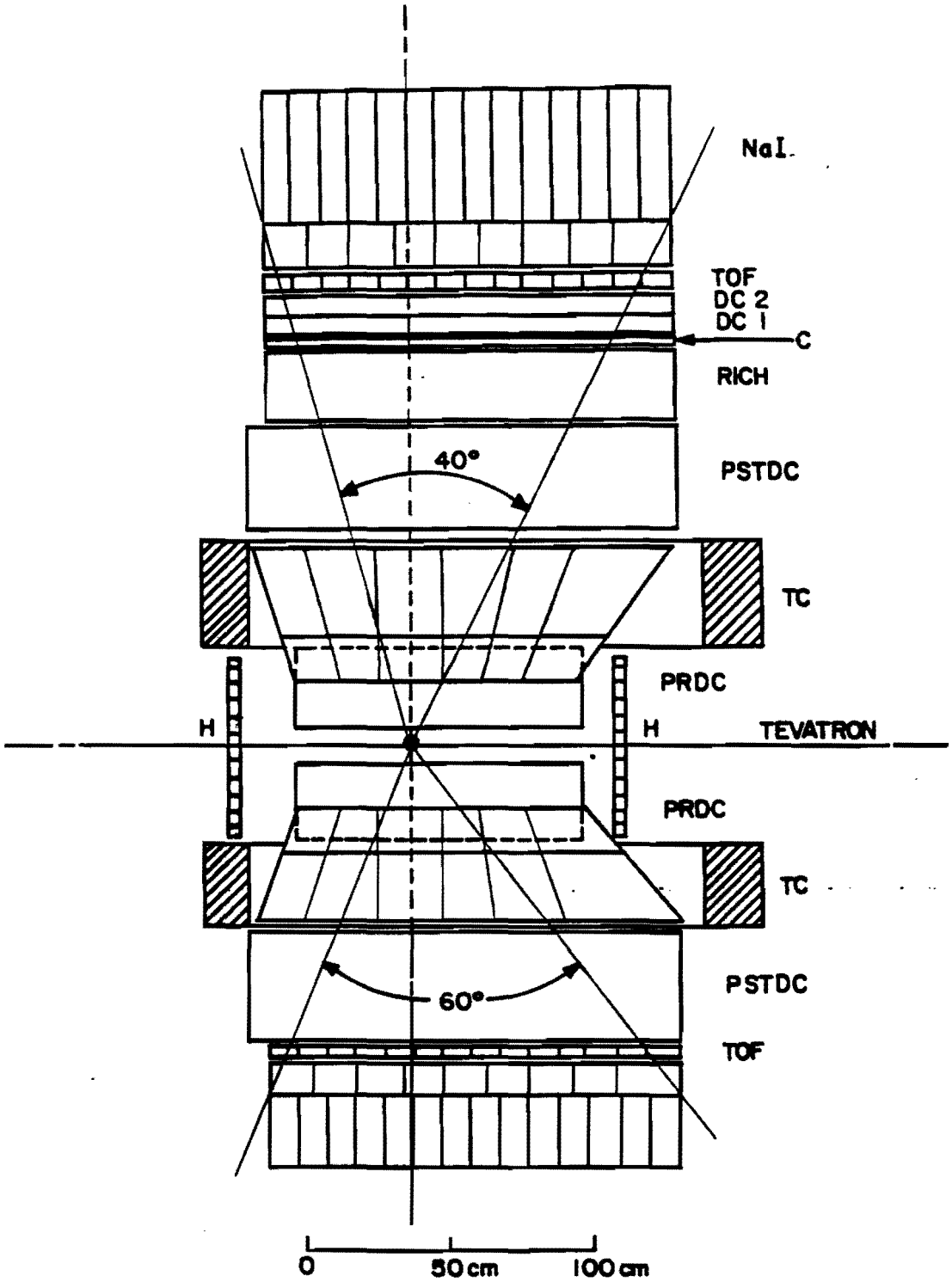

Figure 1.4.1 a. Overview of P787 detector a) Plan view and b) Vertical cross section. H, hodoscope; TC, threshold Cherenkov counter; RICH, ring imaging Cherenkov counter; PRDC, pre-magnet drift chamber; PSTDC, post-magnet drift chamber; C, photon converter; DC1 and DC2, drift chambers; TOF, time-of-flight; NaI, NaI calorimeter; EM2, tunnel side calorimeter

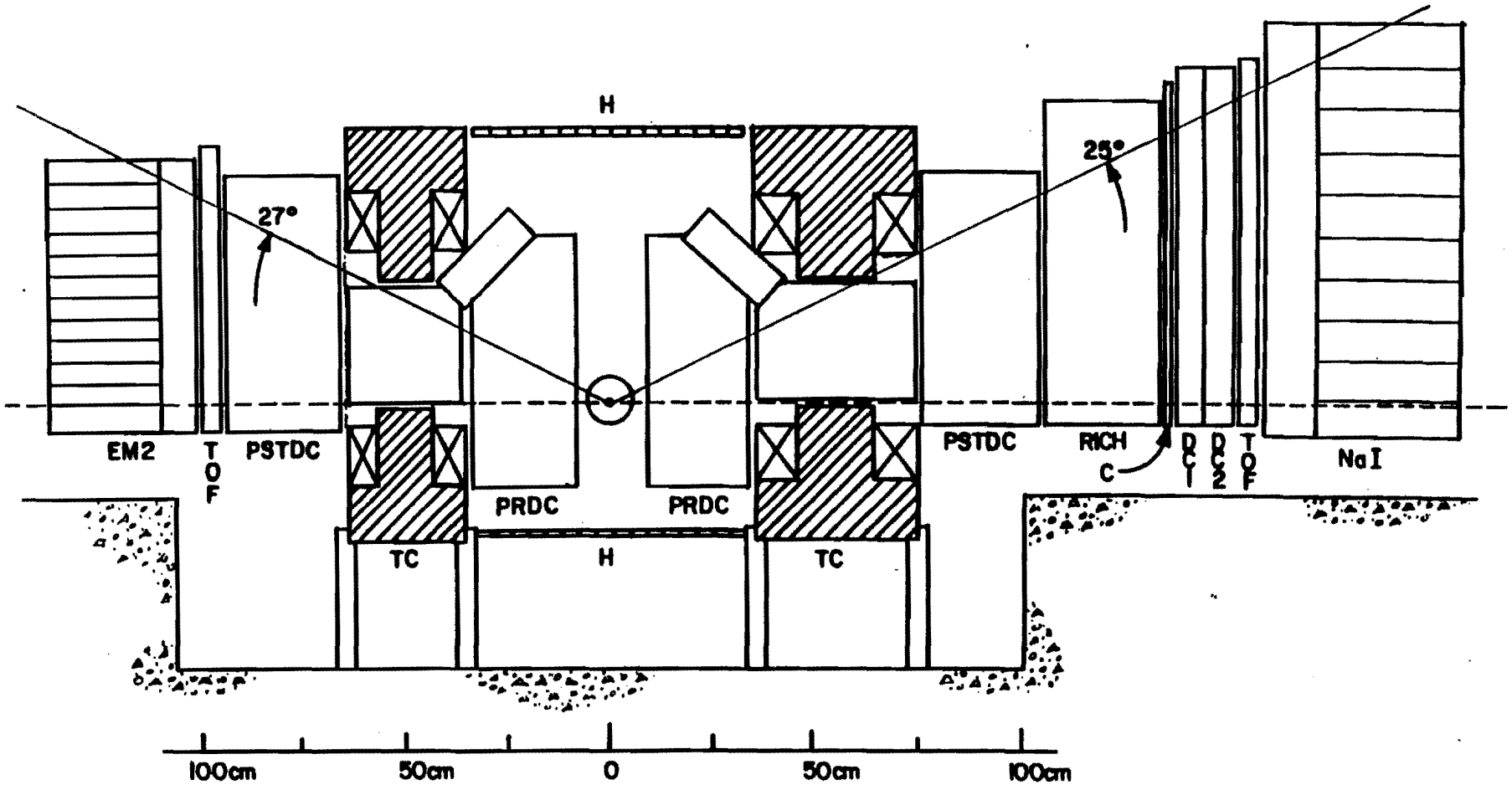

Figure 1.4.1 b Overview of P787 detector a) Plan view and b) Vertical cross section. H, hodoscope; TC, threshold Cherenkov counter; RICH, ring imaging Cherenkov counter; PRDC, pre-magnet drift chamber; PSTDC, post-magnet drift chamber; C, photon converter; DC1 and DC2, drift chambers; TOF, time-of-flight; NaI, NaI calorimeter; EM2, tunnel side calorimeter

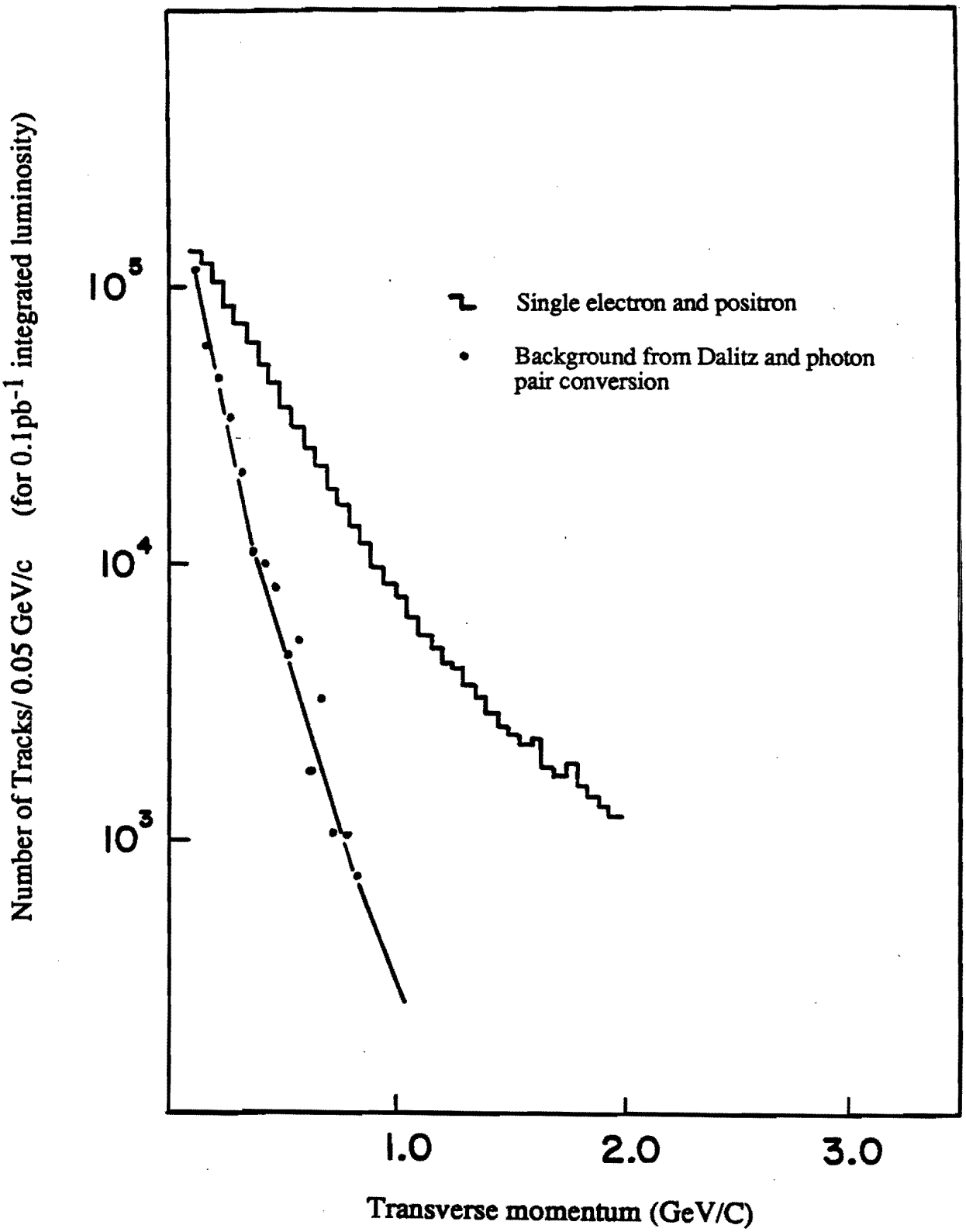

Figure 2.1.1 Detected number of single electrons and positrons compared to the expected background from Dalitz and photon pair production. The background curve includes a rejection factor of 10^{-2}.

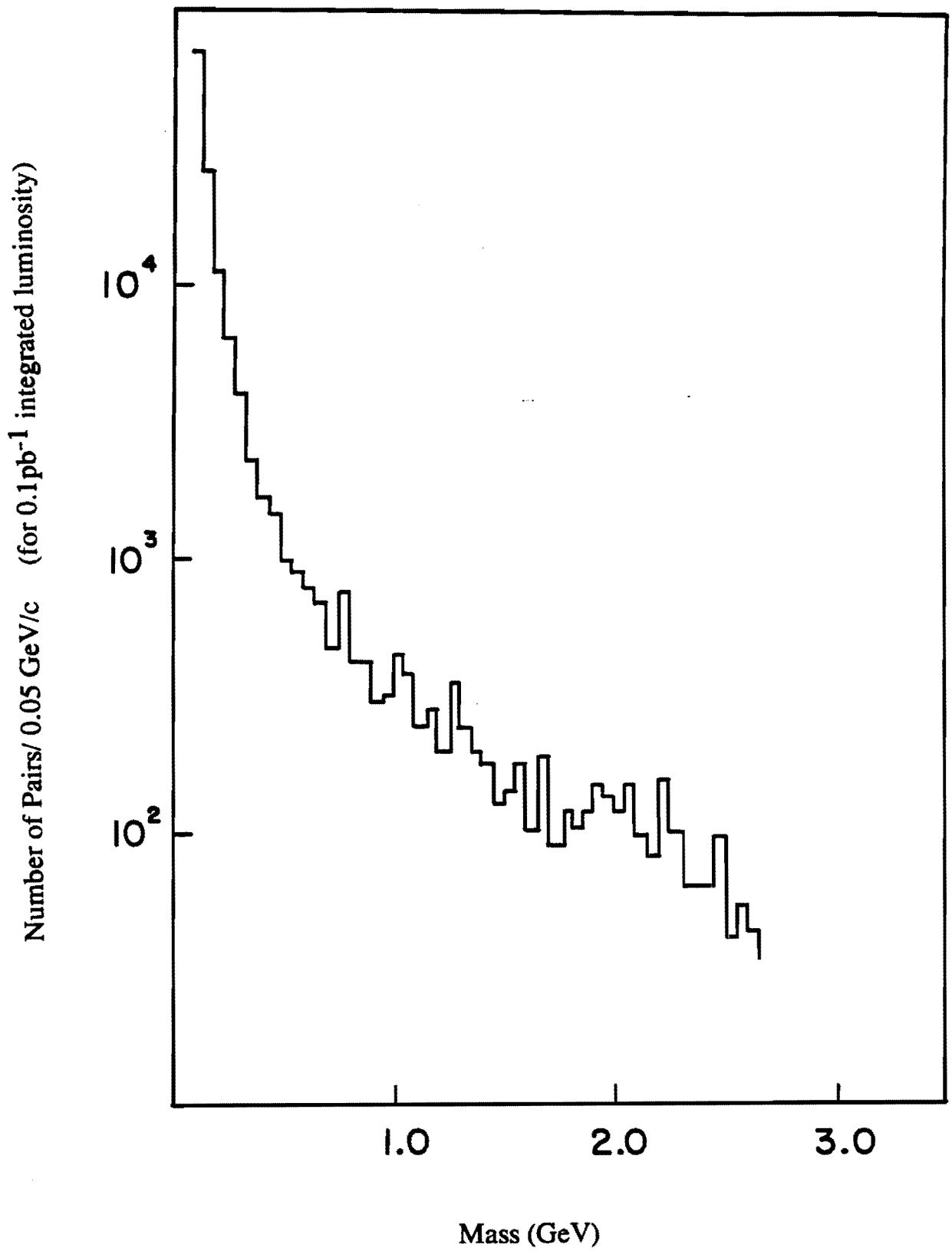

Figure 2.1.2 Detected pair mass distribution.

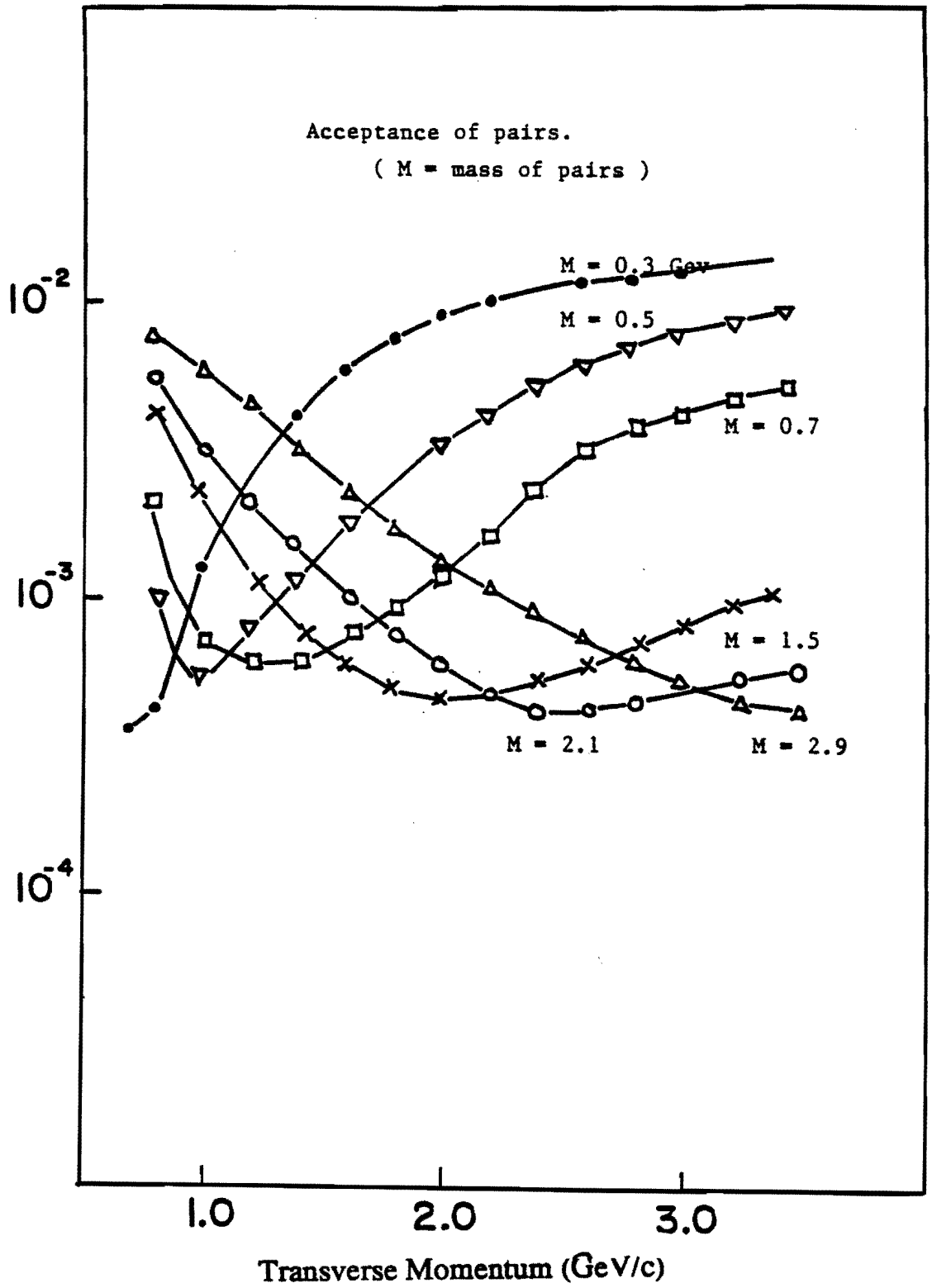

Figure 2.1.3 The probability that a pair can be detected when the pair is produced within the pseudo-rapidity -4.0 to 4.0. Each symbol represents different mass of pairs in GeV/c^2.

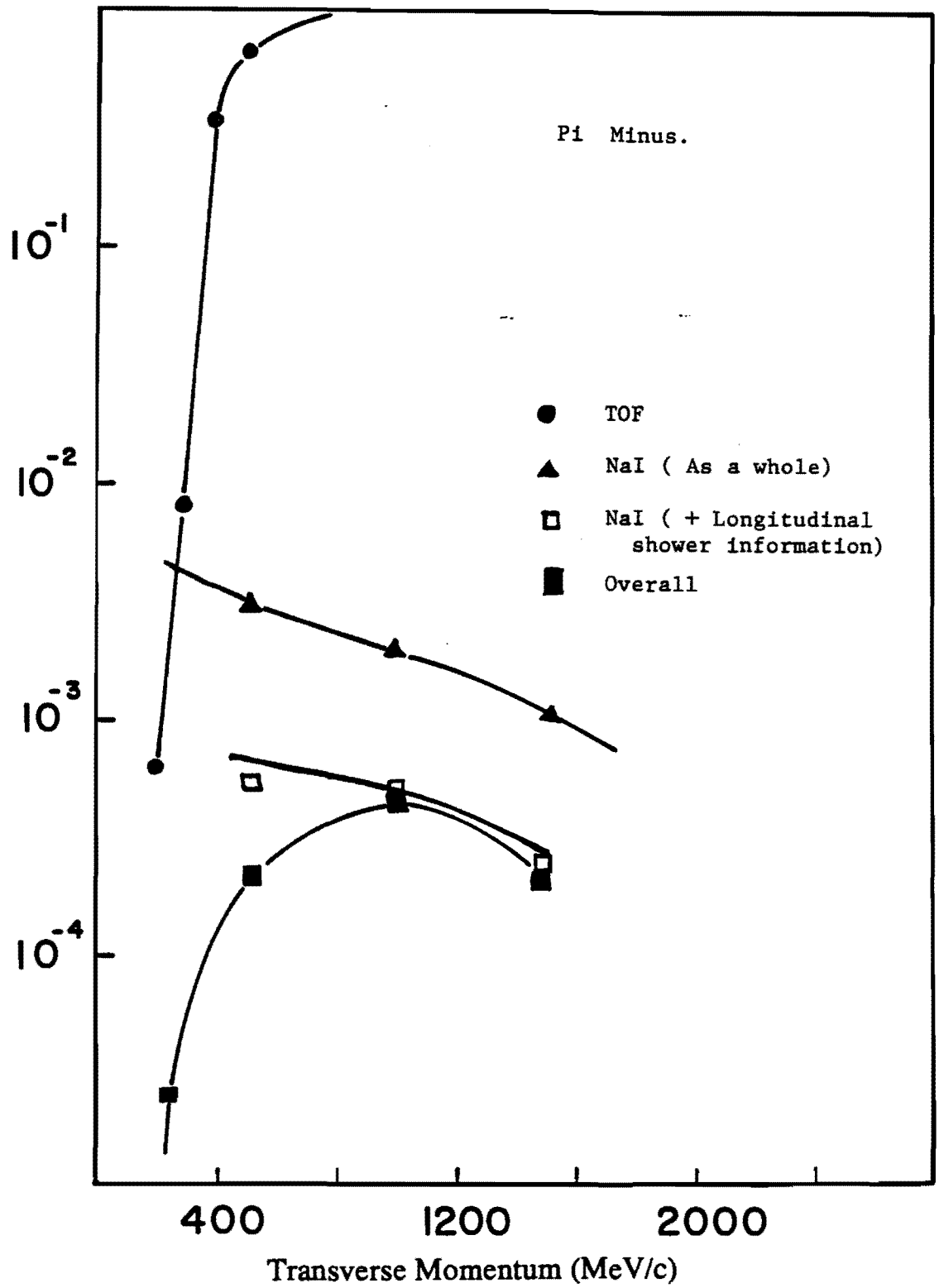

Figure 2.1.4 The π^- rejection probability using various detector components. With the threshold Cherenkov counter, the rejection should improve at least a factor of 20-50.

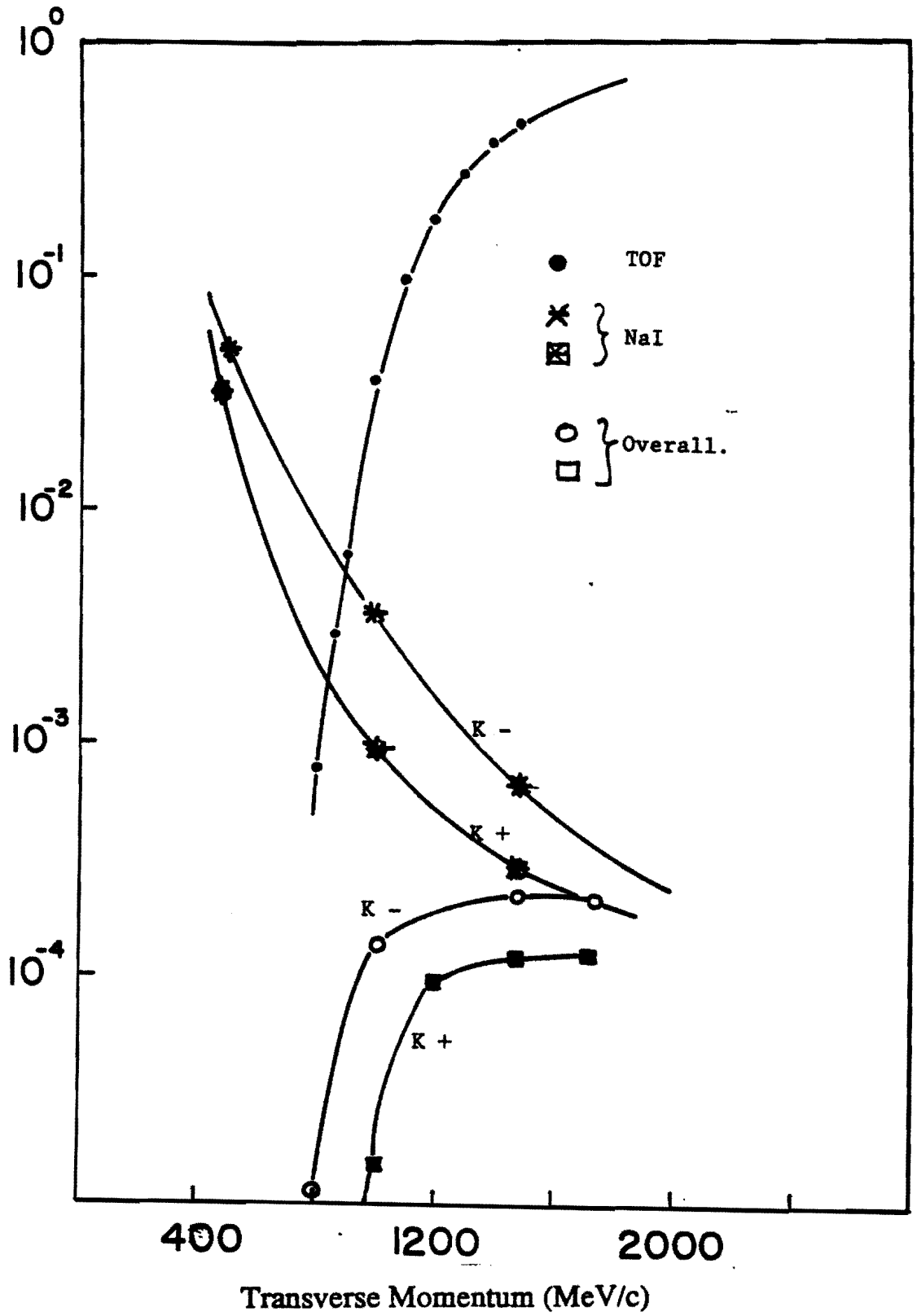

Figure 2.1.5 The Kaon rejection probability using various detector components. With the threshold Cherenkov counter, the rejection should increase by at least a factor of 20-50.

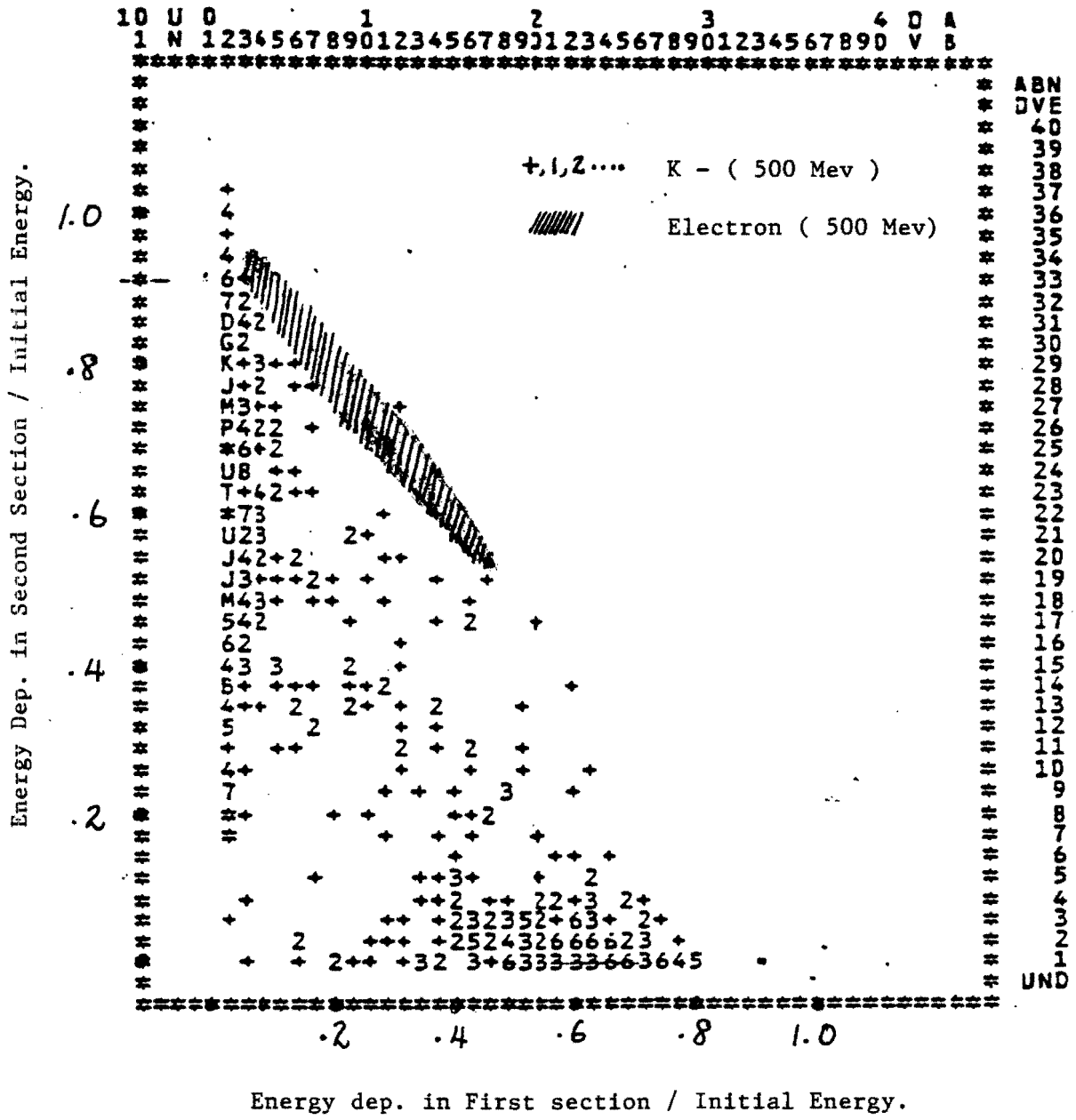

Figure 2.1.6 Fractional energy deposited by e^- and K^- in the first versus second section of the NaI detector.

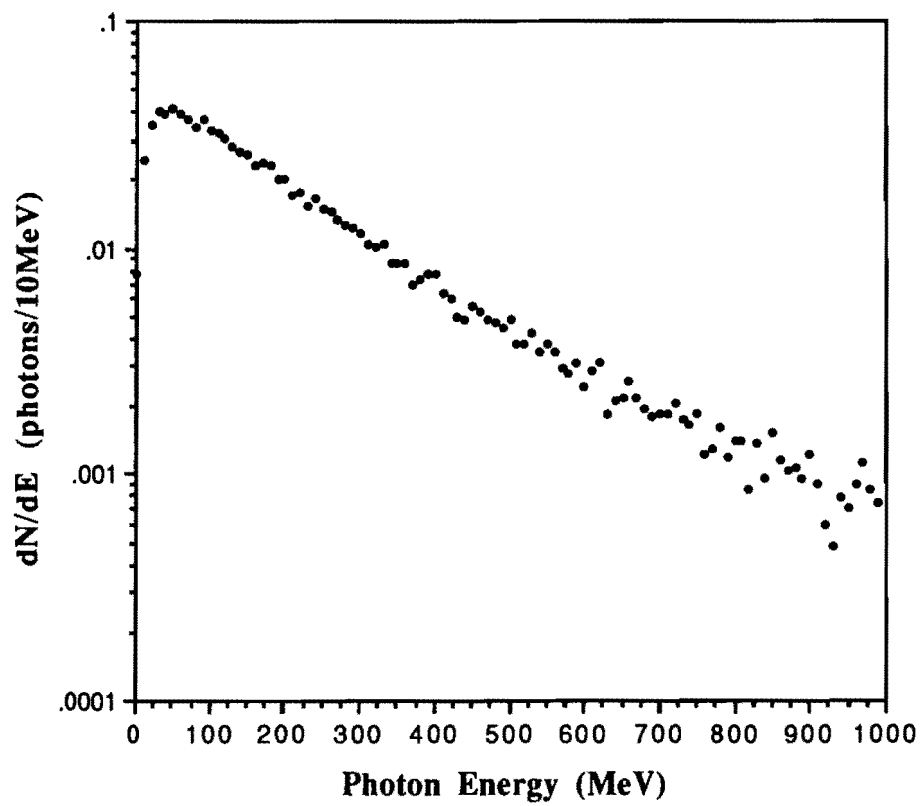

Figure 2.2.1 Photon spectrum into NaI calorimeter from $\bar{p}p$ collisions at $\sqrt{s}$ = 1.8 TeV. (ISAJET prediction)

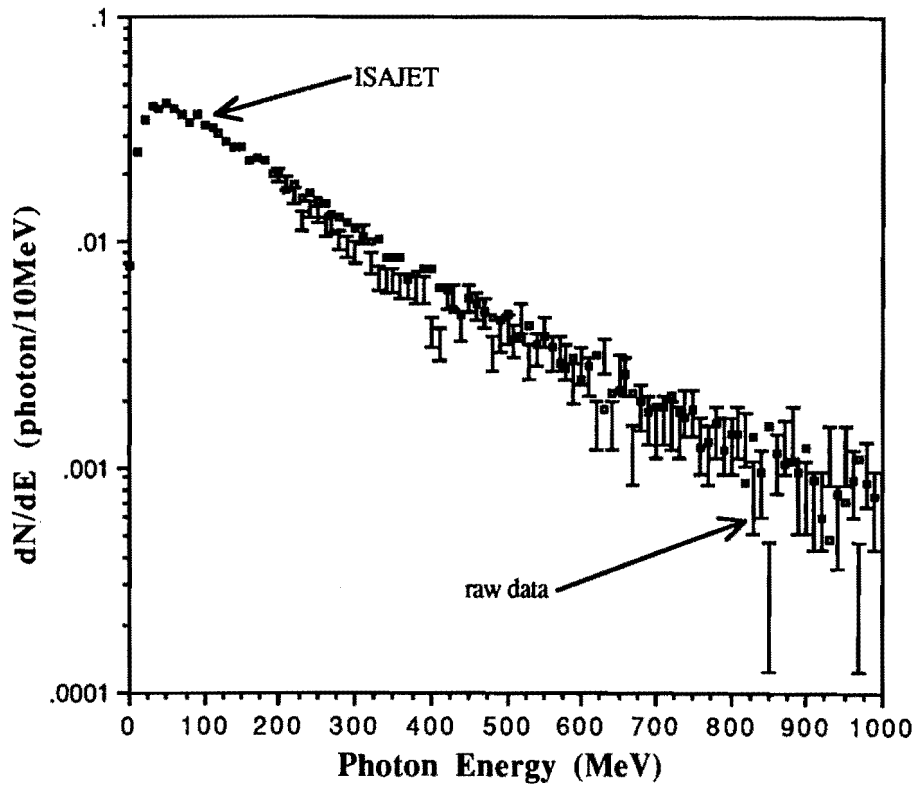

Figure 2.2.3 Comparison of photon energy spectrum measured from E735 NaI calorimeter (raw, uncorrected data) to the prediction of ISAJET.

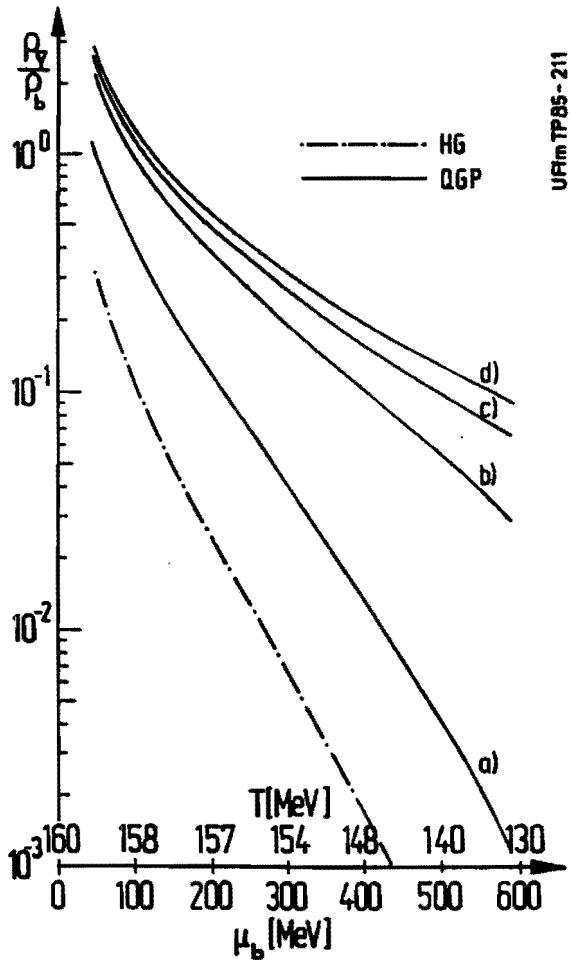

Figure 2.3.1 **Theoretical prediction for the hyperon-baryon ratio as a function of the plasma temperature.** [Koch *et. al.*, 1986]

Fig. 3.1.1 Design of a X - U - V Cell Triplet
Plane View of the Upper Plane

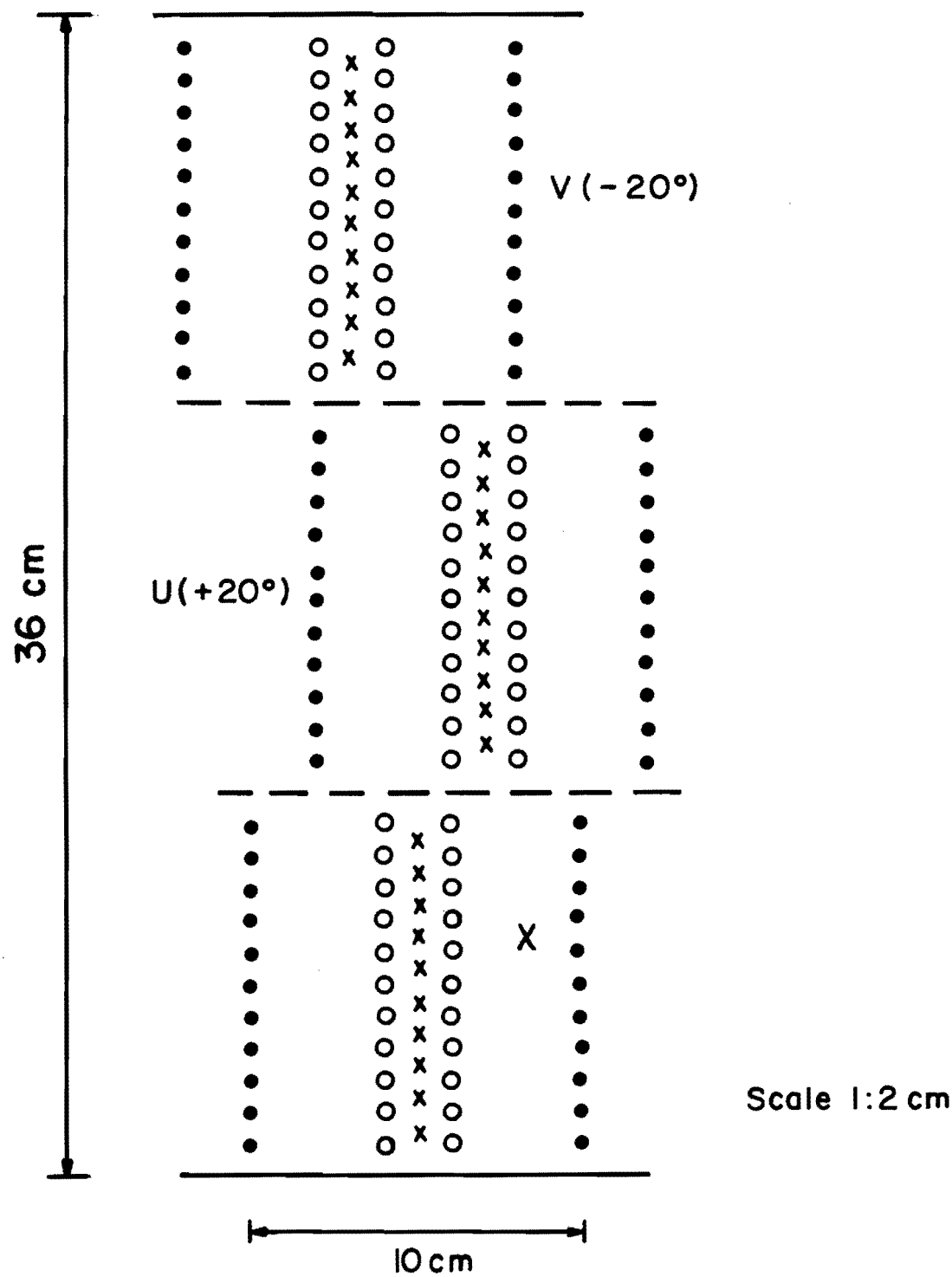

Design of a Single Cell X Chamber Crossection

Fig. 3.1.2

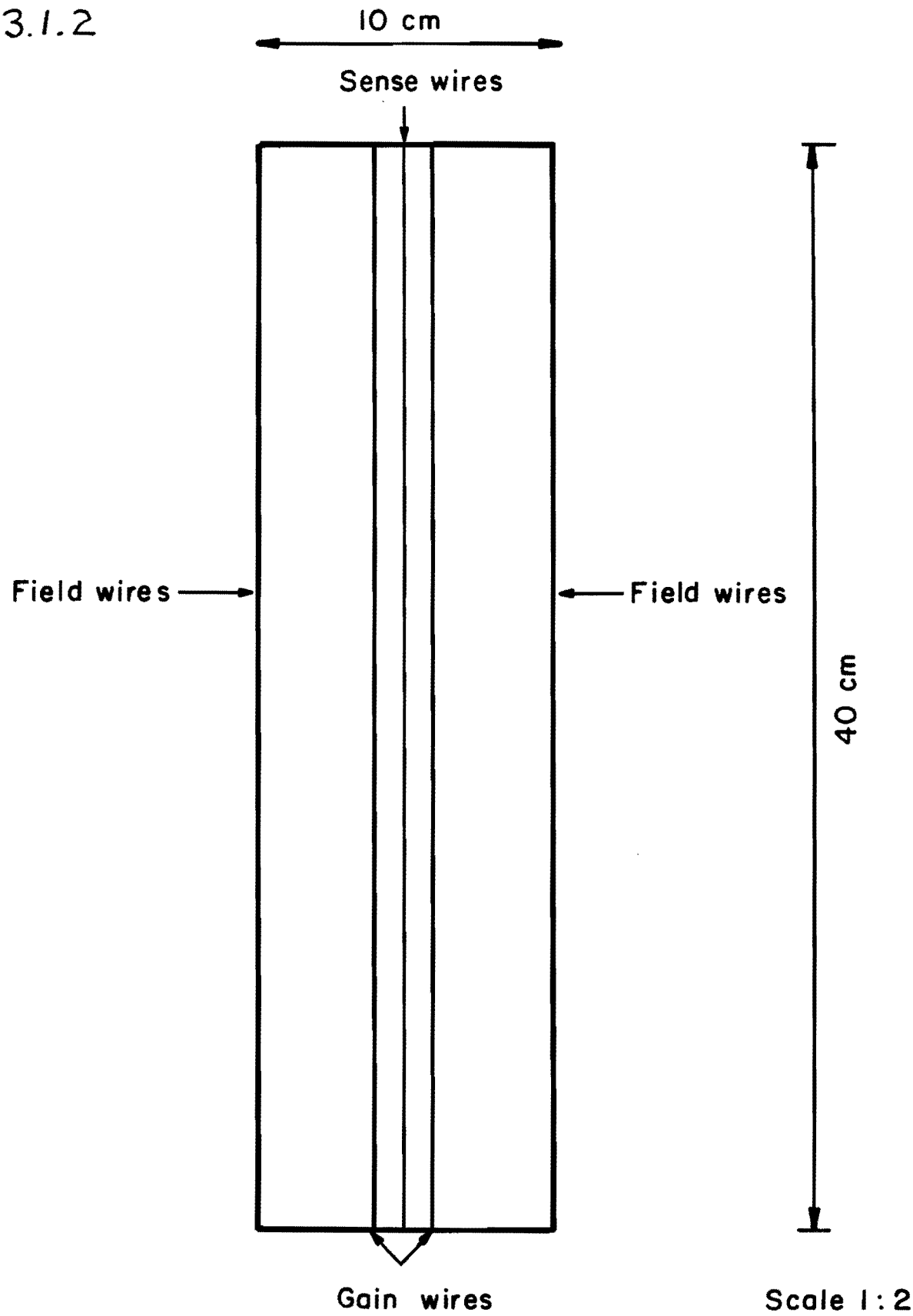

Design of a Single Cell U Chamber
Crossection

Fig. 3.1.3

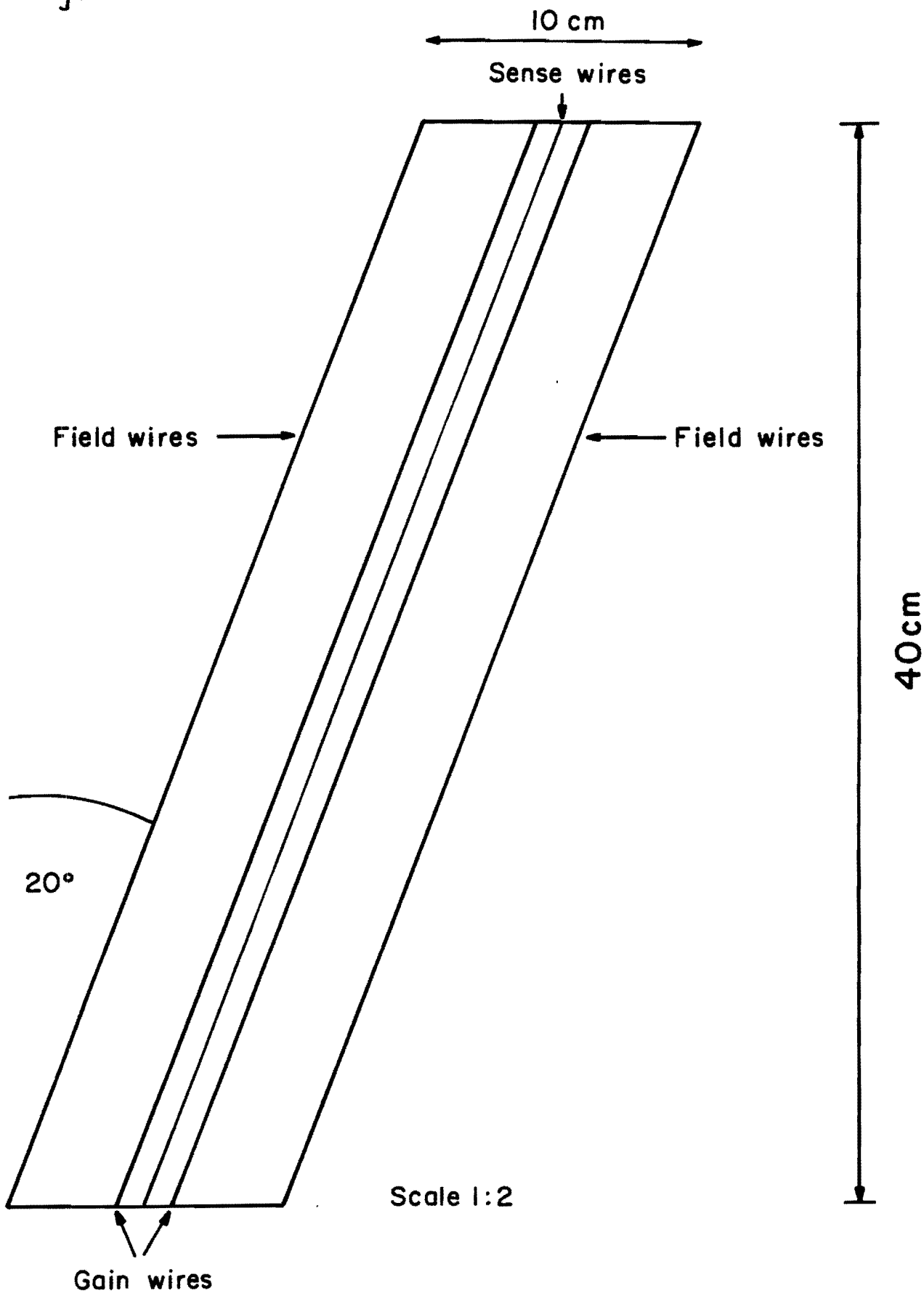

Fig. 3.1.4 Design of the Whole Chamber Triplet
Plane View

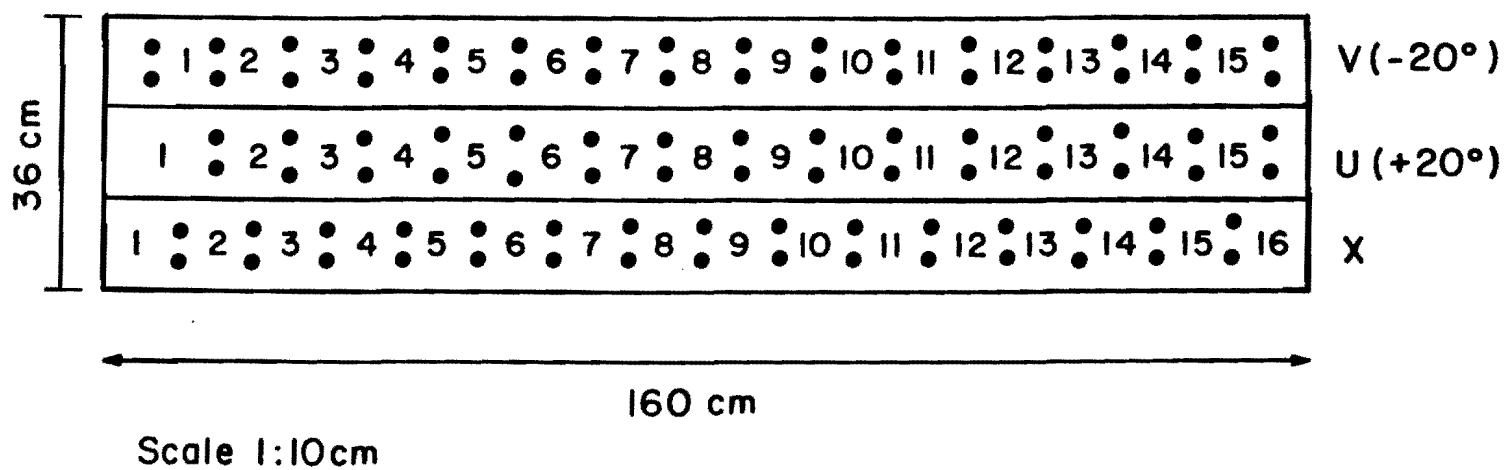

Scale 1:10cm

Fig. 3.1.5

POST MAGNET CHAMBER

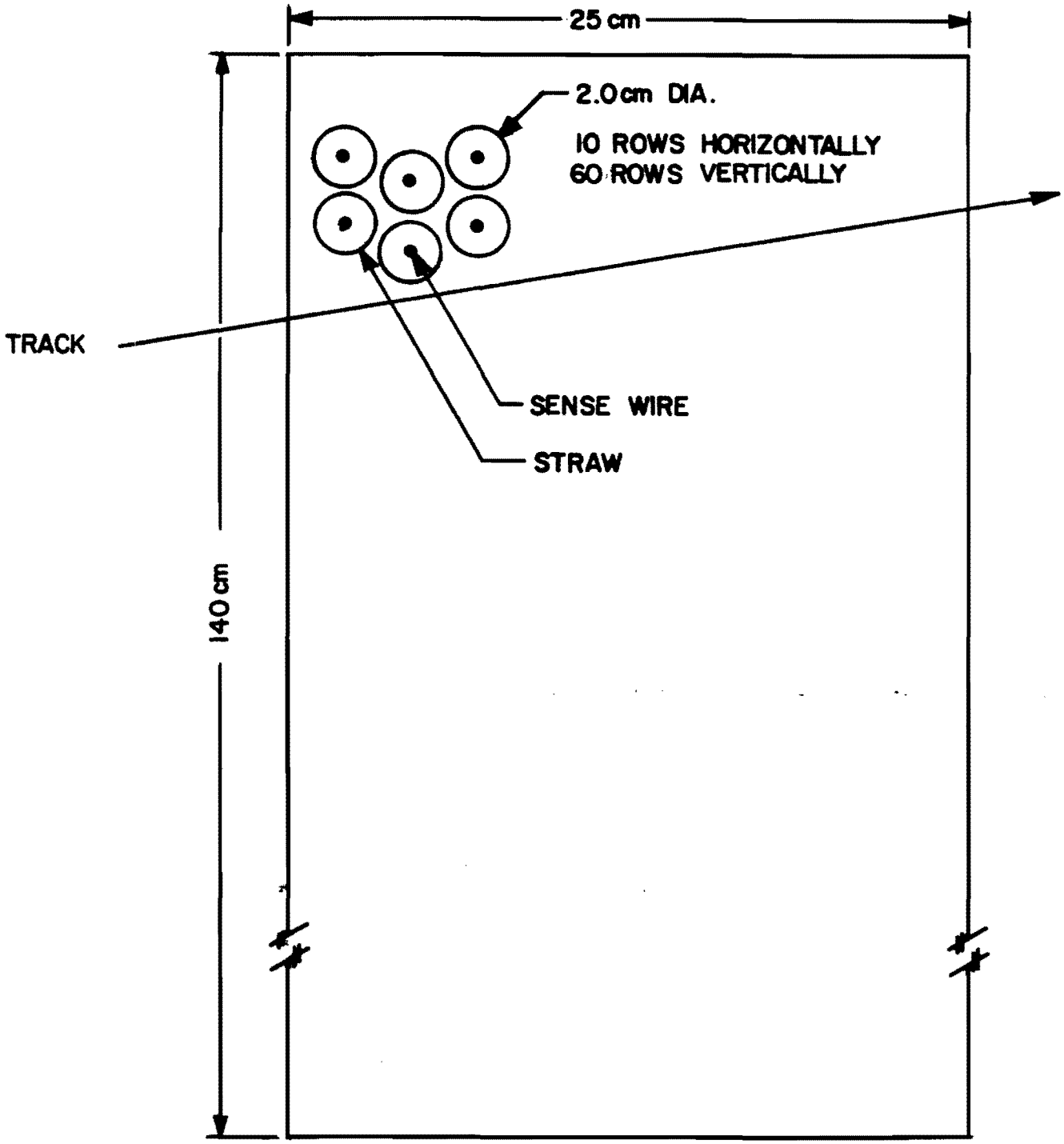

PLAN VIEW

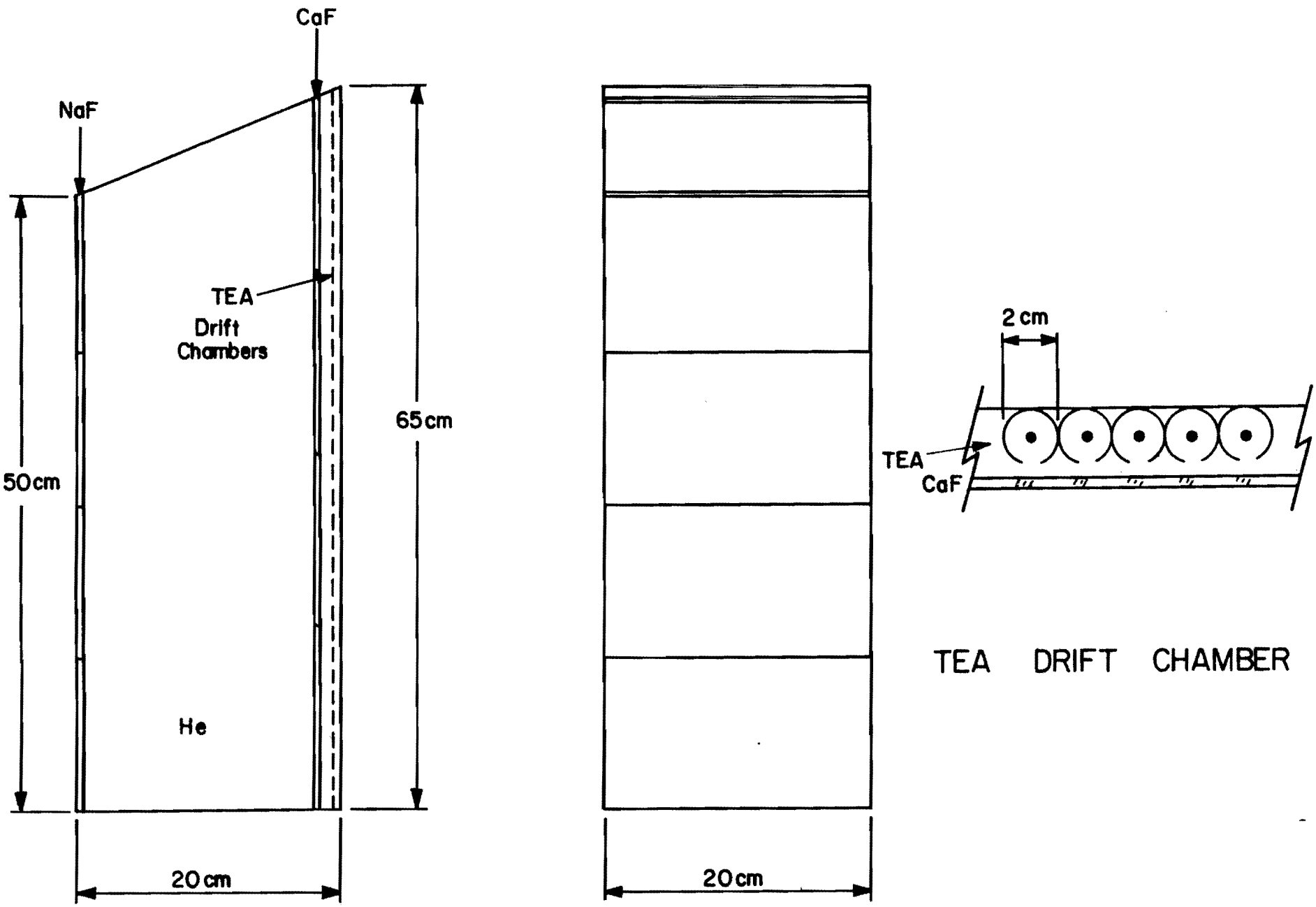

Figure 3.1.6 One of four modules of the proposed RICH counter. A detail of the TEA drift chamber is shown.

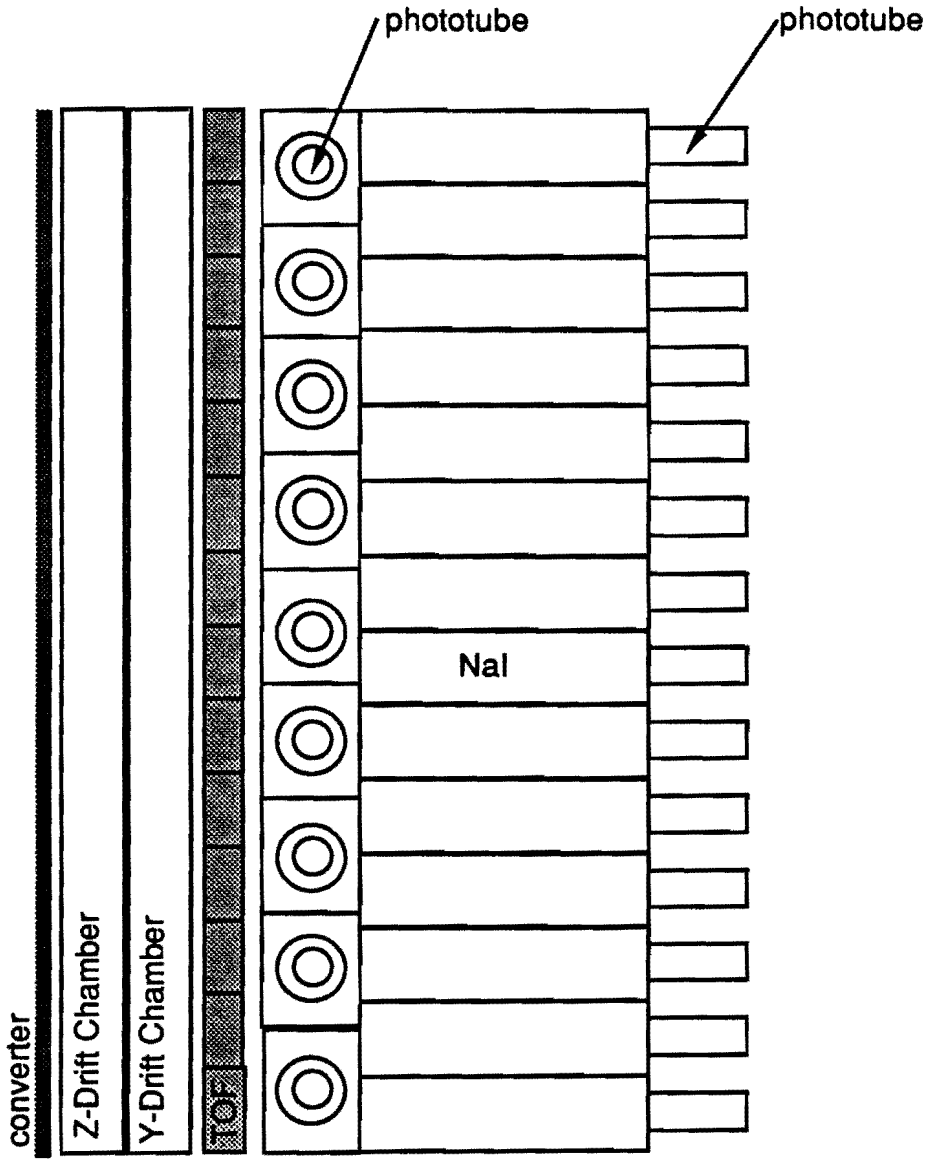

Figure 3.1.7 Detector room electromagnetic calorimeter

Fig. 3.2.1 ON LINE DATA ACQUISITION SYSTEM (P - 787)

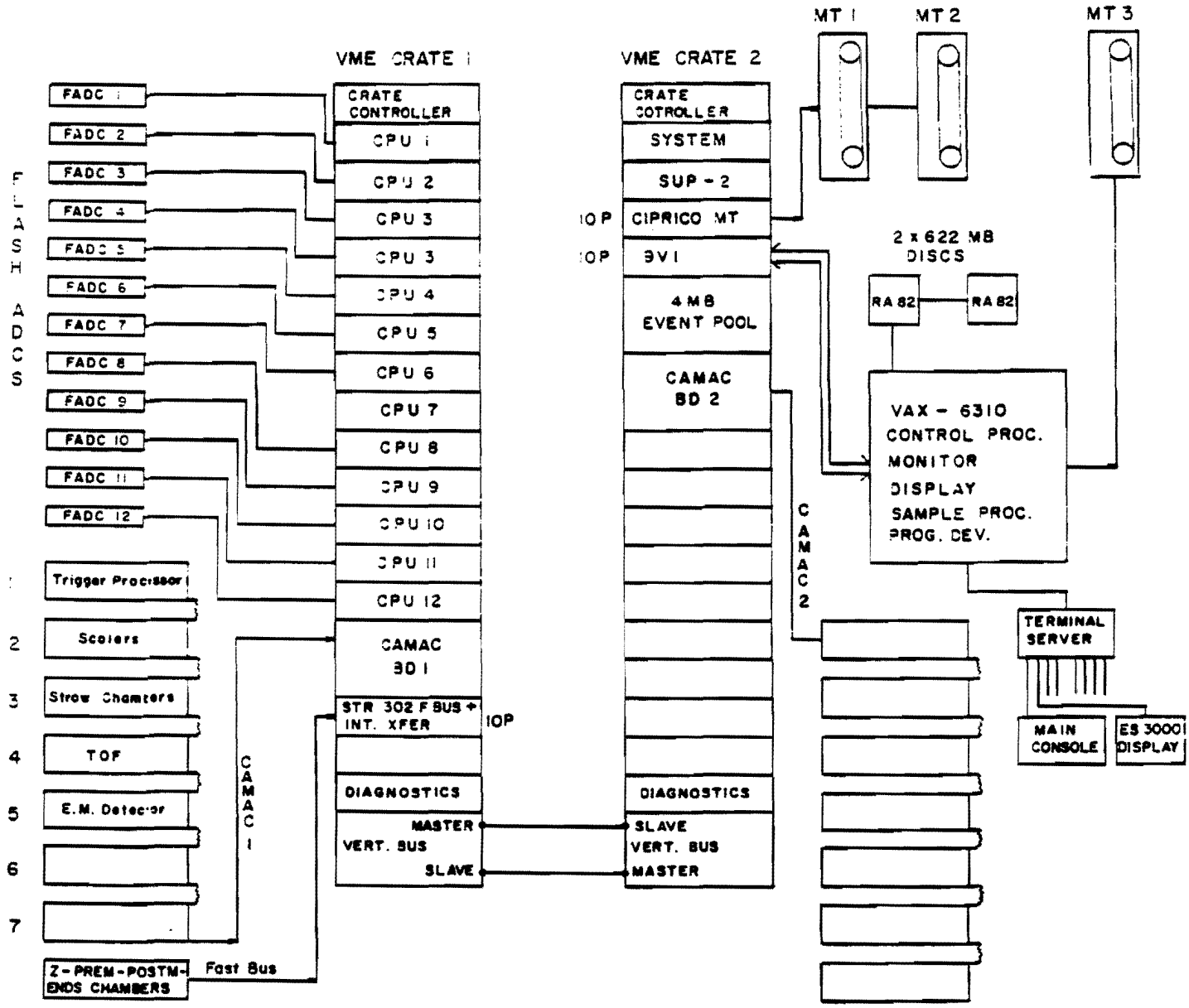

4/28/89

FERMILAB PROPOSAL P787

Multi-signature Search for Quark-Gluon Plasma Formation in High Multiplicity $\bar{p}p$ Interactions at $\sqrt{s}$=1.8 TeV

Duke University
Fermi National Accelerator Laboratory
Iowa State University
University of Notre Dame
Purdue University
University of Wisconsin

Multi-signature Search for Quark-Gluon Plasma Formation in High Multiplicity $\bar{p}p$ Interactions at $\sqrt{s}$=1.8 TeV

April 24, 1989

Fermilab Proposal P787

Submitted by Scientists at
Duke University, Fermi National Accelerator Laboratory,
Iowa State University, University of Notre Dame,
Purdue University, and University of Wisconsin

We propose to measure photon and e^+e^- pair production and to study the low p_t (<3 GeV/c) production characteristics of centrally produced hadrons such as π, ρ, K, K*, ϕ, p, Λ and deuterons in $\bar{p}p$ collisions at $\sqrt{s}$ = 1.8 TeV. This will be done as a function of the energy density of the collision as measured by the charged particle rapidity density. Variation of the above particle production cross sections and transverse momentum spectra with collision energy density will provide information about quark-gluon plasma formation in $\bar{p}p$ interactions at 1.8 TeV. This experiment will also provide unique data for testing hadroproduction models at the highest available energy. To make these measurements we will increase the aperture, momentum resolution and particle identification capabilities of the existing E735 spectrometer and build a second spectrometer arm in the tunnel at the C0 collision hall. Both detector arms will have electromagnetic calorimetry.

Names of the Senior Experimenters

De Pauw University:	V. DeCarlo
Duke University:	A. T. Goshaw
	S. Oh
	W.J. Robertson
	W.D. Walker
Fermilab:	P. C. Bhat
	C. Hojvat
	F. Turkot
Iowa State University:	E. W. Anderson
	C. S. Lindsey
Notre Dame University:	J. Bishop
	N. N. Biswas
	J. M. LoSecco
	V. P. Kenney
	J. Piekarz
Purdue University:	A. T. Bujak
	D. D. Carmony
	Y. I. Choi
	R. J. De Bonte
	L. J. Gutay
	A. S. Hirsch
	N. K. Morgan
	N. T. Porile
	R. P. Scharenberg
	B. C. Stringfellow
University of Wisconsin:	A. R. Erwin
	C. Findeisen
	K. Nelson
	M. A. Thompson

Contents

1 Introduction **4**

1.1 Prologue 4

1.2 Evaluation and Summary of Experiment E735 5

1.3 Overview of P787 Physics Goals 8

1.3.1 Electron-Positron Pair Production 9

1.3.2 Photon Production 10

1.3.3 Hadron Production 11

1.4 Detector Overview 11

1.5 Time Table for Staging P787 13

2 Proposed Measurement and Analysis **16**

2.1 Dilepton Production 16

2.1.1 Introduction 16

2.1.2 Expected Rates 16

2.1.3 Electron Identification 17

2.1.4 Background Rejection of Dalitz Pairs and Photon Conversions (An addendum to this proposal discusses this section in more detail based on recent monte carlo simulations.) 18

2.2 Photon Production 19

2.2.1 Introduction 19

2.2.2 Analysis of the photon data from P787 and preliminary results from E735 20

2.3 Hadron Production 21

2.3.1 Study of Λ production and search for Ξ and Ω production in the central region 22

2.3.2 Low p_t hadron physics 22

2.3.3 p_t of π, K, p, ρ, K*, and ϕ production up to $p_t = 3$GeV/c 23

3 The P787 Detector **24**

3.1 The Spectrometer Components 24

3.1.1 Pre-magnet Drift Chambers (PRDC) 24

3.1.2 Post-magnet Drift Chambers (PSDC) 25

3.1.3 Threshold Cherenkov Counter (TC) 25

3.1.4 RICH Cherenkov Counter (RICH) 26

3.1.5 Spectrometer Room Electromagnetic Calorimeter (NAI) 26
3.1.6 Tunnel Side E.M. Calorimeter (EM2) 28
3.1.7 Multiplicity Hodoscope (H) 28
3.1.8 TOF counters 29
3.1.9 Magnets 29
3.2 Trigger 29
3.2.1 Interaction Trigger 29
3.2.2 Hadron Production Trigger 30
3.2.3 Single and Dilepton Trigger 30
3.3 Data Acquisition System 30
3.4 Accelerator Issues 32

A Theoretical Arguments for Strangeness Enhancement in Deconfined Hadronic Matter 33
A.1 Production Mechanism 33
A.2 Production Rate and Chemical Equilibrium 34
A.3 Conversion from the QGP to Hadronic Phase 34

B Lepton Pair Production from the Centrally Produced Hadronic Matter 35
B.1 Drell-Yan Model for Lepton Pair Production. 36
B.2 Modification of the Drell-Yan Model 36
B.3 The low mass ($m_d < 600$ MeV) region 36

1 Introduction

1.1 Prologue

There is a general theoretical consensus that at temperatures of about 200 MeV and energy densities of about 2 GeV/fm^3 a first order deconfining phase transition of QCD matter will take place [Hagedorn *et al.*, 1980]. There is reasonable expectation that such conditions can be obtained in high energy particle collisions. Theoretical description of the formation, thermalization, and decay of centrally produced hadronic matter is complex. In particular some of the experimental signatures predicted for the existence of a quark-gluon plasma (QGP) can be arrived at without assuming its existence. But while the QGP signatures stem from a central idea, the alternate explanations are subject to a collection of assumptions. The first round of QGP search experiments, E735 at FNAL and heavy ion collisions at CERN, are under analysis, and although there are several suggestive particle production "anomalies," no one experiment has claimed the observation of a QGP. As stressed by Van Hove [Van Hove, 1986], "it will take a unified interpretation of several anomalies to provide the first basis for a serious claim that a QGP has been discovered." The proposed experiment, P787, is designed with this philosophy in mind, namely to look for multiple signatures of QGP formation in a single experiment.

Aside from speculations about the formation of a QGP, the measurement of particle production from highly inelastic $\bar{p}p$ collisions is of fundamental importance in its own right. There is little data on mass identified particle production at low p_t at the Tevatron Collider and the theoretical understanding of the hadronic production mechanism is poor. The measurements made in experiments E735 and P787 will strongly compliment the hard scattering measurements to be made at CDF and D0.

Both our test run in 1987 and the ongoing E735 experiment have shown that a viable experimental $\bar{p}p$ collider program can be sustained at the C0 intersection region. In particular, we have shown [Alexopoulous *et al.*, 1988] that it is possible to measure production characteristics of interactions with central charged particle rapidity densities as high as 32. These extremely high multiplicity events al-

low us to examine the characteristics of hadronic matter compressed to an energy density of up to 7 GeV/fm^3. This energy density is a factor of three higher than that estimated for the onset of QGP formation. The present proposal is intended to appreciably broaden our experimental sensitivity to the production of a QGP and other unusual high energy density $\bar{p}p$ production phenomena. We would enlarge the momentum range of our study of π, K and p production and add measurements of the production of hadron resonances, photons and dilepton pairs. The potential for the discovery of important new high energy physics phenomena in these data is high. The opportunity is also uniquely available to Fermilab if the P787 proposal is approved.

The remainder of this introduction is organized as follows. Section 1.2 evaluates and summarizes the data expected from experiment E735. Section 1.3 then provides a brief overview of the new physics goals of proposed experiment P787. Sections 1.4 and 1.5 provide an overview of the detector and give a time table for staging the experiment. The details of our proposed measurements are presented in Section 2 and a complete detector description is given in Section 3. Some detailed information supporting the proposal is given in the appendices.

1.2 Evaluation and Summary of Experiment E735

Experiment 735 has been installed in the C0 region of the Tevatron Collider since January 1987. We have shown that it is possible to study the momentum spectra of mass identified particles emerging in the central region for very high multiplicity collisions. As shown in Figure 1.2.1, the multiplicity detector was located in the accelerator tunnel and the 90° magnetic, time-of-flight spectrometer was in an adjoining room. This is a unique experiment as it explores the low energy particle spectrum emerging from the highest energy collisions at hadron colliders.

The study of the soft particle spectrum in $\bar{p}p$ collisions at the highest energies is complementary to the research now taking place with relativistic heavy ion collisions, as it explores a different, but significant, range of the variables of interest for the formation of a Quark-Gluon Plasma. These variables are: the size of the region of

hadronic matter created during the collision and the energy density within it. The range of the two variables covered by the present data is summarized in Figure 1.2.2. We have extended the heavy ion collisions to the expectations for the RHIC accelerator and, for the purpose of this comparison we have assumed that experiment E735 could reach a value of $dn/d\eta$ of 50. For the size of the collision region in $\bar{p}p$ collisions we have used a simple linear extrapolation of the preliminary UA1 results [Fincke-Keeler, 1989]. Figure 1.2.2 clearly illustrates the complementarity of the two approaches; heavy ion collisions can explore the large volume of hot hadronic matter while $\bar{p}p$ collisions can explore hadronic matter to very high energy densities.

About 5×10^6 events were collected during the four month 1987 collider run. At that time the Central Tracking Chamber was not installed. All this data has now been analysed, resulting in two publications, each addressing a possible signature of phase transition in hadronic matter. A further article, presenting the results of particle identification utilizing the Time-of-Flight (TOF) system is near completion. In addition, during part of this run an additional 1×10^6 events were collected with converter plates (0.1 and 0.2 radiation lengths) within the spectrometer aperture in order to have a preliminary look at photon production. This data is under analysis and a publication will be ready by summer of 1989. The final sample has of the order of 4000 photons, originating from the collision region. Finally, data collected using a small NaI calorimeter will be used in the design of the $\gamma/e^{\pm}$ calorimeter for P787.

This research is discussed in more detail below.

1. Studies of $< p_t >$ vs. $dn/d\eta$

   The first published article from the 1987 collider run presents the correlation between the average transverse momentum and the associated charged particle multiplicity of the events [Alexopoulos *et al.*, 1988]. The measurement extends previous results from a maximum $dn/d\eta$ of 18 to a value of 32. The UA1 data [Arnison *et al.*, 1982 and Dowell *et al.*, 1988], taken at center of mass energies of 546 GeV and 900 GeV, is in good agreement with our results for the region of overlap in $dn/d\eta$ (see Figure 1.2.3). In agreement with UA1 our data clearly

shows the existence of a plateau in $< p_t >$. The data at the highest multiplicities may indicate a further rise, following the plateau, of $< p_t >$. The high multiplicity data available to E735 from the 1988/89 run will significantly increase the maximum value of $dn/d\eta$ to which the $< p_t >$ vs. multiplicity correlation could be extended. The actual value reached will likely be determined by our ability to correct for backgrounds and sytematics. The new data should settle the question of a second rise of the $< p_t >$ vs. multiplicity.

2. Studies of $\Lambda/\bar{\Lambda}$

   The second published article from the 1987 collider run presents the measurement of strange baryon production (Λ° and $\bar{\Lambda}^\circ$) and its p_t dependence [Banerjee *et al.*, 1988]. The 1987 data contained 400 Λ's. The increase in the number expected from the 1988/89 run could vary from a factor of 5 to a factor of 10. Most of the increased statistics is in the high multiplicity region. This data will allow us to make a first determination of the ratio of Λ production to other charged particles as a function of particle multiplicity. A comparison with the recent preliminary results from the CERN heavy ion experiments, showing a quadratic increase on the ratio Λ/π with multiplicity, will be interesting.

3. The Transverse Momentum Spectra of π's, K's, and p's

   Our pending publication addresses the production of π's, K's, p's and $\bar{p}$'s identified by the TOF system. The p_t dependence of their production will be presented. The statistical accuracy available will permit us to obtain particle ratios up to the order of $dn/d\eta = 15$. The 1988/89 data will increase the maximum $dn/d\eta$ to 20.

At the completion of the 1988/1989 collider run, Experiment 735 would have been taking data for a period of the order of 9 months. The complete experimental setup was available for this run, including the Central Tracking Chamber. In addition, the increased segmentation of the $\bar{p}$ and p TOF counters for this run will provide increased efficiency in determining the vertex position for high multiplicities. During part of this run, a NaI prototype was installed. We estimate that from the 9 months operation we will accumulate

a total of 16×10^6 events. Of these, we predict that of the order of 1×10^6 reconstructed tracks will be available for good events with $dn/d\eta \geq 19$. This represents an increase in the data sample by about 50 times over the first run of the experiment. It should be noted here that the overall number of events recorded is limited by the data recording rate. The dramatic improvement of the accelerator performance and luminosity has allowed E735 to significantly increase the relative fraction of high multiplicity events.

1.3 Overview of P787 Physics Goals

The experience we have gained from experiment E735 has allowed us to design an experiment that appreciably broadens our study of very high energy density $\bar{p}p$ interactions.

We propose to:

- Measure direct e^+e^- pair ($p_t < 3$ GeV/c) and photon ($p_t < 10$ GeV/c) production with a double arm electromagnetic calorimeter.
- Increase the detector aperture, momentum resolution and trigger selection, allowing a broad survey of low p_t meson and baryon production.
- Extend the identified $\pi/K/p$ measurements up to 3 GeV/c and the pion measurement below 150 MeV/c.

The unifying physics goal is to explore the low p_t (<3GeV/c) production region as completely as possible for $\bar{p}p$ collisions at the highest energy density. These measurements will be unique and we believe have considerable potential for the discovery of a quark-gluon plasma. The experiment will also provide a broad survey of low p_t particle production characteristics.

1.3.1 Electron-Positron Pair Production

The production of prompt leptons has been investigated extensively [Mikano *et al.*, 1980]. For e^+e^- pair masses, M, greater than 3 GeV/c^2, the major contributions are from J/ψ decays and Drell-Yan production. For 1.0< M <3.0 GeV/c^2, the decay of charmed mesons is one of the main sources. Recently, the e/π ratios of 1.0 $\times$ 10^{-3} for p_t=0.1 GeV/c and 0.5 $\times$ 10^{-3} for p_t=0.25 GeV/c were observed at the ISR [Akesson *et al.*, 1985]. This is much higher than expected from either hadronic bremsstrahlung or the semileptonic decay of charmed mesons. Not only was an excess of electrons observed but also the electron production rate increased as the square of the charged particle multiplicity.

It was pointed out [Adachi *et al.*, 1981] that the large e/π ratio at low p_t and the multiplicity dependence of the e/π ratio can be explained by thermodynamic models. Leptons would be produced from the annihilation of quark and antiquark in a quark-gluon plasma.

In contrast to most hadrons, which are produced from the later stage of the quark-gluon plasma via surface emission, the leptons (like prompt photons) are expected to be produced throughout the lifetime of the plasma and from the entire plasma volume [Müller, 1985]. Leptons could, therefore, be a much cleaner probe of the plasma stage than the various proposed hadronic probes. For example, the p_t spectrum of dilepton pairs could tell us the internal temperature of the plasma.

In addition to $q\bar{q}$ annihilation, electrons can also come from resonance decays. Effects of plasma formation on these decays could be studied. For example, the ρ meson has a very short lifetime (1.5 fm/c). Once it is formed, it would tend to decay within the plasma volume before it is dissolved. If it decays hadronically (π^+ and π^-), then the decay products would not escape the plasma. If it decays electromagnetically, then the e^+e^- pairs would escape the plasma. In other words, the branching ratio of the hadronic decay mode would be suppressed compared to the electromagnetic decay mode. Using the double arm spectrometer, the production cross section of both decay modes can be measured as a function of p_t and multiplicity. It has also been suggested that the mass and width of the

ρ would be changed if chiral symmetry is restored within the quark gluon plasma [Shuryak, 1981].

We propose to measure: (1) single electron and positron p_t spectra as a function of charged multiplicity; and (2) the invariant mass spectrum and p_t distribution of e^+e^- pairs from the continuum and from vector meson resonances such as ρ, ω, ϕ, and J/ψ. We will measure pairs with mass from 0.1 to 3 GeV/c^2 and p_t less than 3 GeV/c as a function of multiplicity.

1.3.2 Photon Production

We propose extending the scope of our study of low p_t processes by measuring the central production of photons with energies below 10 GeV. Photons provide a qualitatively different view of high energy density $\bar{p}p$ collisions since the direct photon spectrum is sensitive to the parton structure of the collision prior to hadronization. This would be a particularly valuable method of exploring the formation and evolution of a QGP. We would search for an increase of the $\gamma/\pi^{\pm}$ ratio and a change in the shape of the low energy gamma spectrum as a function of the collision energy density as measured by $dn/d\eta$. Any anomalous photon signals would then be correlated with other QGP signatures such as a rise in $< p_t >$, changes in K/π, Λ/p ratios, *etc.* Independent of the formation of a QGP, these photon data will provide constraints on hadroproduction models, being especially sensitive to central π° production.

Interest in the measurement of the low energy direct photon spectrum is enhanced by the observation of unexplained signals from two previous experiments. Data from collisions of K^+p at 70 GeV/c [Chliapnikov *et al.*, 1984] and p-Be at 450 GeV/c [Goerlach *et al.*, 1988] give evidence of large excesses of direct photons at low X_F and p_t. Theoretical attempts to explain these soft photons by standard hadronic production mechanisms have failed [Anderson *et al.*, 1988]. Recently Van Hove [Van Hove, 1988] speculated about the existence of a cold, non-thermal QGP state to explain these low energy photons and other low p_t hadron production phenomena.

1.3.3 Hadron Production

We will improve the π, K and p mass separation and extend identification from 1.2 GeV/c (E735) to 3 GeV/c (P787). These data, along with a larger detector acceptance and improved momentum resolution, will allow us to study a broad spectrum of low p_t hadron production. In particular, we will attempt to measure the $\pi : K : \phi$ and $p : \Lambda : \Xi : \Omega$ ratios as a function of n_c, p_t and $\sqrt{s}$. There are hints of strong variations of these ratios with these variables [Rafelski *et al.*, 1987]. It is important to make definitive measurements within a single experiment, especially at the highest collision energy currently available. The variation of these particle ratios may indicate the onset of new particle production mechanism thresholds. Our collaboration has already observed increases in the Λ/π and K/π ratios as a function of n_c, p_t and $\sqrt{s}$ in E735. A significant increase in these ratios would be an indication of abundant strange quark production via gluon-gluon collisions at high energy densities.

The presence of a low p_t peak in the pion spectrum has been reported in high multiplicity hadronic collisions [Willis, 1988]. Furthermore, low p_t direct photons and low mass dileptons have also been observed in these collisions. To test the idea of an extended (several fm) intermediate parton system [Van Hove, 1988] we will use a shorter flight path TOF detector to identify pions with p_t in the range 60 to 150 MeV/c interval. The detection of these low energy particles would provide important data for measuring the size of the intermediate parton system, which could be a QGP. In general these low p_t data will allow critical tests of ultrasoft hadron production models.

1.4 Detector Overview

The P787 detector will mass identify charged π's, K's, and p's with p_t between 50 MeV/c and 3 GeV/c. Electrons and γ's will be identified for energies less than 10 GeV. The design is based on experience gained from the E735 detector system. As shown in Figures 1.4.1a and 1.4.1b, the proposed detector is a double arm spectrometer. One arm would consist of the present spectrometer with some major modifications, while the other arm would be new. Since the

present E735 spectrometer arm worked very well, we decided to use the same basic design for the new arm: drift chambers for charged particle tracking before and after a dipole magnet (50MeV/c kick). Both arms would also have time of flight counters (250 *ps* FWHM) following the tracking chambers and new electromagnetic calorimeters. A RICH detector in one arm would provide mass identification for charged particles with momenta up to 3 GeV/c. Detailed descriptions of each component are given in Section 3.

The two spectrometer arms have sufficient acceptance to reconstruct mesons and baryons such as ρ's, K^*'s, ϕ's, K°'s, Λ°'s, Ξ's, *etc.* High resolution stereo drift chambers permit clear identification of the K° and Λ° decay vertices. The detector will also discriminate against e^+e^- pairs from Dalitz decays and pair conversions in the beam pipe. The high rejection of these pairs is very important in studying prompt e^+e^- production (see section 2.1.4 for details of background studies). The expected momentum resolution is

$$\frac{dp}{p} = \sqrt{(0.02)^2 + (\frac{0.03}{\beta})^2}$$

The electromagnetic calorimeters are designed to detect gammas and electrons with energy from 10 MeV to 10 GeV with resolution of

$$\frac{dE}{E} = \frac{2\%}{\sqrt{E(GeV)}}$$

The calorimeter in the detector room consists of a front end and an absorber. The front end, consisting of a thin converter, TOF scintillators and drift chambers, rejects low energy neutrals using time of flight and measures the direction of photons. In section 2.2, we present a Monte Carlo study discussing the background rejection and the reconstruction of photons.

The absorber made of NaI is divided into two sections longitudinally to improve electron identification and reject pions by using longitudinal shower profile. Monte Carlo study shows that the calorimeter can reject pions better than 1 in 5000 for the energy range above 100 Mev/c. With the aid of a Cherenkov counter the

rejection will be better than 1 in 10^5. A detailed Monte Carlo study of the pion rejection is described in section 2.1.

The calorimeter in the tunnel side is similar to the one in the detector room with a less sophisticated front end. This detector is designed mainly to measure electrons and positrons. Since the radiation level could be high in the tunnel ($\sim$1 rad/hour) we will fabricate the E.M. calorimeter using radiation resistant, short radiation length materials such as CsI or BGO.

A scintillator hodoscope will cover most of the central region ($-3.2 < \eta < +3.2$). The hodoscope and the spectrometer drift chambers in front of the magnet provide multiplicity and trigger information. The present E735 multiplicity hodoscope will be modified in order to accommodate the new detector system.

A trigger based upon the E735 design will be used for P787. At present, two sets of 15 scintillator counters are located $\pm$200 cm from the interaction region. The trigger requires one or more hits in each set and that they must be in coincidence with the beam crossing. High multiplicity events can be selected preferentially by using the multiplicity hodoscope and a trigger processor especially designed for the experiment.

To enrich the electron and photon sample, an electron trigger system will be based on the pulse height from the electromagnetic calorimeter. The detailed description of the electron trigger is discussed in section 3.2.

1.5 Time Table for Staging P787

For the purpose of presenting the overall schedule for the experiment we shall assume that Fixed Target and Collider runs will alternate starting at the begining of December each year and lasting for about 9 month each. Collider runs will, therefore, be assumed to take place starting 12/01/90 and 12/01/92.

Due to the budgetary and manpower restrictions of our collaboration we have decided to set the following order of priorities to evolve from the present E735 apparatus to the full P787 experiment:

During the remainder of 1989:

1. Approval of P787 from Fermilab's Program Advisory Committee.
2. Complete processing of the E735 data to the DST stage. Physics analysis will continue concurrently with preparation for P787.
3. Studies finalizing the basic parameters of the P787 detector.
4. Detailed design of the spectrometer room electromagnetic calorimeter in order to place the first commercial purchase orders at the begining of the new budgetary year. We estimate of the order of 12 month for delivery.
5. Design and procurement of parts for the second magnet on the tunnel side of the experiment.

1990:

1. Development of prototypes for all the new components with the view to partial installation at C0 for testing during the next collider run starting 12/01/90. This will include one set of pre- and post- magnet drift chambers, one cell of the RICH counter, Be beam pipe, parts of the TOF hodoscope and NaI detector.
2. Construction of the second magnet.
3. Detailed design of the tunnel side electromagnetic calorimeter in order to place the first commercial purchase orders at the begining of the new budgetary year. We estimate of the order of 12 months for delivery.
4. Detailed design of remaining components and trigger electronics.
5. Request for PREP electronics.
6. Detailed design of support structures.
7. Start construction of components based upon the final design.
8. Partial delivery of PREP electronics.

9. Partial installation, including second magnet, at C0.

1991:

1. Continue construction of detector components.
2. *Data taking with partially installed experiment at C0.*

1992:

1. Full availability of additional PREP electronics.
2. Completion of all detector components.
3. *Installation of the full experimental apparatus following the Fixed Target run.*

2 Proposed Measurement and Analysis

2.1 Dilepton Production

2.1.1 Introduction

Analyses of prompt e^+e^- pair production [Mikano *et al.*, 1980] indicates that the dominant production mechanism varies with e^+e^- invariant mass, M. For M>3 GeV/c^2, the production is well explained by the Drell-Yan mechanism [Kajante *et al.*, 1986]. Below 3 GeV/c^2, however, there has been observed an excess above the Drell-Yan prediction. Bjorken and Weisberg [Bjorken *et al.*, 1976] used a model in which partons produced in the collision process contributed to the low-mass dilepton production. Shuryak [Shuryak, 1978] later suggested that these partons may be partons in a QGP. In the very low dilepton mass range, M<600MeV, Domokos and Goldman [Domokos *et al.*, 1981] have also predicted that QGP produced dileptons would dominate. However, McLerran [McLerran *et al.*, 1985] has speculated that these low mass dilepton pairs may be produced from a hadron gas phase.

The P787 experiment will be sensitive to e^+e^- pair production with masses that span the range from about 100 MeV/c^2 to 3 GeV/c^2. We will therefore cover the production range appropriate to a QGP source.

2.1.2 Expected Rates

To make the proposed measurement, we must be able to cleanly identify electron and positrons and be able to reject prompt electron-positron pairs from Dalitz decay and photon pair production. In this section, we present a Monte Carlo study of electron identification and estimate the number of electrons and positrons and the e^+e^- pairs detected for a given luminosity.

Our calculation is based on an integrated luminosity of $0.1pb^{-1}$. The cross-section for lepton pair production from *pp* collision and *p*-nucleus collisions has been measured in various experiments. The

production cross section can be approximated by the expression:

$$\frac{(\frac{d\sigma}{dMdy})_{e^+e^-}}{(\frac{d\sigma}{dy})_{\pi^0}} = \frac{2.0 \times 10^{-5}}{M^2}\ GeV^{-1} \qquad (M\ in\ GeV)$$

This formula was used in our Monte Carlo detector simulation. We assumed that the rapidity distribution of the pairs is flat within our detector geometry, and that the p_t distribution is similar to the hadron p_t spectrum measured in E735.

In Figure 2.1.1, the expected number of single leptons ($e^+ + e^-$) is shown as a function of p_t. The total number of leptons will be of the order of 250,000 to 500,000. We should be able to explore the p_t spectrum as a function of charged multiplicity in detail. In figure 2.1.3, the spectrometer arm acceptance is plotted as a function of p_t for different pair mass, M. The vertical axis is the probability that the pair is identified in the spectrometer when the pair is produced within the pseudo rapidity $-4.0 \leq \eta \leq 4.0$. The typical values are $\simeq 2 \times 10^{-3}$

The simulated dilepton mass spectrum is shown in Figure 2.1.2. We also estimate the number of expected vector mesons (ρ's, ω's, ϕ's and J/ψ's). The number of pairs for a single arm is very small. With the double arm configuration, the number of pairs would be large enough to study vector meson production as a function of multiplicity. The expected number of ρ's, ω's, and ϕ's is about 3000 to 5000 each. The expected number of J/ψ's is about 300. For J/ψ calculation, we use the same p_t slope and cross section measured at UA1 [Bains, 1988].

2.1.3 Electron Identification

The electrons are identified by four methods: (1) Time of flight; (2) comparison of momentum measured in the spectrometer arm to energy measured in the calorimeter; (3) longitudinal shower development in the calorimeter; and (4) Cherenkov counters.

In order to study the pion rejection, we have used EGS3 and Geihsha7 for the electromagnetic shower development and hadron shower development respectively. Figure 2.1.4 and 2.1.5 show the result of the Monte Carlo study for pions and kaons respectively. In

the figure, the rejection factor from different identification method is shown separately. The calorimeter as a whole provides about 1 to 5×10^{-3} rejection (method 2 above). Using longitudinal shower development information improves the rejection by about a factor of 5. The cuts we used to reject hadrons are a function of momentum and about 85% of electrons pass the cuts. The measurement of the longitudinal shower development comes from the absorber which is divided into two sections longitudinally. (5 and 15 radiation lengths). The scatter plot of the energy deposited in the first section versus the second section is shown in Figure 2.1.6 for K^- and electrons. It clearly shows that the electron exhibit a very different shower shape compared to the K^-. TOF will help us to reject low energy pions, kaons and protons. Including the TOF, the hadron rejection is shown in the same figures. With TOF, the rejection is about 3×10^{-4}, which is not quite sufficient. To improve the rejection further, a Cherenkov counter will be used. Although a detailed study is not yet completed, we expect at least an additional factor of 20 to 50 rejection. With the Cherenkov counter, the overall probability of misidentifying pions would be much better than 1×10^{-5}.

2.1.4 Background Rejection of Dalitz Pairs and Photon Conversions (An addendum to this proposal discusses this section in more detail based on recent monte carlo simulations.)

The major background to our signal is from the Dalitz decay of pions and η's and the pair conversion of photons from the beam pipe and from the chamber windows. The radiation length of the Be pipe and the chamber window of the pre-magnet drift chambers is less than 0.5% radiation length.

We have made a Monte Carlo study of this background contribution. We generated 2γ and γe^+e^- decays of π^o's and η's. Some of the gammas are converted to e^+e^- pairs in the beam pipe and the first chamber's windows. Figure 2.1.1 shows the detected e^+ and e^- in the spectrometer arm. Here we assumed that the probability of the background pair rejection is 10^{-2}. (See addendum for a more realistic rejection factor.) The rejection method will be explained very shortly. In the same plot, the expected signal is plotted as de-

scribed earlier. As can be seen, the background is at least an order of magnitude less than the signal.

The background e^+e^- pairs are rejected by three methods. All the available information from the drift chamber just outside the beam pipe must be used.

First, for every identified electron or positron track from the spectrometer arm, the invariant mass will be calculated with other tracks, (other than identified hadrons) not only tracks in the spectrometer arm but also in the pre-magnet drift chamber. We point out that the solid angle of the drift chamber is much larger than the solid angle of the spectrometer arm. We reject the e^+e^- pair if the invariant mass is less than 100 MeV/c^2.

The second method used to reject backgrounds is to look at the charge on each wire along the the track of interest. If the sum of the charges is larger than expected from a single track, we reject the track. This rejects two close tracks from a gamma conversion. To obtain the charge on the wires we plan to use the flash ADC's, which are presently being used in the central tracking chamber, to read out the drift chambers.

The third background rejection method is to look at the unused drift chamber hits near the tracks. This is useful to reject very asymmetric gamma conversions or Dalitz pairs, in which a second electron is of very low energy and cannot be reconstructed.

2.2 Photon Production

2.2.1 Introduction

We propose to measure the central production of photons with transverse momentum between a few 10's of MeV and 10 GeV. This measurement will overlap with the low energy range of photon detection at CDF and D0 and provide new information about the photon production spectrum below a few GeV.

In general, these data will establish constraints on high energy hadroproduction models, being particularly sensitive to central π° production characteristics. Figure 2.2.1 shows the photon energy spectrum near 90° from $\sqrt{s} = 1.8$ TeV $\bar{p}p$ collisions as predicted by an ISAJET simulation. Our photon detector would cover a rapidity

range $-0.23 < y < +0.41$ for which 99.5% of the photons have energy less than 10 GeV.

More specifically, with regard to the main thrust of this experiment, we will be able to measure the shape of the low energy photon spectrum and the rate of photon production relative to charged hadrons. An enhancement of low energy photon production could occur if a QGP was formed. As with other QGP signatures we will measure this low energy photon signal as a function of the energy density of the $\bar{p}p$ collision as measured by $dn/d\eta$. For events containing a QGP, an excess of soft photons could be produced by quark bremsstrahlung and $g + q \rightarrow \gamma + q$ Compton scattering within the plasma. On the other hand, low energy photon production arising from neutral hadron decay (π^o's ,η's ,...) will be proportional to charged hadron production. In addition the shape of photon production spectrum below 100 MeV is dominated by the hadron decay properties and relatively insensitive to production characteristics of the parent hadrons. See Section 2.2.2 below for more details.

Finally we mention that unexplained low energy photon signals have been observed in hadron collisions at lower energies [Chliapnikov *et al.*, 1984 and Goerlach *et al.*, 1988]. Standard hadronic production models, including hadronic bremsstrahlung, have not been able to explain the observed photon excess [Anderson *et al.*, 1988]. We will be able to search for this soft photon production in $\bar{p}p$ collisions at $\sqrt{s} = 1.8$ TeV and, if an excess is observed, correlate it with other expected QGP signatures.

Section 3.1.5 describes the photon detector and reviews tests that have been made at the C0 collision region. Section 2.2.2 discusses the analysis approach we will use to search for an anamolous low energy photon signal.

2.2.2 Analysis of the photon data from P787 and preliminary results from E735

There is little known about the photon production characteristics from 1.8 TeV $\bar{p}p$ collisions. Our data will be used for two purposes. First, to study the photon spectrum from the electromagnetic decays of hadrons and second, to search for excess low energy photon signals.

The most basic analysis is to simply compare the measured photon p_t spectrum to that predicted by various QCD-based hadron production models (ISAJET, LUND, *etc.*). We are in the process of studying the ability of the photon spectrum below 10 GeV to distinguish between various models. A first look at the photon spectrum from hadrons generated by ISAJET is in general agreement with a preliminary measurement we have made using the E735 NaI prototype (see Figure 2.2.3). We will be able to study photon production with lower backgrounds, much higher statistics, better energy resolution and over a larger energy range with the P787 NaI detector.

To search for an excess low energy photon signal, we will estimate the contribution of low energy photons from hadron decay by fitting the photon spectrum above about 200 MeV, and extrapolating to low energies. This extrapolation is highly constrained by the hadron decay properties. This technique has been used in several previous experiments to search for low energy photon signals and has been capable of extracting the soft photons produced by hadronic bremstrahlung [Goshaw *et al.*, 1979 and Chliapnikov *et al.*, 1984]. The sensitivity of the P787 experiment to excess photons in the energy range from a few 10's of MeV to a few 100 MeV is currently under study using Monte Carlo simulations and the data being acquired from the E735 prototype detector.

2.3 Hadron Production

We propose to investigate three different kinematic domains of hadron production as a function of charged particle multiplicity. They are: (1) Production of strange particles (K, Λ, Ξ, and Ω^-) at intermediate p_t, (2) Low p_t (60 MeV/c< p_t <200MeV/c) pion production, and (3) Measurement of the yields of particles ($\pi^\pm$, $K^\pm$, $p^\pm$) and low mass vector mesons with two body decays (ρ, ω, ϕ) up to $p_t \approx$3GeV/c.

These measurements may reveal information on a new form of matter and are of general interest for models of particle production.

2.3.1 Study of Λ production and search for Ξ and Ω production in the central region

In an earlier paper we discussed [Banerjee *et al.*,1988] characteristics of Λ production at $\sqrt{s}$=1.8 TeV. Since our spectrometer arm can identify charged hadrons, it is also interesting to look for the $\Xi \rightarrow \Lambda + \pi$ and $\Omega \rightarrow$K+Λ final states with our improved tracking and acceptance. Monte Carlo acceptance calculations for Ξ and Ω acceptance are underway.

Making reasonable assumptions on production, equilibration and decay of QGP a striking prediction for the Λ/p ratio was obtained [Koch *et al.*, 1986]. The detailed arguments are given in Appendix A and the result for the Λ/p ratio as a function of temperature is given in Figure 2.3.1. It is thus obvious that we must measure the Λ/p ratio as a function of n_c. It is crucial to minimize the background and its variation with n_c under the Λ peak. In order to achieve that, we will build a high resolution, stereo drift chamber with multi-hit capability for accurate Λ decay vertex determination (see section 3.1.1). In addition with the help of the drift chamber on the tunnel side, the primary vertex location will be accurately determined. Particle identification will be improved by the double signature of a Cherenkov counter and TOF. Finally, we will make a three constraint fit to all Λ candidates. Thus we will obtain a clear signal for the Λ/p ratio variation as a function of charged particle multiplicity.

2.3.2 Low p_t hadron physics

Reports of sharp peaks of $d\sigma/dp_t^2$ at p_t <100MeV/c have been reported. [Willis, 1988] Tying together the above results with low p_t lepton and photon enhancement, Van Hove [Van Hove, 1988] suggested that they are all the manifestations of a cold QCD plasma. Since we can measure all three signatures in one experiment we can have conclusive experimental evidence for the existence or nonexistence of such a system. These events may also be related to enhancements in rapidity density $dn/d\eta$ as discussed by Peschanski [Bialas and Peschanski, 1988].

The measurement will be made with the tunnel side magnetic-TOF spectrometer (see Figure 1.4.1) with the magnetic field in the

magnet lowered to ~1kG. We would make this measurement during the 1991 collider period.

2.3.3 p_t of π, K, p, ρ, K*, and ϕ production up to p_t = 3GeV/c

Using the magnetic-TOF spectrometer in E735, we were able to obtain mass indentified p_t distributions for π, K, and p up to 1.5 GeV/c. With the help of a Cherenkov counter the range of mass identification can be extended to 3 GeV/c. Since the single arm acceptance for ρ, K* and ϕ increases with p_t, we will be able to measure the n_c dependence of ϕ and, with lesser acceptance, that of ρ and K*.

3 The P787 Detector

The P787 experimental apparatus is shown in Figures 1.4.1a and 1.4.1b. A detailed description of the individual components is given in the following sections. With the exception of the proposed RICH counter, our collaboration has successfully built similar devices for E735. Although the general description of each component is accurate, the detail will change as more design studies are made. For example, the exact number of sense wires assigned to each chamber view and some of the readout details may change. The individual components are also identified by the abbreviations shown in the apparatus figures.

3.1 The Spectrometer Components

3.1.1 Pre-magnet Drift Chambers (PRDC)

Two of these chambers are required, one for each spectrometer arm. We have borrowed extensively from our experience with E735 Central Tracking Chamber (CTC) by adopting a similar design for the drift cells, as shown in Figure 3.1.1. Each drift cell will consist of 10 sense wires and 22 field shaping wires. Cells are separated by an additional 11 high voltage wires. A total of 46 cells divided into 3 views x, u, v will form one chamber. The overall geometry of the x cells is shown in Figure 3.1.2 and of the u and v cells in Figure 3.1.3. The dimensions of a full chamber, including the cell locations are shown in Figure 3.1.4.

The two chambers will have a total of 920 sense wires. The same gas as for the CTC will be utilized (Argon, 4% methane, 1% CO_2), with a drift velocity of the order of 30 microns/ns. Readout of the pre-magnet chamber will utilize the 100 MHz flash ADC system in use with the E735 CTC. Because the FADC system provides multi-hit capability, only one end of each sense wire will be read. As with the CTC, we would expect a position resolution of less than 250 microns and a two track separation of the order of 3mm.

3.1.2 Post-magnet Drift Chambers (PSDC)

Two post-magnet drift chambers are required, one for each spectrometer. Their design follows from our experience with the straw drift chambers presently in use in E735. These are required because of the large angular range of the traversing particles. To obtain a more compact geometry we have chosen 2 cm diameter straws. The straw arrangement is shown in Figure 3.1.5. Like in E735, they will operate with Argon-10% Methane gas. We expect a resolution of the order of 200 microns. The small diameter straws allow us to increase our multi-track capability and the efficiency for detecting tracks correlated in space. Each post-magnet chamber consists of two sections. One with vertical wires (10 rows of tubes) and the other with slanted wires (6 rows of tubes). A total of 960 sense wires per chamber will be instrumented with the same type of single hit TDC electronics presently used for the E735 spectrometer straw chambers.

3.1.3 Threshold Cherenkov Counter (TC)

A final decision on the necessity of the Threshold Cherenkov counters to be installed within the two magnet gaps awaits a more detailed Monte Carlo study. The purpose is to provide e/π separation at momenta below 1.0 GeV/c. Freon 12 at atmospheric pressure is one candidate for the radiative media. Each counter will contain 6 or more cells constructed from thin aluminized mylar reflectors in order to keep the expected particle occupancy per cell to less than one. Cherenkov light will be reflected backwards and towards the top of the magnet by a series of thin planes of aluminized mirror installed on the downstream end of the detector. Ray-tracing studies are presently under way to study the photon efficiency of such a geometry. In addition, two possible detection schemes are under evaluation:

- Winston cones and light guides transmiting the light to phototubes on top of the magnets;
- a compact TEA chamber separated from the radiator by a quartz window installed just below the magnet coil. The design

of this chamber will be identical to the one to be built for the RICH counter below. A larger number of cells could then be considered.

3.1.4 RICH Cherenkov Counter (RICH)

The RICH counter under development follows closely a counter recently discussed in the literature [Arnold *et al.*, 1988]. The proposed counter is designed for particle identification below 3 GeV/c and has the advantage of a very short length, 20 cm, as sufficient number of photons are emitted from the 5 mm thick NaF radiator. The length of the counter is determined by the requirement that the radii of the rings become measurable in the photosensitive TEA or TMAE drift chamber. Due to the proximity of the electromagnetic calorimeter a TEA chamber appears more convenient in order to avoid operating at higher than room temperatures.

As shown in Figure 3.1.6, the counter will be built in 4 modules 20 cm wide and approximately 50 cm high at the NaF entrance radiator and 65 cm high at the exit CaF_2 window. Within each module the NaF radiator will be constructed of 4 x (5" x 8") and the CaF_2 drift chamber window of 4 x (6.5" x 8") crystals. The type of readout and optimum segmentation is under study. Two possibilities exist:

- A MWPC with about 5 mm wire spacing for charge amplification in conjunction with 1 cm x 1 cm pads for position readout. A total of 5200 electronic channels would then be required.
- A modification of the post-magnet straw drift chambers with open slots for the entrance of the photoelectrons. Charge division, in conjuction with the FADC pre-magnet chamber system, could be used for measuring the position along the wire. Eighty channels of FADC would then be necessary.

3.1.5 Spectrometer Room Electromagnetic Calorimeter (NAI)

The layout of the electromagnetic detector is shown in figure 3.1.7. It consists of a thin (0.1 radiation length) copper converter followed by y and z drift planes, a time of flight (TOF) scintillator hodoscope and a calorimeter composed of an array of NaI blocks.

The copper radiator will convert 5 to 8% of the incident photons, producing e^+e^- pairs which will traverse the drift planes. The drift planes are made up of 1.5 cm diameter straw tubes with four z measuring planes (vertical tubes) and four y measuring planes (horizontal tubes). Our experience with 5 cm diameter drift tubes in the E735 spectrometer shows that we should be able to determine spatial position of charged tracks in the drift planes to an accuracy of 200 microns. ~~There will be four z planes and four y planes~~.

The trajectory of a converting photon will be determined by measuring the positions of the produced e^+e^- in the y and z planes and reconstructing from these points the slopes for the gamma. This trajectory is then projected back to the beam line. Simulation studies with the shower program EGS indicate that we can use this method to predict the point of origin of the converted gammas at the beam line to within 10 cm (sigma) for photon energies as low as 50 MeV. The beam interaction vertex position will be known to a few mm from the reconstruction of produced charged tracks in the drift planes nearest the beam line.

The TOF hodoscope, situated between the drift planes and the calorimeter, will be used to determine whether a photon which converts in the copper radiator is synchronous with the beam interaction. Particles from the $\bar{p}p$ interaction which subsequently scatter in the spectrometer magnet yoke can result in neutrons, K^o's and photons which will enter the electromagnetic detector. They will arrive at the detector later in time than photons traveling directly from the beam interaction and can be discriminated against. The TOF hodoscopes employed in E735 provide timing resolution of 250 picosec FWHM. We should be able to reject photons that are out of time by 1 nanosec (4 sigma).

The NaI calorimeter consists of a 10 x 15 array of 10 cm square blocks; the front face is 125 cm from the beam line. The depth of the calorimeter will be 20 radiation lengths so as to be a total absorber for incident photons up to 10 GeV energy (punch through for 10 GeV photons $< 1.5\%$). The calorimeter will include a 0 radiation length NaI active converter in front of it which will provide information used to distinguish between charged hadrons and electrons incident on the calorimeter.

The signal from each NaI block will be split into two. One will

5

have high gain (full ADC count for 400 MeV energy deposition) and the other will have low gain (full ADC count for 10 GeV energy deposition). This will provide good energy resolution over a large dynamic range.

3.1.6 Tunnel Side E.M. Calorimeter (EM2)

The tunnel side electromagnetic calorimeter will be similar to the one in the spectrometer room except that it will not have a front-end with drift chambers and TOF. However this detector will be subject to considerable radiation exposure over the entire length of the experiment. The actual choice of material (CsI, BGO, *etc.*) is presently under study.

3.1.7 Multiplicity Hodoscope (H)

The scintillator counter hodoscope will serve the same functions for P787 as it did for E735. Online, it will provide a fast indication of the event multiplicity so the trigger system can scale down the number of low multiplicity events written to tape in favor of the more interesting high multiplicity events. Offline, the hodoscope will serve in combination with the inner drift chambers to determine the charged multiplicity in the central region.

As much of the previous system will be used as possible. Although, the counters will have received as much as 15Krad by the end of the 1988-89 run, they still should be usable up to 50Krad dose [Lindsey *et al.*, 1987]. Any counters which show deterioration will be repaired or replaced.

In Figure 1.4.1a are shown the P787 endcap counter arrays' position. The two inner rings (of 24 counters each) from E735 will be brought closer to the intersection region in order to avoid particles showering from the edges of the magnet iron. Figure 1.4.1b shows the new position of the "barrel" counters (which previously surrounded the central tracking chamber). They will now cover the region above and below the beampipe.

This arrangement reduces the segmentation from 240 counters to about 120. Used in combination with the inner drift chambers, this should be sufficient for the trigger and for offline multiplicity deter-

mination. If further study shows that more segmentation is required, other counters can be added using either the previous counters or making new ones.

3.1.8 TOF counters

The TOF arrays used for triggering and interaction time measurement during E735 would need to be reconstructed to allow for the new geometry around the beam pipe. The TOF1 and TOF2 arrays from E735 would be dismantled and reconstructed to build the TOF counters at the entrance of the two electromagnetic calorimeters.

3.1.9 Magnets

The present E735 spectrometer magnet will be used with only minor mechanical modifications and a change in position in the C0 pit floor.

The second magnet design will follow closely the design of the first. A smaller magnet is required. We expect that the same mechanical drawings and tooling for the first magnet could be utilized with only some dimensional changes.

3.2 Trigger

3.2.1 Interaction Trigger

The lowest level trigger on the experiment is that of the detection that an interaction has taken place at the time of the crossing. As for the E735 detector this trigger will be provided by two sets of TOF counters located approximately 2.1 meters upstream and downstream of the C0 interaction point. This distance allows for a clean separation between beam-beam events and those originating upstream or downstream of the interaction region (beam-gas events). In addition, interactions due to beam present in neighboring bunches can also be rejected by timing. The TOF/TRIGGER counter hodoscopes "P" and "PBAR" utilized for E735, with a time resolution of 250ps FWHM are perfectly adequate for P787 as well. Two sets of Beam Halo Veto hodoscopes from E735, located approximately 4.5 m on either side of the interaction point provide a

more clear time separation for beam-gas events associated with near bunches. During experiment E735 an "interaction trigger" rate of the order of 400 Hz was measured for CDF luminosities of the order of 1×10^{30}.

3.2.2 Hadron Production Trigger

A Trigger Processor (TP), providing trigger scaling based upon the hodoscope hit multiplicity will be utilized to reduce the 400 Hz first level trigger rate. This TP will be an upgraded version of the one that has worked well in E735.

3.2.3 Single and Dilepton Trigger

For a clean lepton signal, that is to optimize the amount of lepton events recorded on tape, a rejection of the order of 1×10^{-2} is necessary with respect to triggers originating from pions.

3.3 Data Acquisition System

The data acquisition system for FNAL P787 will utilize a VAX-6310 computer and an existing VME system, developed for FNAL E735, extended into a second crate. A possible configuration is shown in Fig. 3.2.1. The data from FADC's, CAMAC and FASTBUS are read out in parallel by front-end VME microcomputers, preprocessed and stored in their local memory buffers. The DMA device, under control of a supervisory processor, copies segments of an event from FEP's into contiguous, multievent buffers in memory ("stand alone" on VME bus), formatting the event appropriately for magnetic tape interface.

The mode of transfer (maximum or limited-rate, with or without-hold) is decided by the Supervisor on an event by event basis in order to minimize a bus and dual-port memory arbitration overhead. The Supervisor maintains an Output Queue, it administers DMA transfers to magnetic tape in an asynchronous manner. Every n^{th} event (n=1,2...) is transferred to the VAX for monitoring hardware performance, online track reconstruction, full event display, *etc.* The VAX may also request a specific type of event. There are two 6250

Bpi, 125 Ips tape drives in the system. A third tape drive on VAX-6310 is used to read (analyse) events taken earlier.

The existing VME system is based on Microsys' CPU07 microcomputer boards supporting standard (24 bit) addressing. Assuming, that no extended (32 bit) addressing CPU boards are introduced into the existing VME system (which potentially may create hardware, as well as software incompatibility problems), the proposed configuration does not give much room for further expansion: the 16 MByte address space is almost fully utilized.

This problem can be circumvented by connecting two crates in DR11W-DR11W type manner for which we have the necessary hardware. In that configuration two crates would operate as two independent 16 MByte computers, communicating with each other with a protocol similar to that of the CD driver. Additional advantage of that kind of solution would be a 50% decrease of bus traffic and consequently a substantial increase in system performance. In this "loosely coupled" system the front-end processors and interfaces to experimental apparatus would be kept all in one crate, the data buffers, magnetic tape and host interfaces in another crate. Additional CPU's (ACP-RISC type) could be easily incorporated into the system within the second crate for online or offline data analysis.

The data acquisition programs are written mostly in RTF68K FORTRAN, some real-time routines in AS68K assembler. Both are available from CERN. They run as native compilers on CPU07 computer under CPM-68 operating system. This makes the system virtually independent from a host computer. This has proven to be very convenient, especially on a test stage of program development and hardware testing. The compilers are able to generate code for 68000, 68010 and 68020 processors. Data acquisition software runs without support of any operating system after it is downloaded from hard disk by one of the VME computers. The RTF68K cross-compiler under VMS exists. A greatly inproved version of RTF68K which supports FASTBUS and DR11W interfaces is now available from CERN.

3.4 Accelerator Issues

In order to increase the lower momentum limit of particles towards the two spectrometer arms and to minimize the number of photon conversions, we would like to request the replacement of the existing aluminum beam pipe with a beryllium one. Assuming that the Tevatron proton abort line will not be utilized during collider running, the new beam pipe should be centered on the Tevatron beam and of dimensions comparable to the beryllium pipe presently installed at B0 (CDF).

A Theoretical Arguments for Strangeness Enhancement in Deconfined Hadronic Matter

In order to compute quantitive predictions for strangeness production in Centrally Produced Hadronic Matter (CPHM) one has to make general assumptions as well as detailed parametrizations. In this section we give a brief description of the important steps and results based on the paper of Koch *et al.*[Koch *et al.*, 1986].

A.1 Production Mechanism

There are two commonly accepted consequences of the standard model:

1. Both the gluon (g) density and small x collision cross section increases rapidly with $\sqrt{s}$.

2. There is a large cross section for strange quark (s) production via the elementary process:

$$g + g \rightarrow s + \bar{s}$$

   Based on considerable experimental evidence, it is further assumed that if the size of CPHM is greater than r$\geq$ 2 fm and the number of produced particles is sufficiently large, then:

3. The concept of temperature (T) (hadron thermodynamics) is meaningful. The parameter which controls decisively the predictions of strange quark abundance and yet least amenable to direct measurement is the strange quark mass (m_s). Fitting the stable particle mass spectrum one can deduce:

4. $m_s \simeq$170 MeV. Since the Deconfined Hadronic Matter or Quark Gluon Plasma (QGP) in CPHM has T$\geq$170 MeV, a profuse strange particle production is expected. We have to emphasize that the basic pair production subprocess $g + g \rightarrow s + \bar{s}$ is in principle the same for both phases of hadronic matter: hadron gas and QGP. However in the case of separated hadrons reaction 1 can only take place during the actual collision process,

which means that strange quark production has a strict constraint in space, time and phase space. On the otherhand, if QGP is formed with a reasonable space-time extension at high T with a very large phase space, a large enhancement of strange quark production is expected (r>2 fm, t$\simeq 2 \times 10^{-23}$ sec, T$\geq$ 170 MeV).

A.2 Production Rate and Chemical Equilibrium

In order to predict the strangeness abundance, one has to calculate the strangeness production rate per unit volume and the time constant for chemical equilibrium. The equilibrium time (t) must be less or of the order of QGP lifetime: t$< 2 \times 10^{-23}$ sec. The calculation assumes (1) the subprocesses

$$g + g \rightarrow s + \bar{s}$$

$$q + \bar{q} \rightarrow s + \bar{s}$$

and (2) Bose-Einstein and Fermi-Dirac distributions for the momentum distribution of the quarks and gluons. The results show that t depends on the strength of the coupling constant, the mass of the strange quark and the temperature. When $m_s \leq$ T and T$\simeq$ 200 MeV, one finds that t is comparable or less than the QGP lifetime (2×10^{-23} sec). In general, strange quark production will become more strongly enhanced with higher t and coupling strength and with lower m_s.

A.3 Conversion from the QGP to Hadronic Phase

The entropy of QGP is proportional to the number of quarks and gluons from which it is made. Since quark pairs form mesons and gluons in $g \rightarrow q + \bar{q}$ transitions also form mesons, after QGP $\rightarrow$ hadrons phase transition entropy would decrease. To be consistent with the Second Law of Thermodynamics, one has to assume that there must be a third elementary process in hadronization. Since a $q\bar{q}$ pair is in a color singlet state in only one out of nine cases, a $q\bar{q}$ pair must usually radiate a gluon in order to recombine into a meson.

1. The three elementary processes which dominate hadronization are

$$q + \bar{q} \rightarrow \pi$$

$$q + \bar{q} \rightarrow \pi + g$$

$$g \rightarrow q + \bar{q}$$

The breakup process is assumed to proceed in a single direction: quarks coalesce to form hadrons. The inverse reactions are neglected. The above assumptions are combined with the Combinatorial Breakup Model, which assumes:

2. Quarks are distributed among final state hadrons by two constant probabilities: one for meson and one for baryon production. For example:

$$N_{nucleon} = \frac{\beta}{3!} \times N_q^3$$

$$N_Y = \frac{\beta}{2!} \times N_q^2 \times N_s$$

$$N_p = \alpha \times N_q \times N_{\bar{q}}$$

3. Combining thermal and chemical equilibrium with gluon radiation corrections $N_q, N_{\bar{q}}$ and N_s can be calculated and the prediction for ρ_Y/ρ_N ratio can be calculated (See Fig. 2.3.1). There is an order of magnitude enhancement for this ratio in QGP compared to hadron gas.

B Lepton Pair Production from the Centrally Produced Hadronic Matter

From lepton number conservation, leptons and antileptons are produced in pairs. Let Q_μ denote the sum of dilepton four momenta, then the mass of the dilepton system (m_d) is $m_d = \sqrt{Q_\mu Q_\mu}$. For the purpose of experimental study, the dilepton mass spectrum has been divided [Kajante *et al.*, 1986] into three regions:

$m_d > 3$ GeV	(Drell-Yan region)
1 GeV$< m_d <$ 3 GeV	(QGP region)
140 MeV $< m_d <$ 600 MeV	(Hadronized gas region)

B.1 Drell-Yan Model for Lepton Pair Production.

According to this model the origin of the dileptons is electromagnetic: Constituents of the colliding hadrons annihilate into virtual (timelike) photons which convert into dilepton pairs. For massive lepton pairs ($m_d > 3$ GeV) the theoretical results are compatible with experiments. However, for small dilepton masses and small transverse momenta, the Drell-Yan formula needs to be corrected.

B.2 Modification of the Drell-Yan Model

Bjorken and Weisberg [Bjorken *et al.*, 1976] considered the contribution of partons which were produced in the collision process. Thus the parton density function in inelastic hadron-hadron collision can be at least five times larger than the density function extracted from hadron structure function νW_2, which was measured by lepton probes. This modification brings the theoretical prediction in agreement with experiments. This implies that the excess lepton yield is made up of low-mass ($m_d < 3$ GeV) dileptons produced at high total transverse momentum. Viewing the time development of the QGP, McLerran and Toimela concluded [McLerran *et al.*, 1985] that massive, high p_t dileptons are emitted in the early stages of the collision. Thus there is a relationship between the age of the plasma and the dilepton mass. Approximately one has t $\propto$ m_d^{-1} [Adachi *et al.*, 1981].

B.3 The low mass ($m_d <$ 600 MeV) region

For this mass range there are contradictory predictions. While Domokos and Goldman predict [Domokos *et al.*, 1981] that QGP produced dilepton pairs dominate this mass range, McLerran predicts that these pairs are emitted from the matter after it has cooled down [Kajante *et al.*, 1986] below the hadron gas phase.

References

[Adachi *et al.*, 1981]
Adachi *et al.*, Phys. Rev. **D23**(1981) 1106;
Shuryak, Phys. Reports **61C**(1980) 71.

[Akesson *et al.*, 1985]
Akesson *et al.*, Phys. Lett. **152B**(1985) 411.

[Alexopoulous *et al.*, 1988]
Alexopoulous *et al.*, Phys. Rev. Lett. **60**(1988) 1622.

[Anderson *et al.*, 1988]
Anderson *et al.*, LUND pre-print LUTP 88-1.

[Arnison *et al.*, 1982]
Arnison *et al.*, Phys. Rev. Lett. **118B**(1982) 167.

[Arnold *et al.*, 1988]
Arnold *et al.*, NIM **A273**(1988) 466.

[Bains, 1988]
Bains, Ph.D. Thesis, University of Birmingham (1988) 99.

[Banerjee *et al.*, 1988]
Banerjee *et al.*, Phys. Rev. Lett. **62**(1988) 12.

[Bialas and Peschanski, 1988]
Bialas and Peschanski, Phys. Lett. **207B**(1988) 59.

[Bjorken *et al.*, 1976]
Bjorken and Weisberg, Phys. Rev. **D13**(1976) 1405

[Chliapnikov *et al.*, 1984]
Chliapnikov *et al.*, Phys. Lett. **B141**(1984) 276.

[Domokos *et al.*, 1981]

Domokos and Goldman, Phys. Rev. **D23**(1981) 203.

[Dowell *et al.*, 1988]
Dowell *et al.*, (1988) CERN-EP188-137.

[Fincke-Keeler, 1989]
Fincke-Keeler, Ph.D. thesis, University of Victoria (1989).

[Goerlach 1988]
Goerlach, Proc. 24th Int. Conf. on High Energy Physics, Munich (1988).

[Goshaw *et al.*, 1979]
Goshaw *et al.*, Phys. Rev. Lett. **43**(1979) 1065.

[Hagedorn *et al.*, 1980]
Hagedorn and Rafelski, Phys. Lett. **97B**(1980) 136;
McLerran and Svetitsky, Phys. Lett. **98B**(1981) 195
Kuti, Polonyi and Szlachanyi, Phys. Lett. **98B**(1981)199;
Van Hove, Phys. Lett. **118B**(1982) 138;
Bjorken, Fermilab Pub. 82/44-PHY;
Kogut *et al.*, Phys. Rev. Lett. **51**(1983) 869;
Engels *et al.*, Nucl. Phys. **B205**(1982) 545.

[Kajante *et al.*, 1986]
Kajante *et al.*, Phys. Rev. **D34**(1986) 2746;
Kajante and McLerran, Ann. Rev. Nucl. Part. Sci. **37**(1987) 293.

[Koch *et al.*, 1986]
Koch *et al.*, Phys. Reports **142**(1986) 162;
Barz *et al.*, Nucl. Phys. **A484**(1988) 661.

[Lindsey *et al.*, 1987]
Lindsey *et al.*, NIM **A254**(1987) 212.

[McLerran *et al.*, 1985]
McLerran and Toimela, Phys. Rev. **D32**(1985) 1109.

[Mikano *et al.*, 1980]
Mikano *et al.*, Phys. Rev. Lett. **D22**(1980) 2107;
Blockus *et al.*, Nucl. Phys. **B201**(1982) 205;
Adams *et al.*, Phys. Rev. **D27**(1971) 1983;
Anderson *et al.*, Phys. Rev. Lett. **37**(1976) 799.

[Müller 1985]
Müller, *The Physics of the Quark Gluon Plasma*, Springer-Verlag, (1985)46;
Kajante and McLerran, Ann. Rev. Nucl. Part. Sci. **37**(1987).

[Rafelski *et al.*, 1987]
Rafelski and Danos, Phys. Lett. **192**(1987) 432.

[Shuryak, 1978]
Shuryak, Phys. Lett. **78B**(1978) 150;

[Shuryak, 1981]
Shuryak, Phys. Lett. **107B**(1981) 103.

[Shuryak, 1988]
Shuryak, *The QCD Vacuum, Hadrons and the Superdense Matter*, World Scientific (1988);

[Van Hove, 1986]
"Prospects for Production and Detection of a Quark-Gluon Plasma," 5th International Conference of Ultra-Relativistic Nucleus-Nucleus Collisions (Quark Matter '86).

[Van Hove, 1988]
Van Hove, CERN-TH, 5236/88.

[Willis 1988]
Willis, Nucl. Phys. **A478**(1988) 151.

Figures

Figure 1.2.1	The E735 detector.
Figure 1.2.2	Hadronic matter energy density versus radius. The regions accessible for $\bar{p}p$ collisions at FNAL and for heavy ion collisions at CERN and RHIC are shown.
Figure 1.2.3	$< p_t >$ versus $dn/d\eta$ as measured in experiments E735 and UA1
Figure 1.4.1	Overview of P787 detector a) Plan view and b) Vertical cross section. H, hodoscope; TC, threshold Cherenkov counter; RICH, ring imaging Cherenkov counter; PRDC, pre-magnet drift chamber; PSTDC, post-magnet drift chamber; C, photon converter; DC1 and DC2, drift chambers; TOF, time-of-flight; NaI, NaI calorimeter; EM2, tunnel side calorimeter
Figure 2.1.1	Detected number of single electrons and positrons compared to the expected background from Dalitz and photon pair production. The background curve includes a rejection factor of 10^{-2}.
Figure 2.1.2	Detected pair mass distribution.
Figure 2.1.3	The probability that a pair can be detected when the pair is produced within the pseudo-rapidity -4.0 and 4.0. Each symbol represents different mass of pairs in GeV/c^2.
Figure 2.1.4	The π^- rejection probability using various detector components. With the threshold Cherenkov counter, the rejection should improve by at least a factor of 20-50.
Figure 2.1.5	Kaon rejection probability using various detector components. With a threshold Cherenkov counter, the rejection should increase by at least a factor of 20-50.
Figure 2.1.6	Fractional energy deposited by e^- and K^- in the first versus second section of the NaI detector.
Figure 2.2.1	Photon spectrum into NaI calorimeter from $\bar{p}p$ collisions at $\sqrt{s}$=1.8TeV. (ISAJET prediction)
Figure 2.2.3	Comparison of photon energy spectrum measured from E735 NaI calorimeter (raw, uncorrected data) to the prediction of ISAJET.
Figure 2.3.1	Theoretical prediction for the hyperon-baryon ratio

	as a function of the plasma temperature. [Koch *et al.*, 1986]
Figure 3.1.1	Design of a X-U-V Cell Triplet Plane View of the Upper Plane
Figure 3.1.2	Design of a Single Cell X Chamber Cross Section
Figure 3.1.3	Design of a Single Cell U Chamber Cross Section
Figure 3.1.4	Design of the Whole Chamber Triplet Plane View
Figure 3.1.5	Post-magnet Chamber
Figure 3.1.6	One of four modules of the proposed RICH counter. A detail of the TEA drift chamber is shown.
Figure 3.1.7	Detector Room Electromagnetic Calorimeter
Figure 3.2.1	On Line Data Acquisition System (P787)

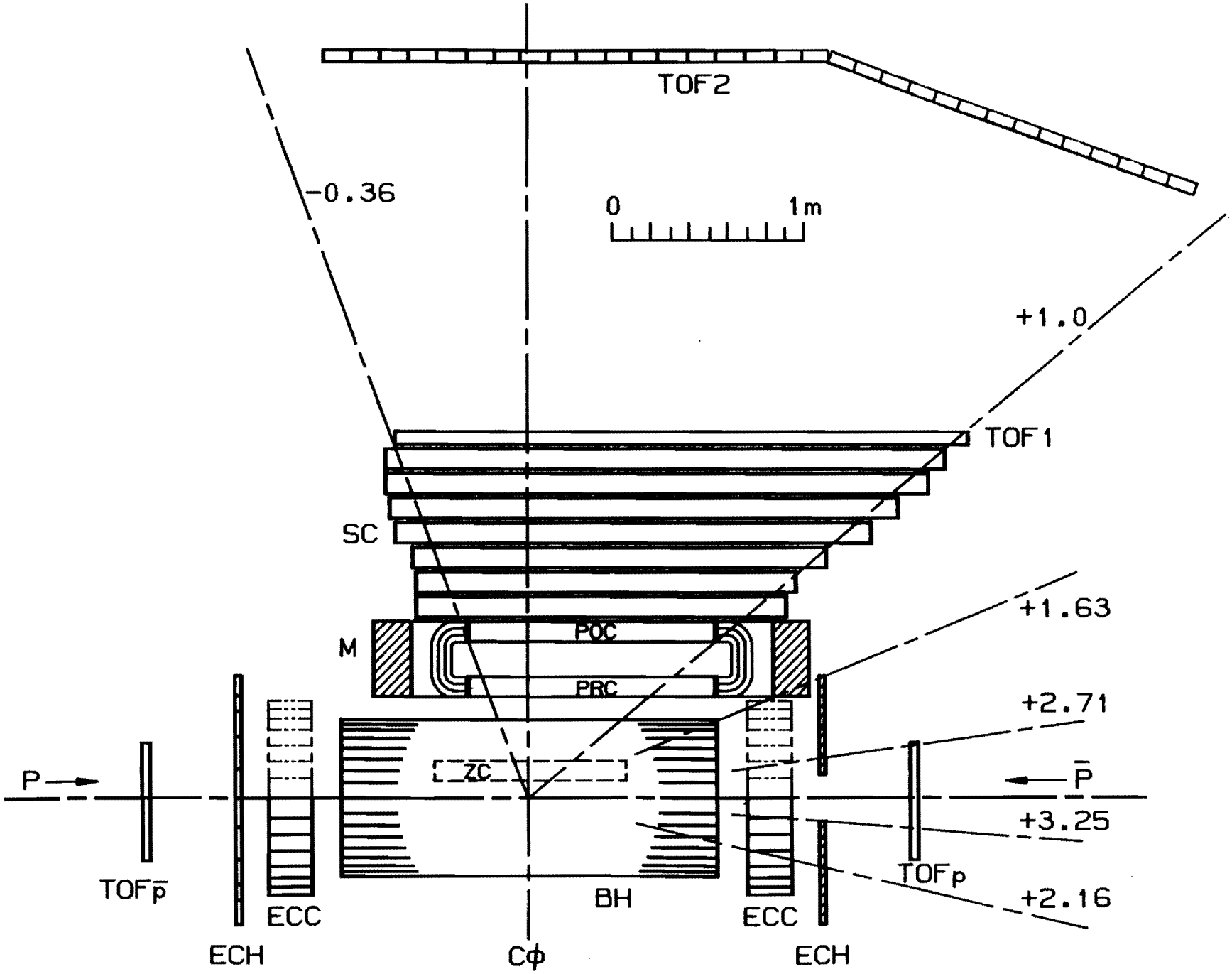

Figure 1.2.1 The E735 detector.

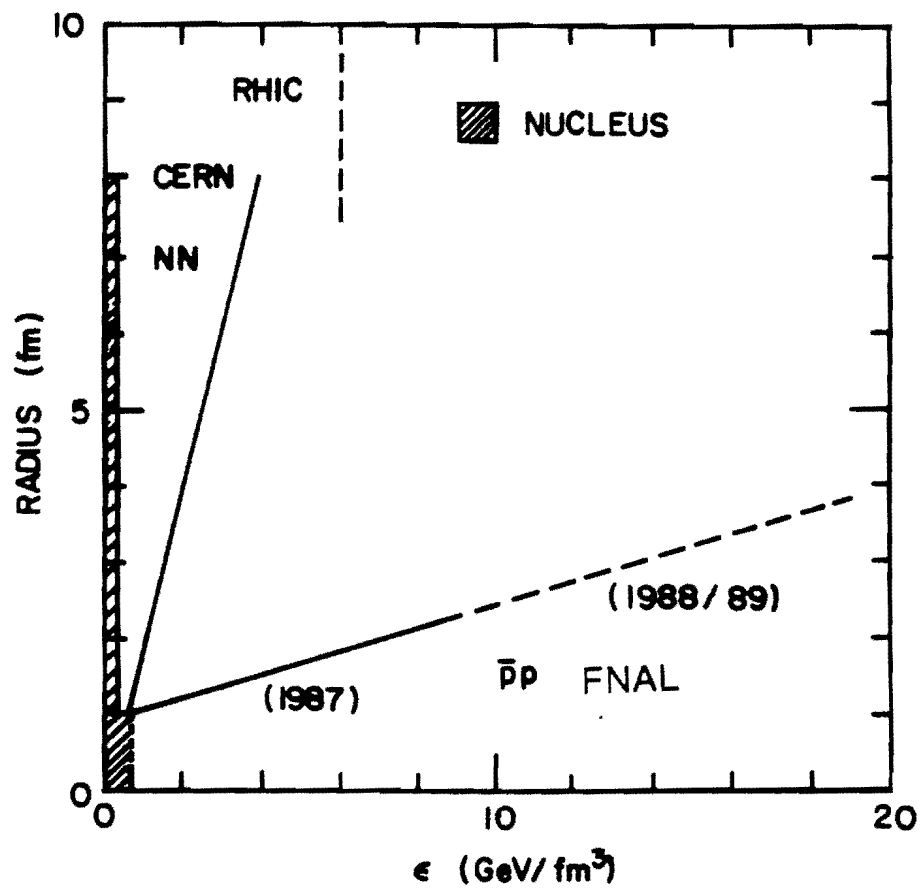

Figure 1.2.2 Hadronic matter energy density versus radius. The regions accessible for $\bar{p}p$ collisions at FNAL and for heavy ion collisions at CERN and RHIC are shown.

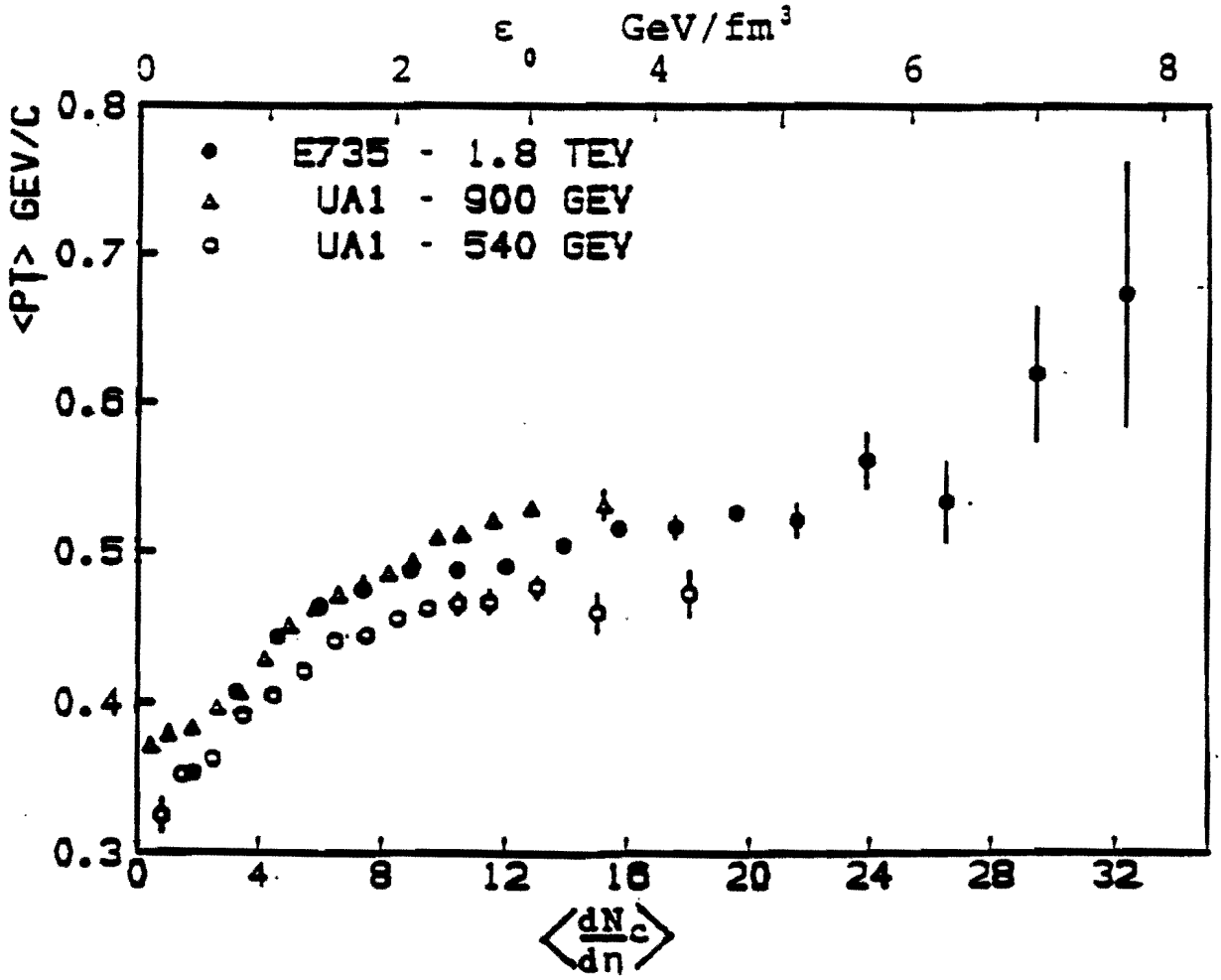

Figure 12.3 $< p_t >$ versus dn/dη as measured in experiment E735 and UA1.

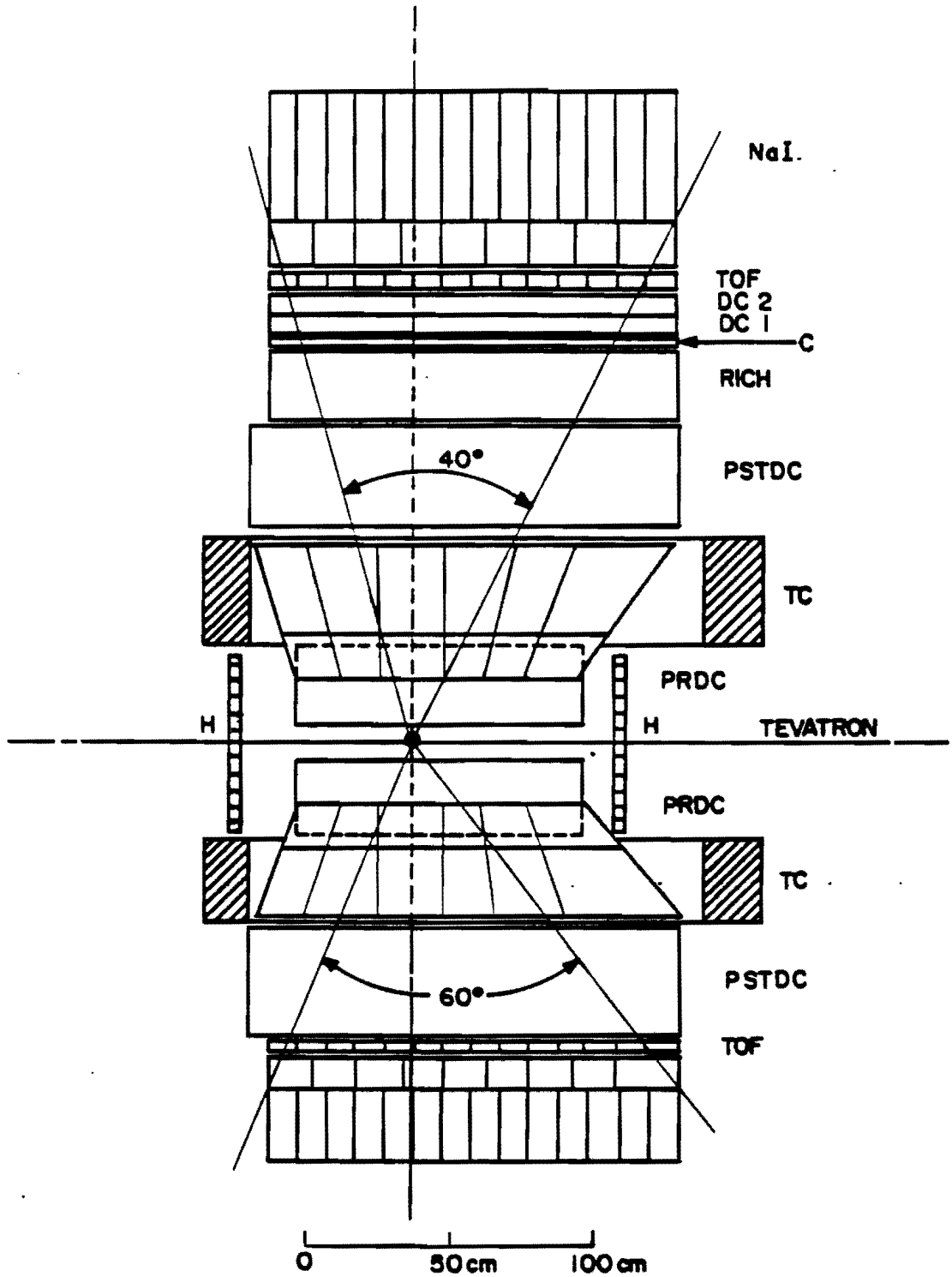

Figure 1.4.1 a. Overview of P787 detector a) Plan view and b) Vertical cross section. H, hodoscope; TC, threshold Cherenkov counter; RICH, ring imaging Cherenkov counter; PRDC, pre-magnet drift chamber; PSTDC, post-magnet drift chamber; C, photon converter; DC1 and DC2, drift chambers; TOF, time-of-flight; NaI, NaI calorimeter; EM2, tunnel side calorimeter

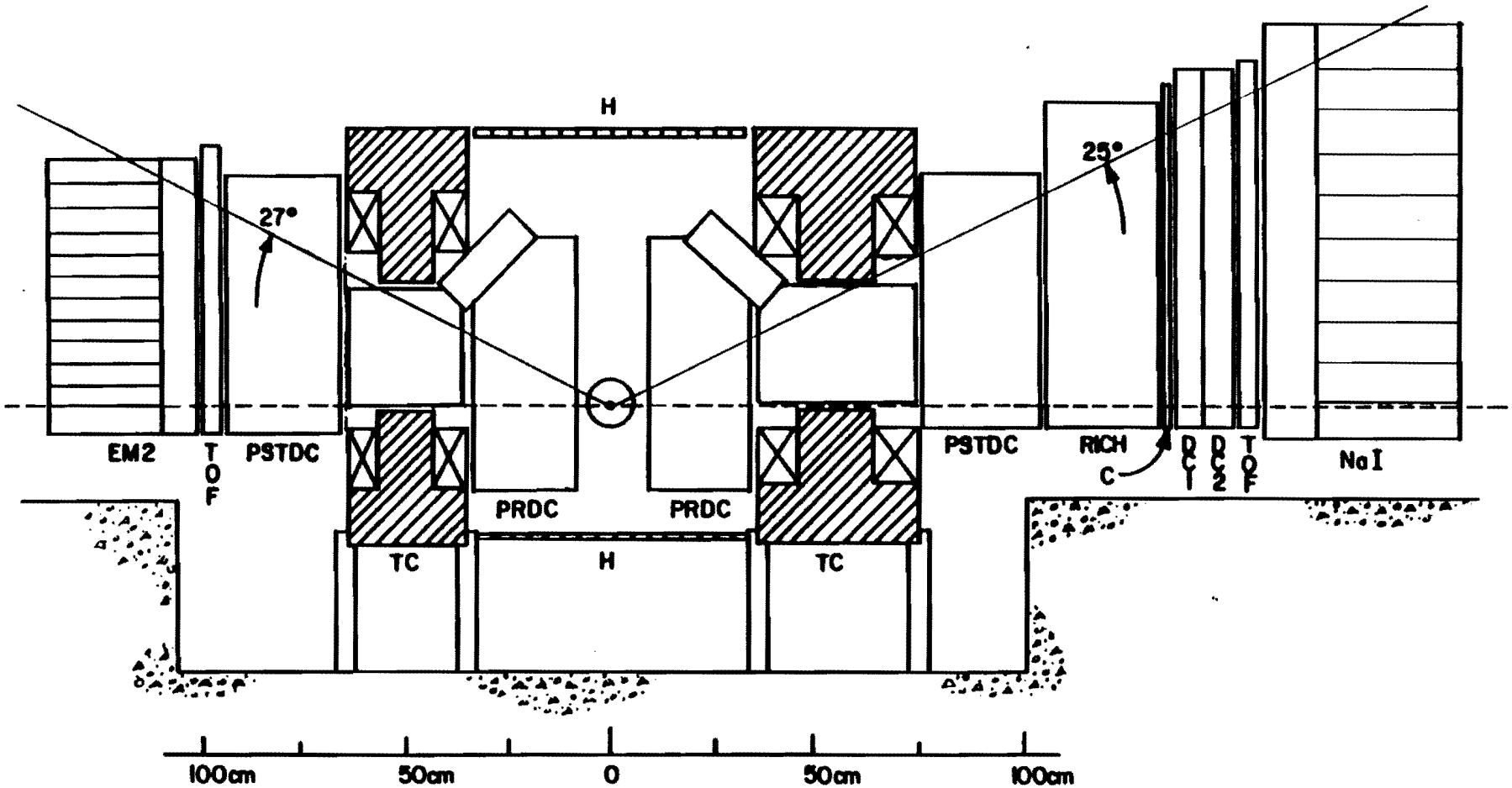

Figure 1.4.1 b Overview of P787 detector a) Plan view and b) Vertical cross section. H, hodoscope; TC, threshold Cherenkov counter; RICH, ring imaging Cherenkov counter; PRDC, pre-magnet drift chamber; PSTDC, post-magnet drift chamber; C, photon converter; DC1 and DC2, drift chambers; TOF, time-of-flight; NaI, NaI calorimeter; EM2, tunnel side calorimeter

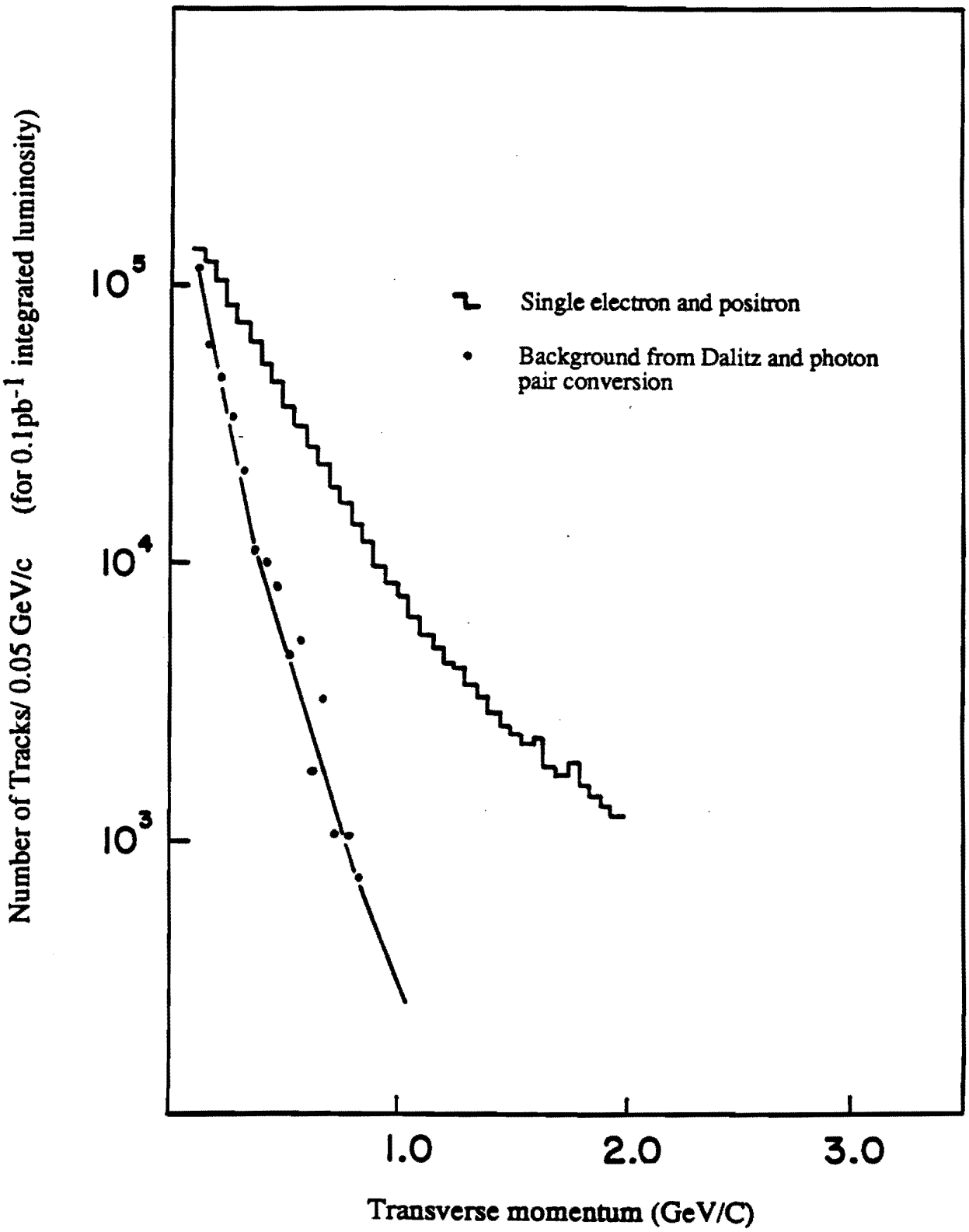

Figure 2.1.1 Detected number of single electrons and positrons compared to the expected background from Dalitz and photon pair production. The background curve includes a rejection factor of 10^{-2}.

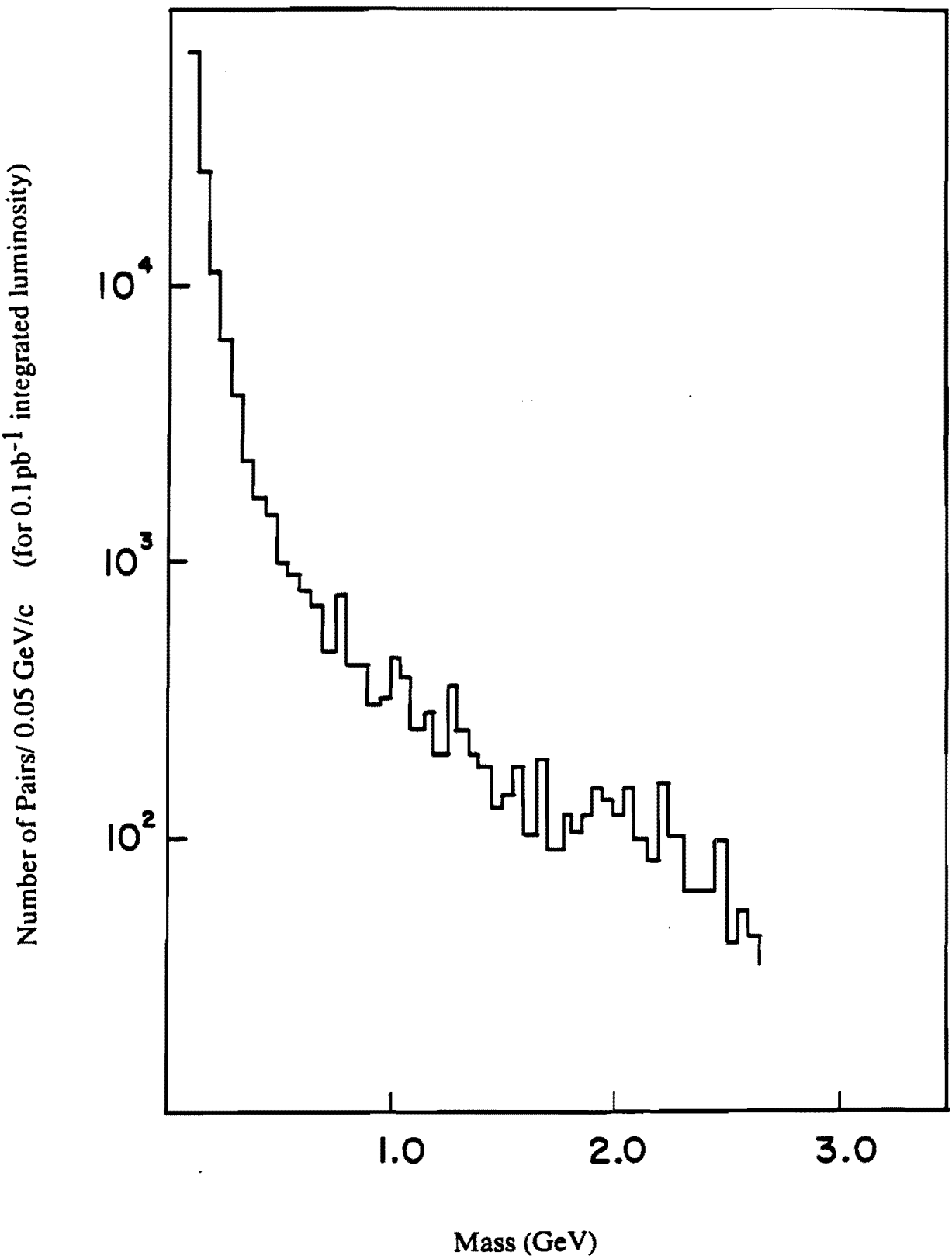

Figure 2.1.2 Detected pair mass distribution.

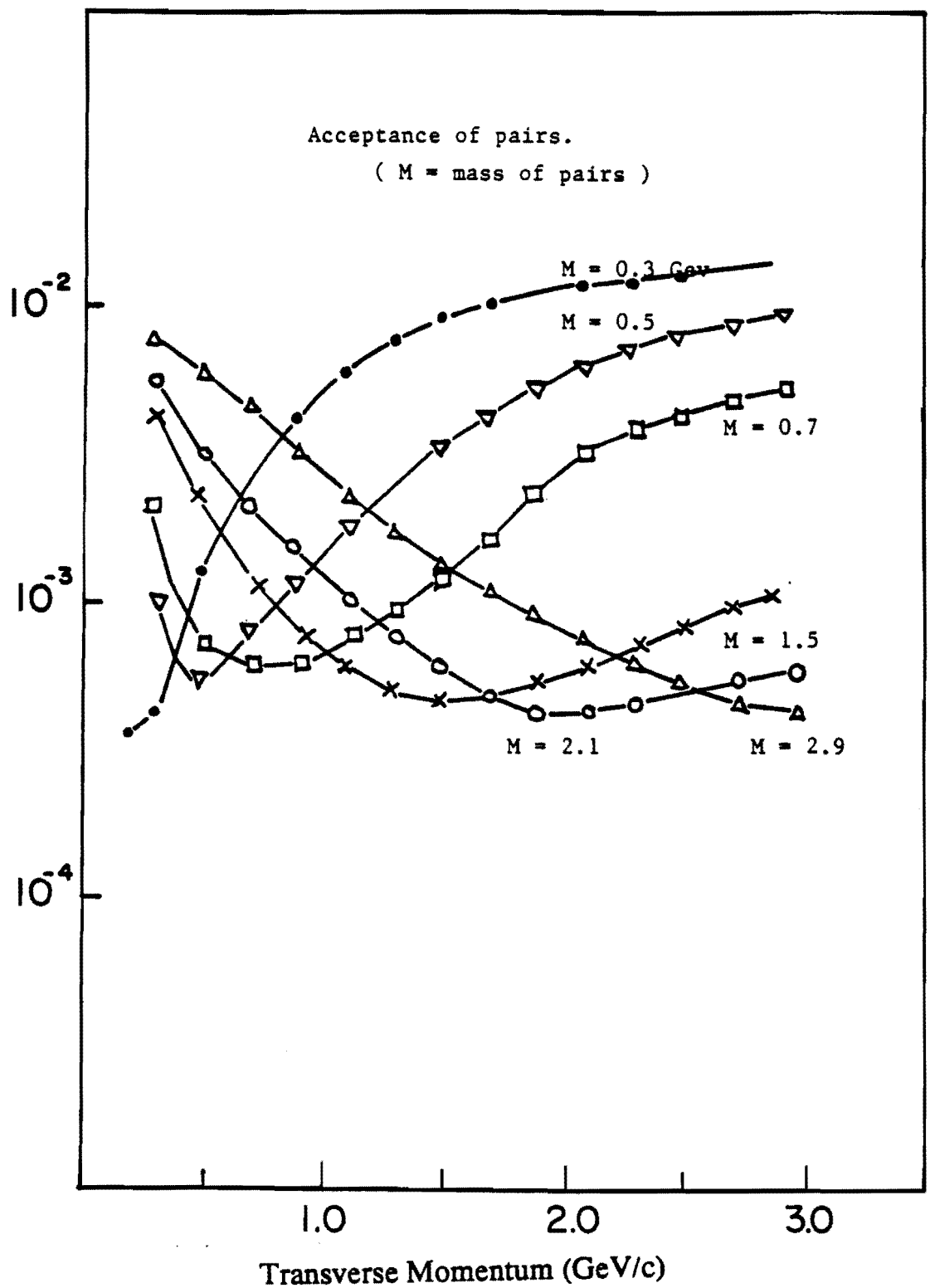

Figure 2.1.3 The probability that a pair can be detected when the pair is produced within the pseudo-rapidity -4.0 to 4.0. Each symbol represents different mass of pairs in GeV/c^2.

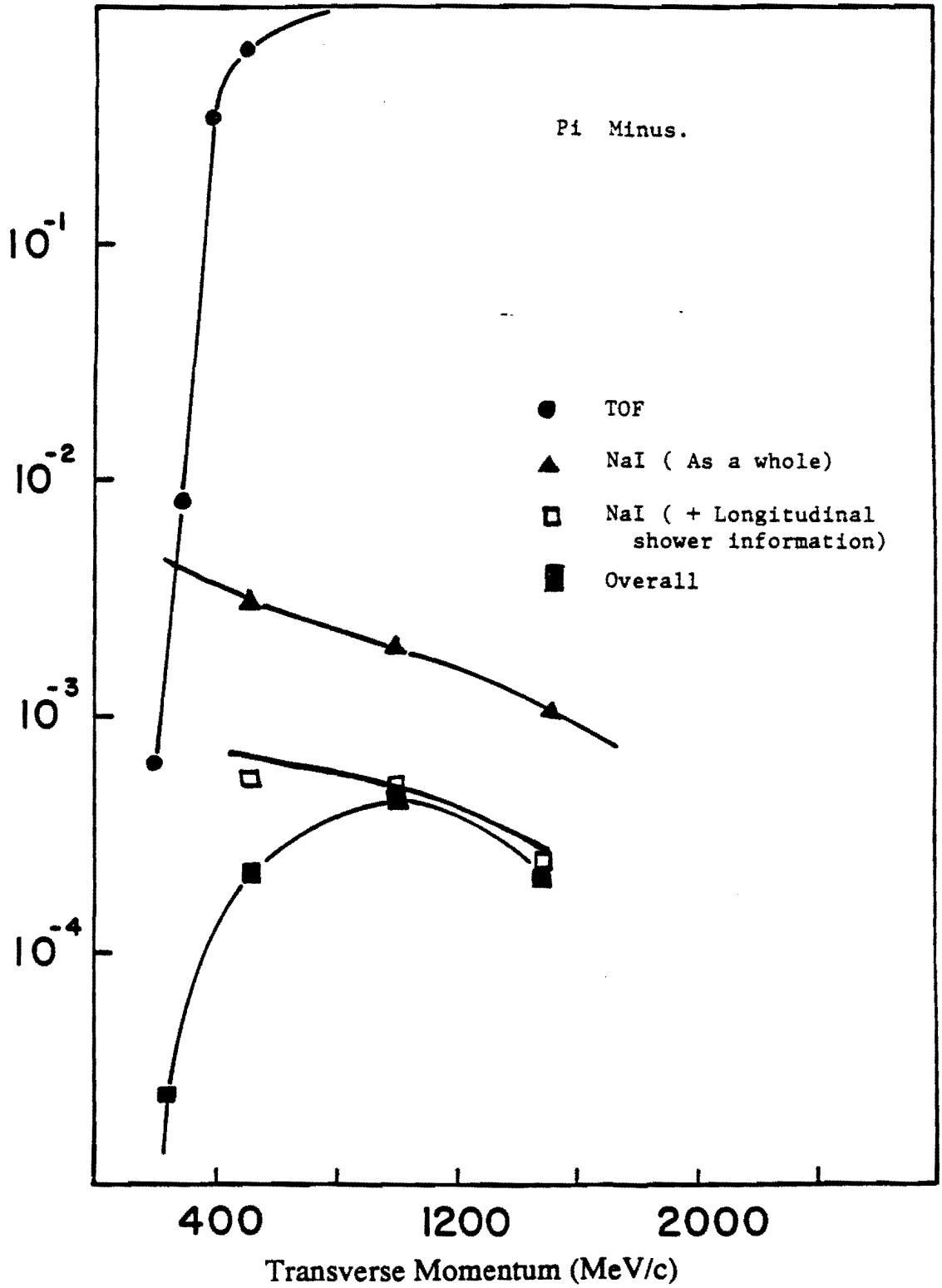

Figure 2.1.4 The π^- rejection probability using various detector components. With the threshold Cherenkov counter, the rejection should improve at least a factor of 20-50.

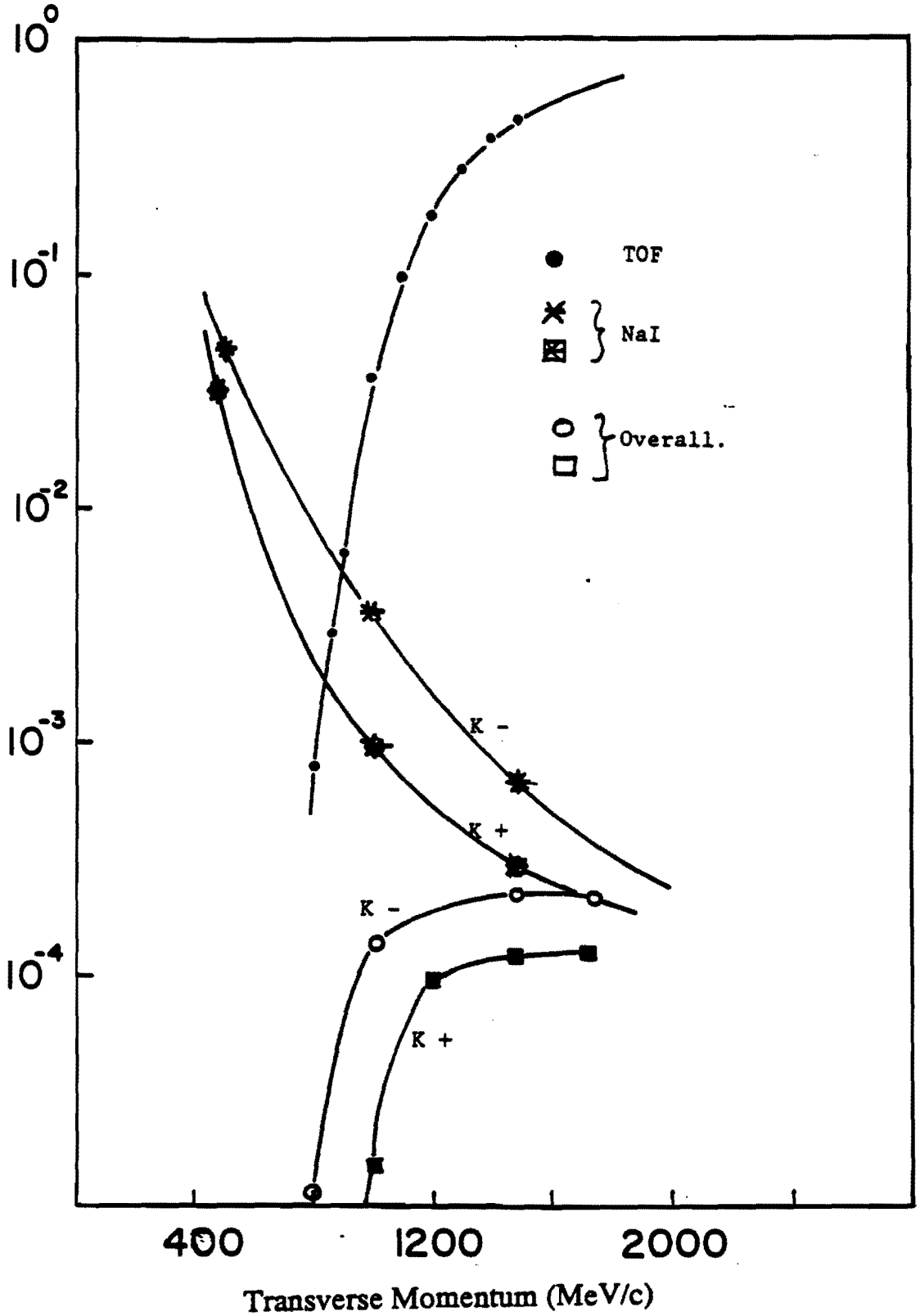

Figure 2.1.5 The Kaon rejection probability using various detector components. With the threshold Cherenkov counter, the rejection should increase by at least a factor of 20-50.

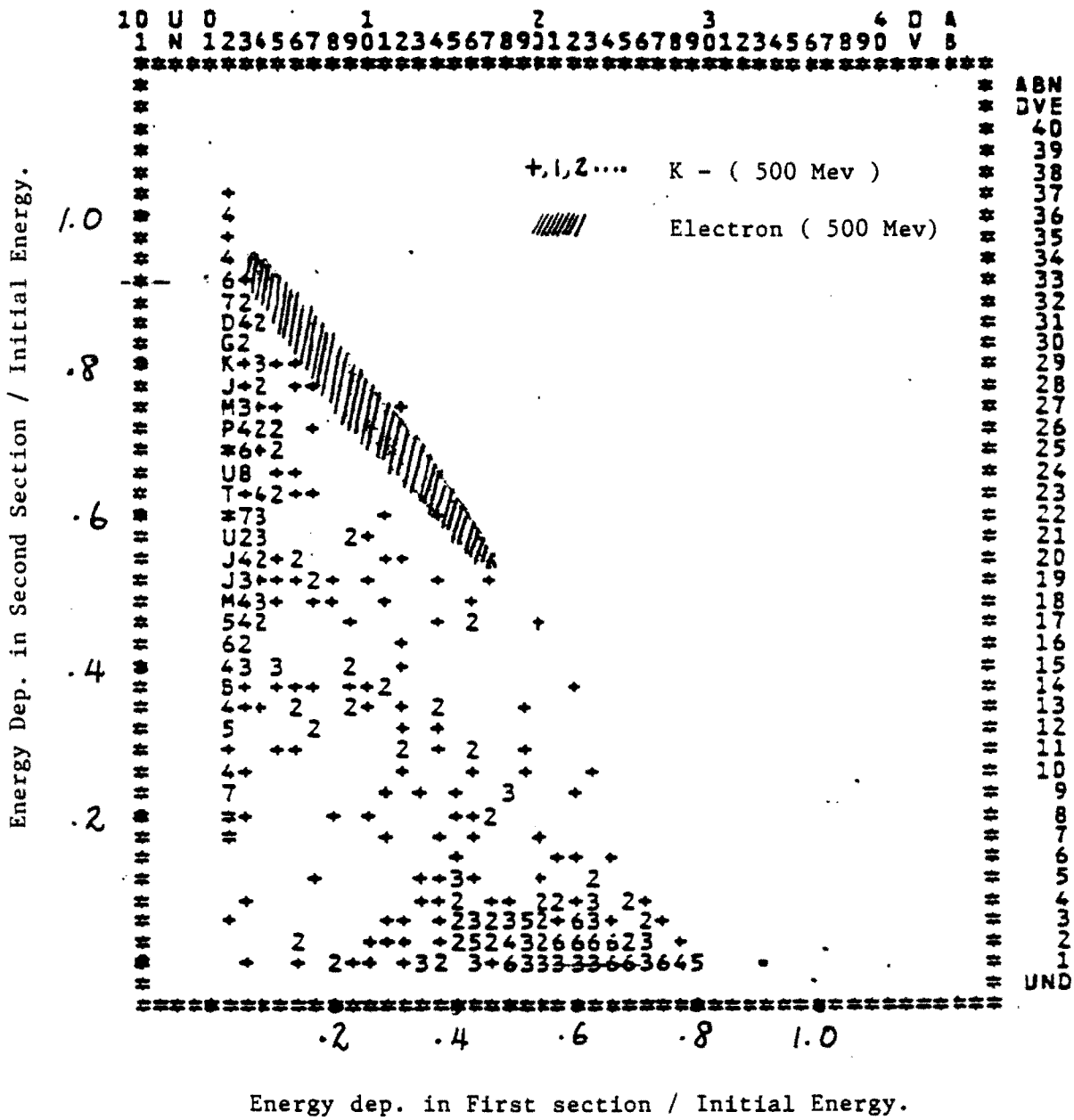

Figure 2.1.6 Fractional energy deposited by e^- and K^- in the first versus second section of the NaI detector.

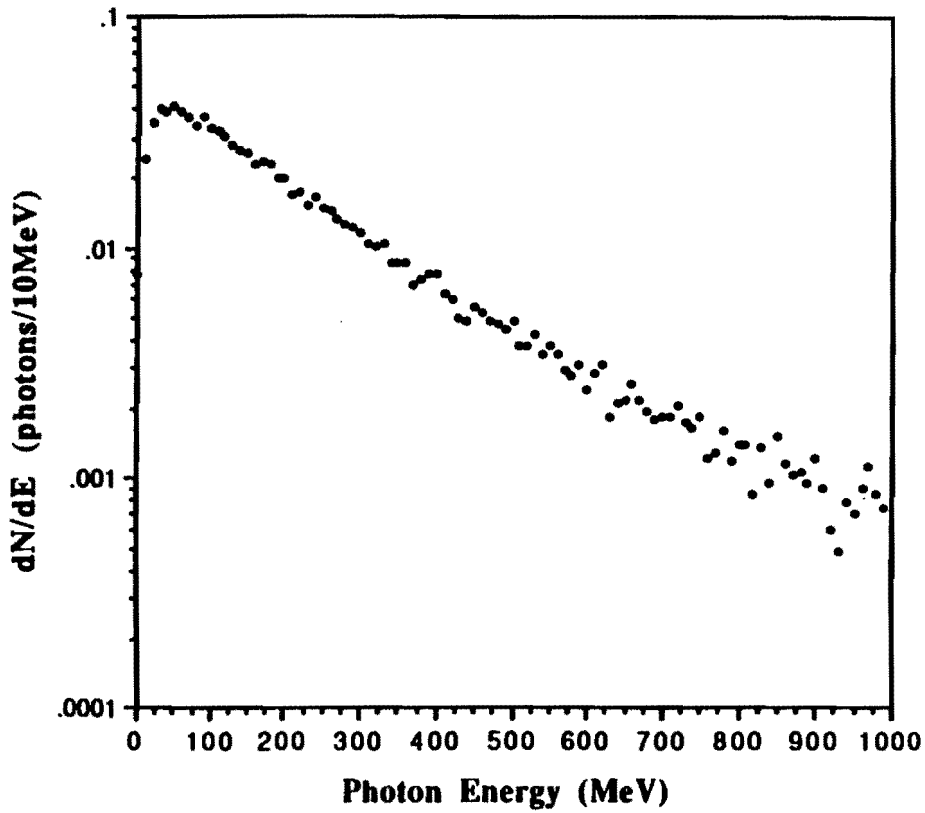

Figure 2.2.1 Photon spectrum into NaI calorimeter from $\bar{p}p$ collisions at $\sqrt{s}$ = 1.8 TeV. (ISAJET prediction)

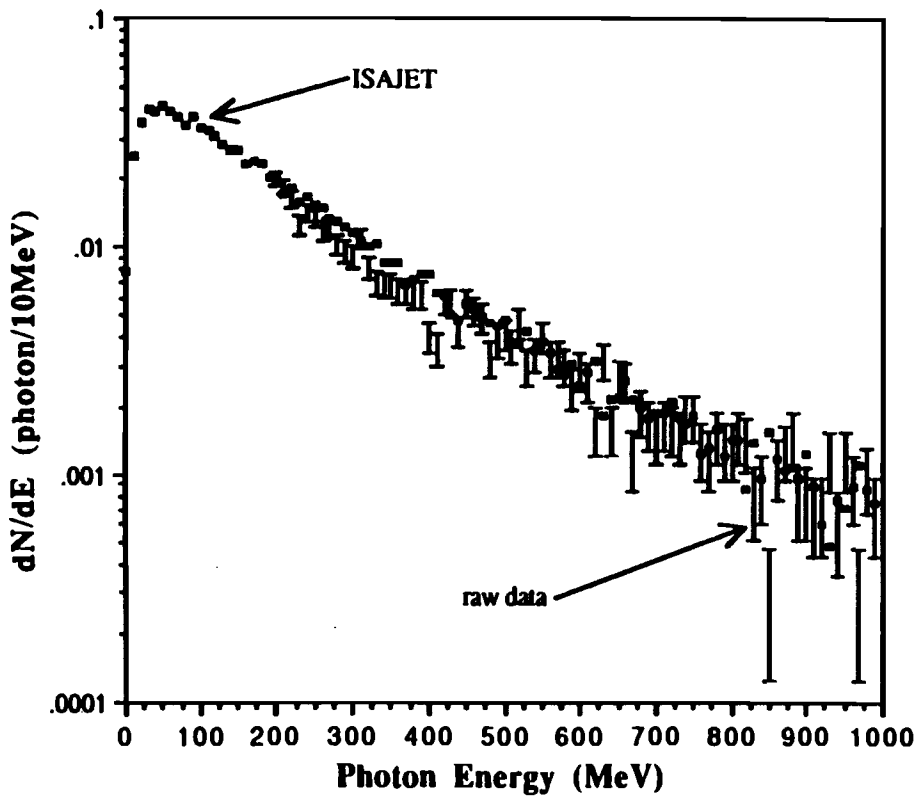

Figure 2.2.3 Comparison of photon energy spectrum measured from E735 NaI calorimeter (raw, uncorrected data) to the prediction of ISAJET.

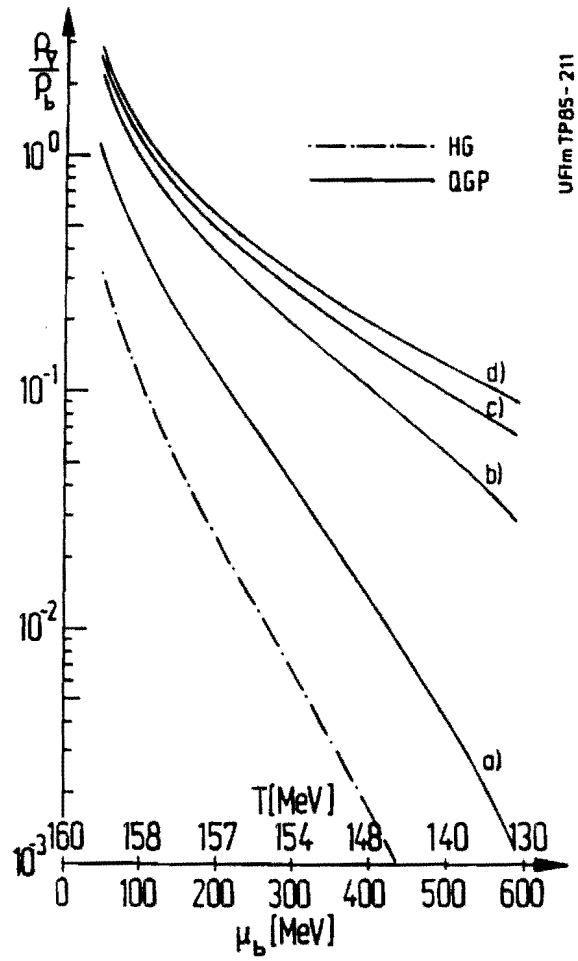

Figure 2.3.1 Theoretical prediction for the hyperon-baryon ratio as a function of the plasma temperature.

Fig. 3.1.1 Design of a X - U - V Cell Triplet
Plane View of the Upper Plane

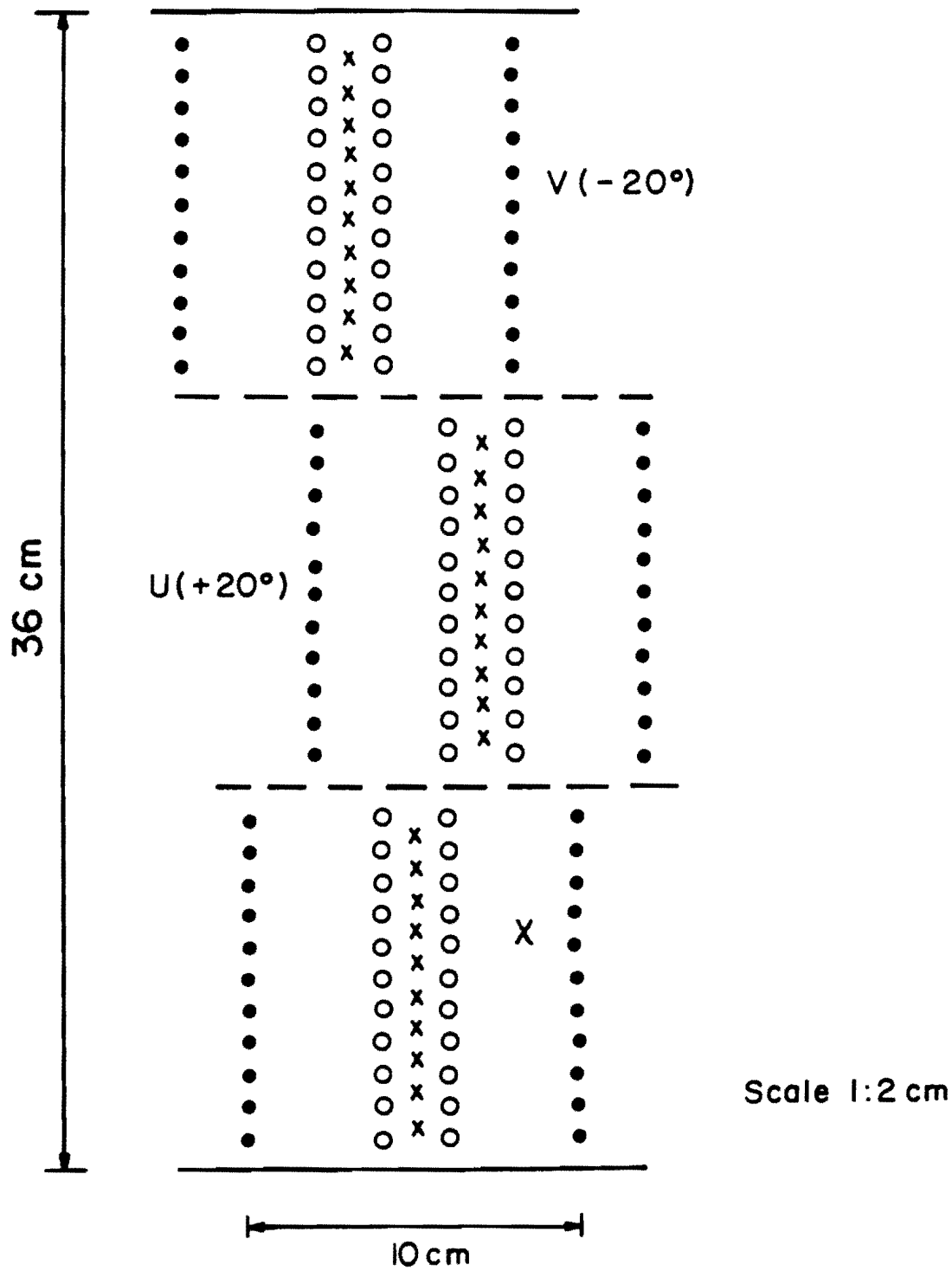

Design of a Single Cell X Chamber Crossection

Fig. 3.1.2

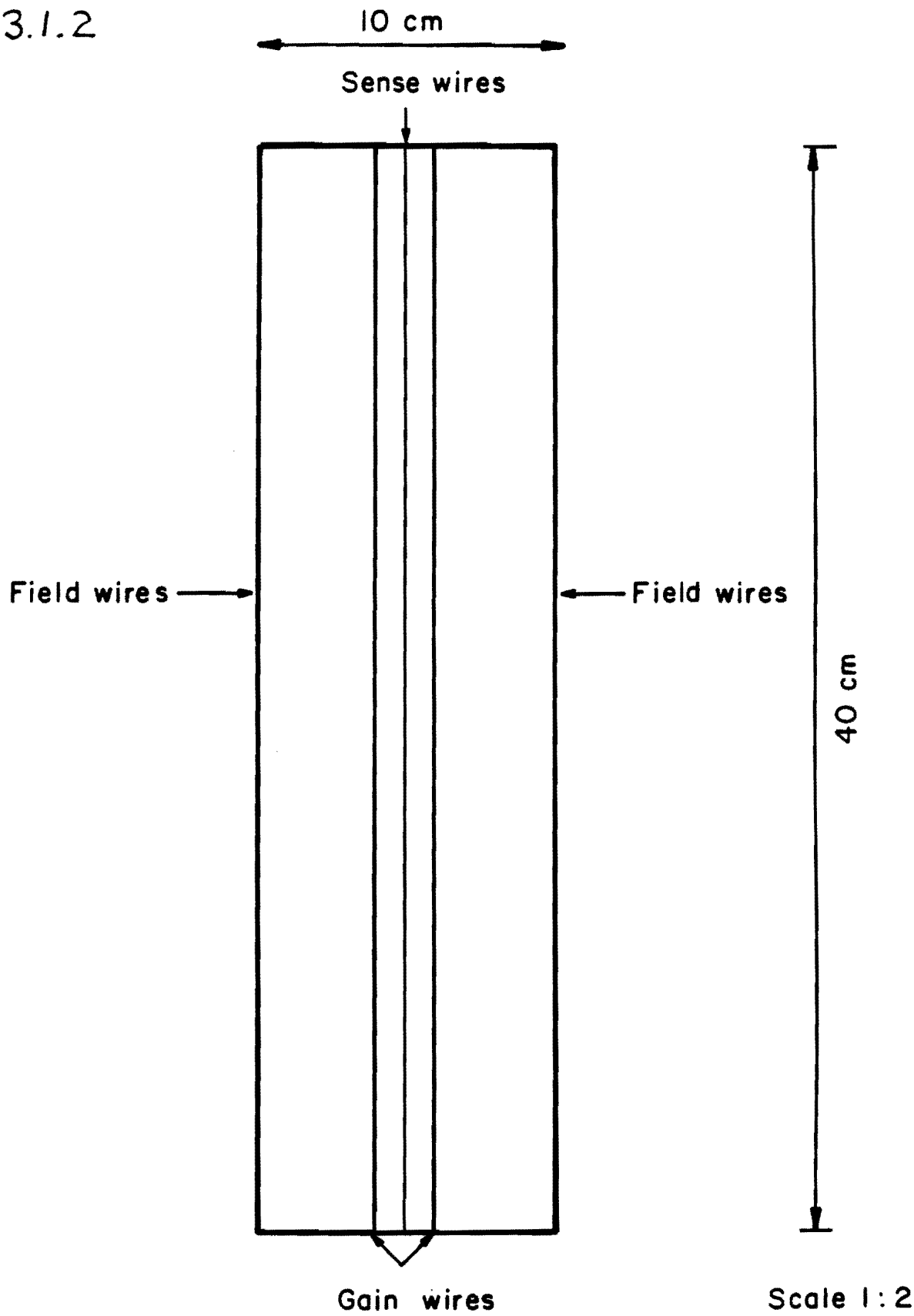

Design of a Single Cell U Chamber
Crossection

Fig. 3.1.3

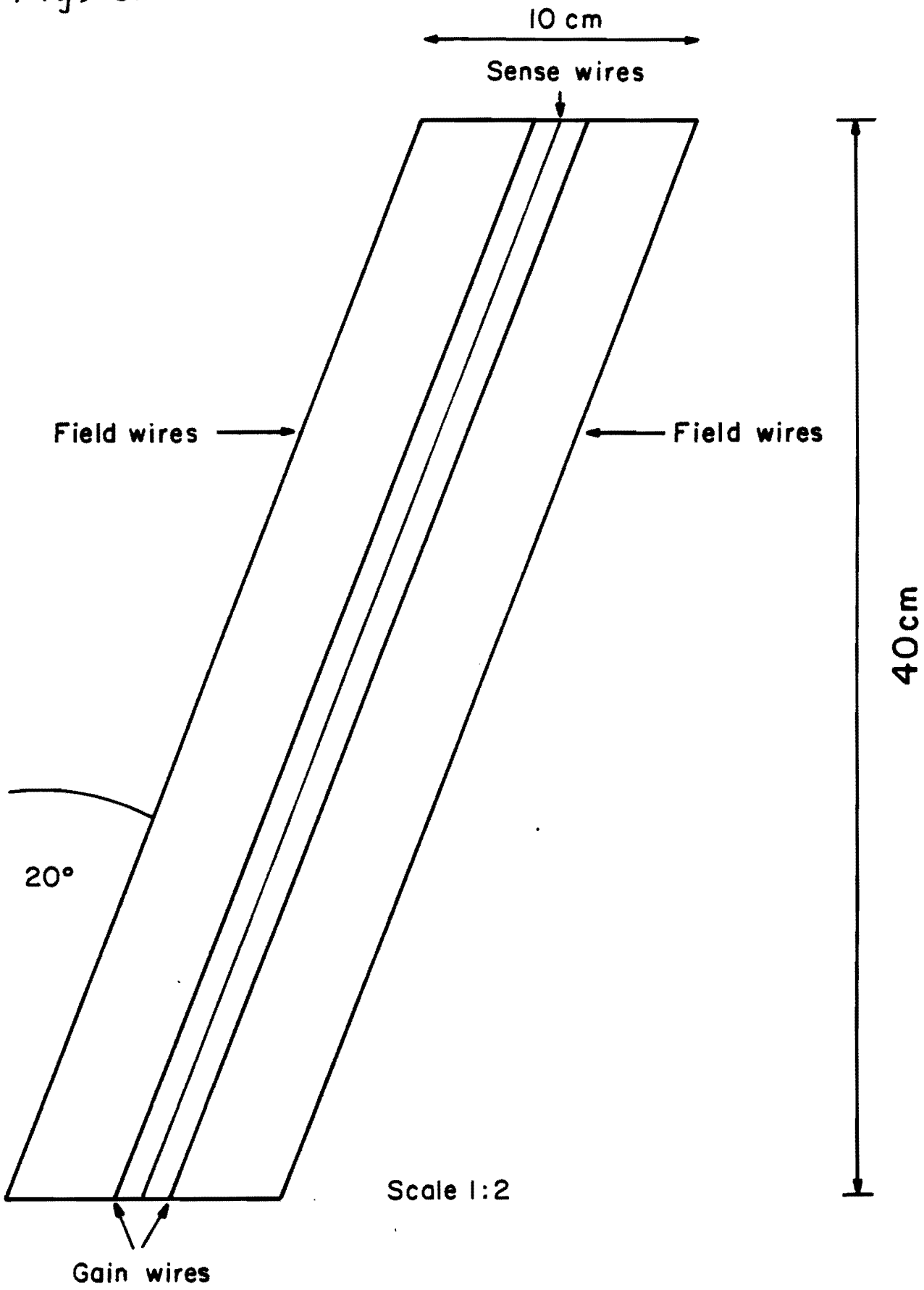

Fig. 3.1.4 Design of the Whole Chamber Triplet
Plane View

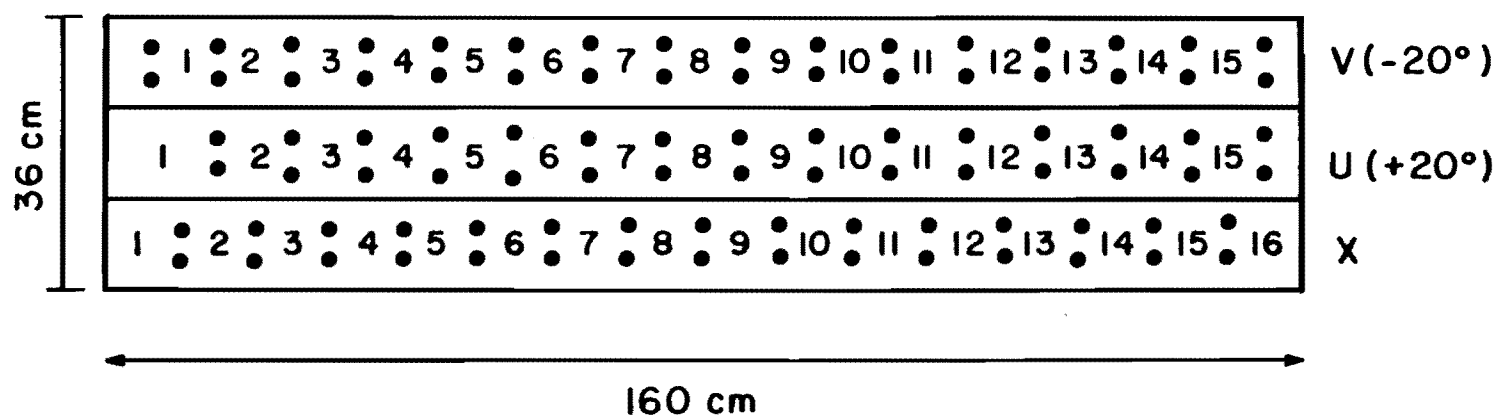

Scale 1:10cm

Fig. 3.1.5

POST MAGNET CHAMBER

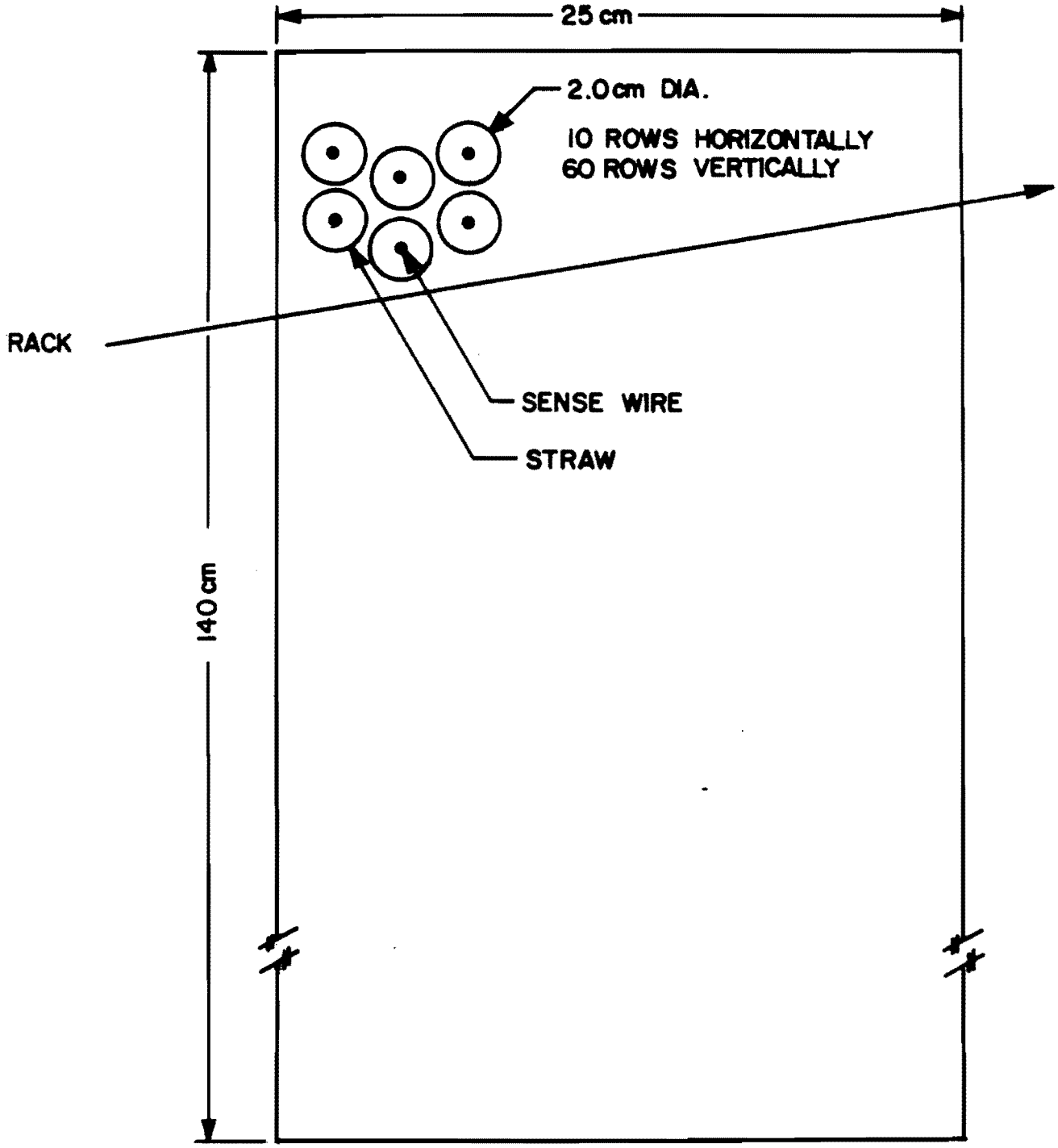

PLAN VIEW

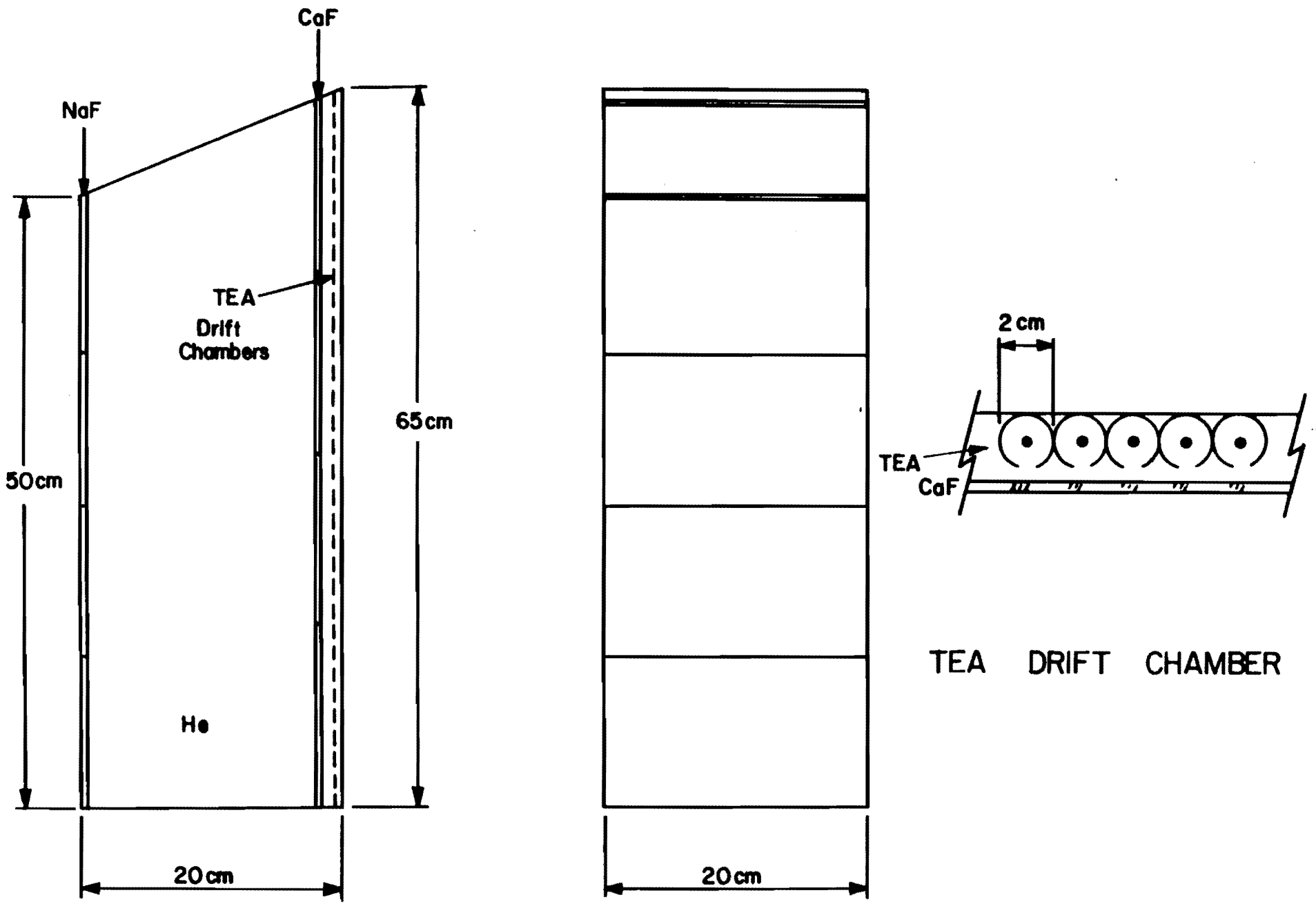

Figure 3.1.6 One of four modules of the proposed RICH counter. A

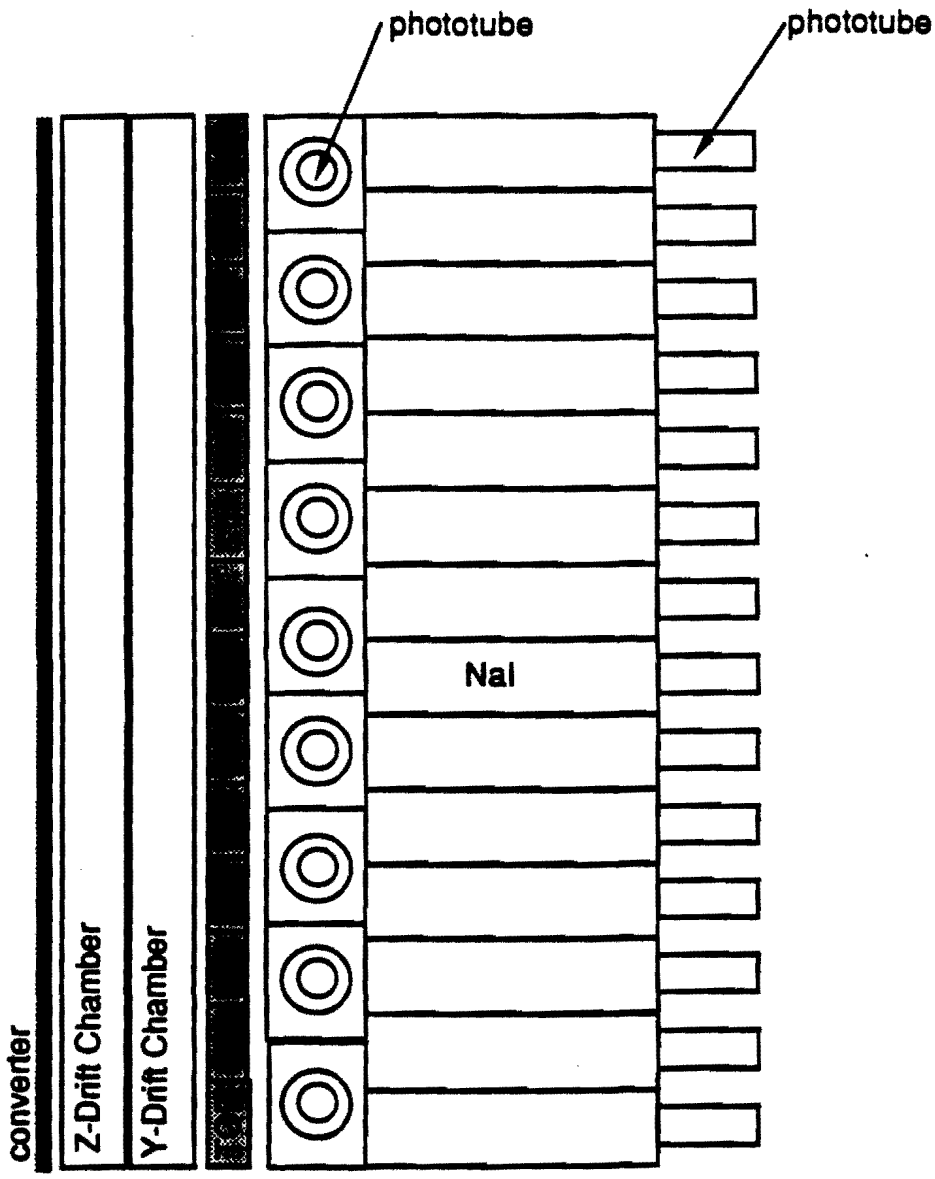

Figure 3.1.7 Detector room electromagnetic calorimeter
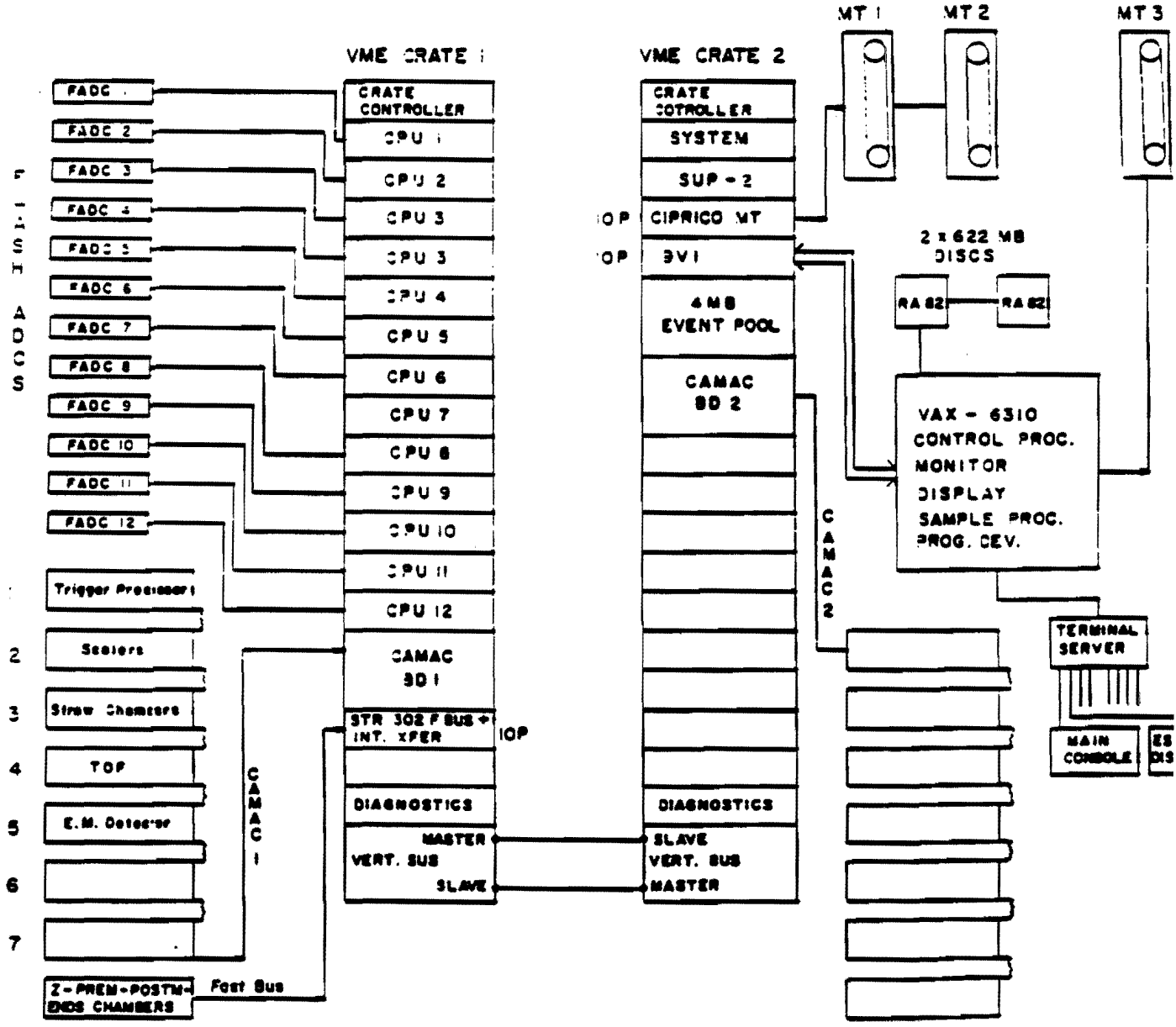
Fig. 3.2.1 ON LINE DATA ACQUISITION SYSTEM (P-787)